Seeding and structural variability in α-synucleinopathies

Doctoral Thesis

In partial fulfillment of the requirements for the degree “Doctor rerum naturalium (Dr. rer. nat.)” in the Molecular Medicine Study Program at the Georg-August University Göttingen

Submitted by
Niccolò Candelise

from Cosenza, Italy
Göttingen 2018

Members of the Thesis Committee

Supervisor

Prof. Dr. Mathias Bähr

Göttingen University Medical School, Dept. Neurology.

Second member of the thesis committee

Prof. Dr. Tiago Outeiro

Department of Experimental Neurodegeneration; Center for Nanoscale Microscopy and Molecular Physiology of the Brain. University Medical Center Goettingen.

Third member of the thesis committee

Prof. Dr. Alexander Flügel

Institute for Neuroimmunology and Multiple Sclerosis Research
University Medical Center Göttingen
Georg-August University

Date of disputation:

Abstract 7

List of Figures 8

List of Tables 10

List of Abbreviations 10

1. Introduction 12

1.1 Protein aggregation and misfolding diseases 12

1.1.1 Protein misfolding and aggregation *12*

1.1.2 Factors affecting aggregation *14*

1.1.3 Prion-like behaviour and the concept of strains *15*

1.2 α-synuclein in physiology and pathology 17

1.2.1 Biology of α-synuclein *17*

1.2.2 Clinical features of α-synucleinopathies *19*

1.2.3 Spreading of α-synuclein *21*

1.2.4 α-synuclein strains *23*

1.3 Methods in protein aggregation 26

1.3.1 Tinctorial properties of protein aggregates *26*

1.3.2 Study of the architecture of protein aggregates 27
1.3.3 Protein misfolding assays and
The Real-Time Quaking-Induced conversion (RT-QuIC) 28

2. Aim of the project **32**

3. Methods **35**
3.1 Patients 35
3.2 Isolation of α-synuclein seeding competent fraction 36
3.3 Total α-synuclein ELISA 37
3.4 Real Time-Quaking Induced Conversion 37
3.5 Proteinase K digestion and Western blotting 38
3.6 Oligomeric α-synuclein ELISA 39
3.7 Dot Blot 39
3.8 Surface-Plasmon Resonance 40
3.9 Raman spectroscopy 40
3.10 Transmission Electron Microscopy 41
3.11 AFM analysis 41
3.12 Statistical analysis 42
3.13 Ethical issues 42

4. Results **43**
4.1. Validation of the Lewy pathology and α-synuclein aggregation by RT-QuIC **43**
4.1.1 Histochemical profile of the Lewy pathology do not differ between DLB and PD 43
4.1.2 Enrichment of the α-synuclein-containing fraction 44
4.1.3 The α-syn-SCFs contain equal level of α-synuclein among groups 46

4.1.4 Ruling out self-aggregation 47

4.1.5 DLB-seeded, but not PD-seeded reactions, promote the conversion of α-synuclein during the RT-QuIC 48

4.2 Biochemical validation of the RT-QuIC products **52**

4.2.1 Detection of PK resistant α-synuclein in DLB seeded RT-QuIC reactions 52

4.2.2 Monomeric α-synuclein is reduced after the RT-QuIC in DLB seeded reactions 54

4.2.3 Fibrillar and oligomeric α-synuclein species are generated during RT-QuIC in DLB seeded reactions 56

4.3 Structural analysis of α-synuclein aggregates generated by RT-QuIC **59**

4.3.1 Analysis of the background noise in Raman spectroscopy 59

4.3.2 Analysis of the Raman intensity along the coffee-ring 61

4.3.3 Detection of β-sheet structures in DLB-seeded RT-QuIC reactions by Raman spectroscopy 62

4.3.4 Fibrillar structures are detected by EM and AFM 64

5. Discussion **69**

5.1 Isolation of an α-synuclein containing, seeding prone fraction 69

5.2 Seeding of α-synuclein in DLB and PD patients 71

5.3 Biochemical evidences of α-synuclein aggregates

in DLB-seeded RT-QuIC reactions *72*

5.4 Structural evidences of α-synuclein aggregates in DLB-seeded RT-QuIC reactions *73*

5.5 Structural variability underlies potential α-synuclein strain typing *74*

5.6 Considerations on selective vulnerability *78*

6. Summary and Conclusions **81**

7. Bibliography **82**

Abstract

In the present work, we were interested in applying the Real-time quaking-induced conversion (RT-QuIC) for the detection of the seeding activity of Dementia with Lewy bodies (DLB) and Parkinson's disease (PD) brain derived α-synuclein seeds. and analyzing the structure and morphology of the α-synuclein aggregates generated via RT-QuIC. A different seeding and conversion ability support the existence of α-synuclein conformational variants in both α-synucleinopathies.

To this aim, brain materials derived from neuropathologically well-characterised cases with DLB, PD and controls have been processed by filtration and centrifugation steps to obtain an α-synuclein seeding competent fraction, deployed as seed for the RT-QuIC. Biochemical and morphological analyses of RT-QuIC products were conducted by western blot, dot blot analysis, Raman spectroscopy, atomic force microscopy and transmission electron microscopy analyses. We observed a different seeding activity between DLB and PD, which resulted in the generation of a PK-resistant and fibrillary α-synuclein species in DLB seeded reactions, while PD and control seeds failed in the conversion of wild type α-synuclein substrate.

The structural variance between DLB and PD seeding kinetics and products indicated the existence of different α-synuclein stains in these groups. Our study contributes to the understanding of the clinical heterogeneity observed among α-synucleinoèpathies and opens news avenues for the future development of strain-specific therapies.

List of Figures

Figure 1. Free energy landscape of protein folding 13
Figure 2. α-synuclein structure 18
Figure 3. Strains selection 24
Figure 4. Kinetic of protein aggregation 29
Figure 5. Schematic workflow for Raman spectroscopy 41
Figure 6. Paraffin embedded histological sections of FCx and SNc of DLB and PD samples 44
Figure 7. Seeding activity of α-synuclein in different isolated fractions 45
Figure 8. Detection of α-synuclein in the α-syn-SCF 46
Figure 9. Confirmation of the α-synuclein amount among samples 47
Figure 10. Self-aggregation of α-synuclein in the RT-QuIC assay 48
Figure 11. RT-QuIC seeded with FCx derived material 49
Figure 12. RT-QuIC seeded with SNc derived material 50
Figure 13. Detection of PK-resistant α-synuclein fragments in FCx seeded RT-QuIC samples 53
Figure 14. Detection of PK-resistant α-synuclein fragments in SNc seeded RT-QuIC samples 53
Figure 15. Detection of monomeric α-synuclein before and after the RT-QuIC 55
Figure 16. Surface Plasmon Resonance 56
Figure 17. Detection of fibrillar α-synuclein before and after the RT-QuIC 57

Figure 18. Detection of oligomeric α-synuclein before and after the RT-QuIC 58
Figure 19. Background signals from different Raman supports 59
Figure 20. Background signals from the components of the RT-QuIC reactions 60
Figure 21. Raman shift of α-synuclein as a function of concentration 61
Figure 22. Raman signal along the radius of the coffee ring 62
Figure 23. Raman spectra of the amide I band region of the samples before RT-QuIC processing 63
Figure 24. Deconvolution of the Amide I band 63
Figure 25. Raman spectra of AQ and BQ samples 64
Figure 26. AFM on BQ samples 65
Figure 27. TEM on BQ samples 66
Figure 28. Morphological characterization of the RT-QuIC products under AFM 67
Figure 29. Morphological characterization of the RT-QuIC products under TEM 68
Figure 30. α-synuclein seeding-conversion mechanism 72

List of Tables

T**able 1.** List of materials	33
Table 2. Clinical features	35
Table 3. Overview of diagnostic accuracy	51
Table 4. Comparison among α-synuclein RT-QuIC protocols	77
Table 5. Recapitulatory table of the two-way ANOVA	79

List of abbreviations

(in order of appearance, most relevant highlighted in bold)

PCD = Protein Conformational Disorder

CJD = Creutzfeldt-Jakob Disease

GSS = Gerstmann-Sträussler-Scheinker syndrome

FFI = Fatal Familial Insomnia

PrP^{C} = cellular Prion Protein

PrP^{Sc}= Scrapie prion protein

PK = Proteinase K

AD = Alzheimer's Disease

NAC = Non-Amyloid-β Component

LB = Lewy Bodies

LN = Lewy Neurites

DLB = Dementia with Lewy Bodies

PD = Parkinson's Disease

PD-D = Parkinson's Disease associated Dementia

RBD = REM-sleep Behaviour Disorder

CNS = Central Nervous System

iDLB = Incidental Dementia with Lewy Bodies

PNS = Peripheral Nervous System

MSA = Multiple System Atrophy

ThT = Thioflavin-T

PFF = Pre-Formed Fibrils

EM = Electron Microscopy

AFM = Atomic Force Micoscopy

RT-QuIC = Real-Time Quaking-Induced Conversion

PMCA = Protein Misfolding Cyclic Amplification

CSF = Cerebrospinal Fluid

BH = Brain homogenates

Ctrl = Controls

FCx = Frontal Cortex

SNc = Substantia Nigra pars compacta

w/V = Weight to Volume ratio

AQ = After the RT-QuIC

BQ = Before the RT-QuIC

TEM = Transmission Electron Microscope

AUC = Area under the curve

IHC = Immunohistochemistry

α-syn-SCF = α-synuclein seeding-competent fraction

SPR = Surface Plasmon Resonance

KD = Dissociation constant

1. Introduction

1.1 Protein aggregation and misfolding diseases

1.1.1 Protein misfolding *and aggregation*

The correct function of living organisms strictly depends on the concerted functions of a network of thousands of proteins [1-3], which need to assume a specific structure to exert their functions. Protein folding is a tightly regulated process that depends on the aminoacid sequence of the protein. A nascent polypeptidic chain may arrange in conserved structures, such as α-helices and β-sheets, or display random-coiled architecture with no repetitive motifs. The distribution of these structures within a protein defines its tertiary structure, that is the way the protein disposes itself in the three-dimentional space. The process of protein folding is dependent on the energetic landscape of a protein. Thermodynamic constrictions force a protein to assume the conformation that minimizes the free energy of the system. Protein folding is regulated chaperones, which prevent the formation of nonfunctional structures by helping the protein reaching a local energetic minimum, defining the functional structure of the protein [4, 5]. However, some proteins may be able to adopt an alternative conformation which is typically β-sheets enriched [6-8]. Most of the disease-related proteins appears to be intrinsically disordered [9-12], owing a low complexity region facilitating the transition to β-sheets enriched structures and show poor binding to chaperones [13]. Most neurodegenerative diseases share the presence of aggregated, β-sheet enriched proteins in form of plaques and fibrils, therefore are collectively defined as protein conformational disorders (PCDs) [14-21]. β-sheets are formed of alternated strands linked by hydrogen bonds between the N-terminal and C-terminal moiety of the peptide, connecting one strand to the other [1, 22]. Upon adequate conditions, virtually every protein can change its conformation and accomodate into a β-sheet enriched structure [23], leading to the formation of amorphous aggregates and amyloid fibrils, representing the absolute free energy minimum among the various conformations a protein can adapt [24] (Figure 1). Even globular proteins, under the proper conditions, have been shown to form aggregates [25].

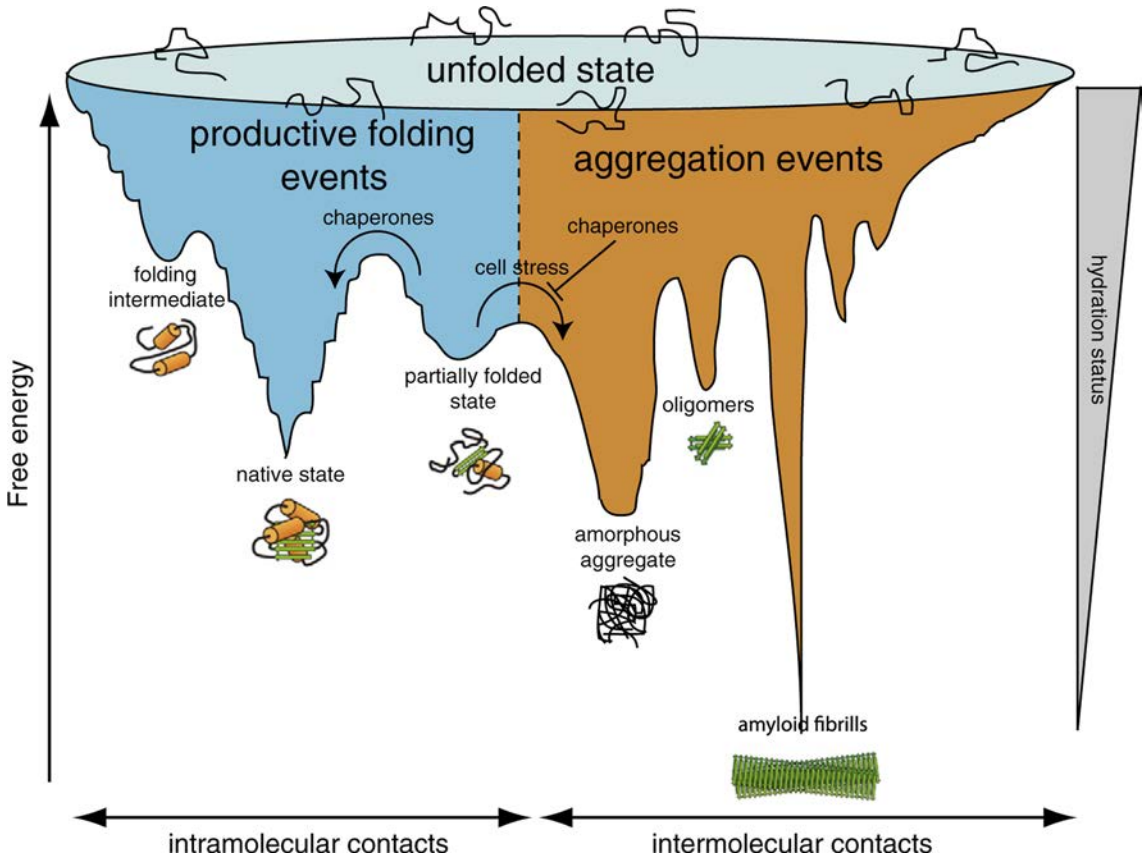

Figure 1. Free energy landscape of protein folding.

The diagram shows the energetic states a protein can adopt while folding. Stressful events, or changing in the micro-environment in which the reaction takes place may displace chaperones and lead the protein to an aggregated state, either as amorphous aggregate, oligomer or amyloid fibril. The decrease of hydration state, by increasing the local protein concentration, pushes toward the formation of fibrils, as well as the intermolecular forces that may intervene between exposed regions of two proteins [24].

Studies conducted with X-ray fibre diffraction and solid-state magnetic nuclear resonance [2, 26-28] have shown that amyloid fibrils are composed of several protofilaments, transitory structures which consist of β-sheet structures possessing β-strands running perpendicular to the length of the fibril, in a structure termed cross-β conformation [29]. The formation of this conformation is favoured by intermolecular hydrogen bonds, hydrophobic interaction and water exclusion from the inner core of the fibril. The sum of these forces allows the misfolded protein to overcome its intermediate, metastable stages and lean toward the minimal energy level of the amyloid [30]. Nevertheless, it is still unclear whether misfolding triggers protein aggregation or whether oligomerization and establishment of intermolecular forces induces the conformational changes. Therefore, different models have been proposed following kinetic studies. According to the polymerization hypothesis [1, 31, 32], the critical event of protein conformational di-

sorders is the formation of oligomers, which act as a seed to induce misfolding. In this model, misfolding follows the formation of oligomers in a nucleation dependent polymerization, similar to crystal formation [1]. From a kinetic point of view, this model implies a slow lag phase, in which unfavourable interactions occur before the oligomeric nucleus is formed and starts growing into fibrils. The conformational hypothesis, on the other hand, implies that the protein is stable both in its native conformation and in the misfolded one. According to the nucleation model [1, 33, 34], the misfolding may be either spontaneous or induced, and the amyloid formation is not necessarily the end point of the conformational switch. Lastly, the conformation/oligomerization hypothesis offers an intermediate approach, with mild conformational changes leading to an unstable intermediate with amyloidogenic properties, stabilized by intermolecular interactions with other β-sheet enriched molecules, thereby aggregating into fibrils. According to this view, the misfolding into the pathogenic species is triggered by structural changes, while complete misfolding is dependent on the oligomerization process [1, 7].

1.1.2 Factors affecting aggregation

Besides intermolecular forces and genetic variants, a plethora of environmental factors have been found to affect protein misfolding and aggregation [35]. Being a thermodynamic dependent process, protein aggregation may be influenced by physical factors, such as temperature, molecular crowding or other forces increasing entropy, as well as chemical factors such as variations of the pH or the presence of other proteins or biomolecules (i.e., nucleic acids, phospholipids and proteoglycans).

- Low pH promotes protein aggregation by increasing the net surface charge and enhance side chain repulsion, allowing the exposure of the aggregation-prone hydrophobic core [38]. Changes in the environmental pH affect, for instance, the amyloidogenic properties of β-2-microglobulin [36] and, similarly, the growth of α-synuclein fibrils, which is magnified at mildly acidic pH values (5,8) [37].

- Nucleic acids and polysaccharides own a high binding affinity for amyloid proteins and are therefore suggested to act as template, or as scaffold, for protein aggregation [39]. Electrostatic interactions between the peptide chain and the phosphate groups of

nucleic acids are favoured, thereby promoting the aggregation. The interaction between nucleic acids and amyloid proteins may increase the local concentration of the latter, facilitating protein aggregation through exposed hydrophobic domains with neighbour proteins [40, 41]. Indeed, nucleic acids have been shown to enhance α-synuclein aggregation [42, 43], as well as prion protein, SOD1, amyloid-β and tau [43].

- Lipid bilayers reduce the activation energy barrier required for proteins to accommodate into the amyloid state [44] by interacting with the positively charged surface of amyloidogenic proteins unmasking the hydrophobic core of the proteins.

- Thermodynamic events such as increasing temperature and concentration, or the application of an external force to the system, cause an increase in the entropy of the system increasing the chances of misfolding and aggregation.

Lastly, both *in vivo* and *in vitro*, protein aggregation is dramatically enhanced by the presence of a single misfolded unit, which posses the ability to transmit its conformational information to neighbour molecules in their native state, giving rise to self-propagating molecules which, according to the protein-only theory postulated for prion protein [45], represent the etiological cause of most, if not all, protein conformational disorders.

1.1.3 Prion-like behaviour and the concept of strains

The term prion was originally introduced by Stanley Prusiner in 1982 [14] to define the peculiar properties of the *pr*oteinaceous *in*fectious particle found in scrapie, a form of spongiform encephalopathy affecting sheep. The same component was subsequently pinpointed as the culprit of a class of infectious, inherited and sporadic human diseases, namely Creutzfeldt-Jakob Disease (CJD), Gerstmann-Sträussler-Scheinker syndrome (GSS) [46], Fatal Familial Insomnia (FFI) [47] and Kuru, an endemic pathology of Papua New Guinea affecting the Fore tribe due to their cannibalistic tradition [46]. Prions were shown to be resistant to inactivation by heating and by methods aimed to modify nucleic acids. Moreover, they were shown to be insoluble in non-denaturating detergents and partially resistant to protease treatment [46]. Foremost, the term prion underlies the requirement of infectivity, although the spreading in the absence of a nucleic acid

was unprecedented [45], putting the basis for a newfangled field in biology. The pathogenic informations that underlie the occurrence of prion diseases was ascribed to the conformation the protein adapts [22]. Upon the conformational switch of the cellular prion protien (PrP^{C}), the pathogenic scrapie isoform (PrP^{Sc}) was found to form rod-shaped particles with a structure indistinguishable from amyloids [49]. According to the widely accepted protein only hypothesis, the propagation of prions requires the formation of a homotypic complex between the two forms of PrP [45], leading to the conversion from the native form to the pathogenic conformation. The newly generated β-enriched molecule may act as a seed, by contacting other native forms (often termed substrate) and impose the conversion of the secondary structure from α-helices to β sheets, thus establishing a positive feedback that will eventually cause the aggregation into plaques and fibrils, affecting neurones and spreading through the organism. Nowadays, it is widely accepted [1, 2] that most, if not all, neurodegenerative diseases are caused by the misfolding and subsequent prion-like behaviour of one or more proteins. Moreover, a single misfolded molecule may misfold into different conformations, giving rise to different clinical picture and therefore different diseases. Separate conformations of the same protein are referred as strains.

The term “strain” was introduced to explain the differences in the pathological phenotype in goats when intracerebrally inoculated with sheep scrapie [49-51]. After infection, goats would either show clinical syndromes dominated by nervous (“drowsy”) symptoms or scratching behaviour, indicating that they could be related to different inocula. Therefore, researchers [51] borrowed the term strain from virology (at the time, prion pathologies were believed to be caused by very slow viruses [52]) to indicate the different clinical outcomes following goat and mice infection with scrapie sheep material. Importantly, the incubation period and brain lesion pattern were stable after several passages [53, 54]. The inoculation from the same scrapie source resulted in a different distribution of lesions and different incubation time among different mice lines, whereas no differences in these parameters could be detected within the same line.

After the breakthrough of the prion hypothesis [14], it became apparent that the properties of a strain were encoded exclusively in its structure. Strains were hence viewed as a population of conformational variants that compete for the same source (i.e., the native version of the misfolded protein) as a function of the environmental conditions. The predominant variant within a clinical frame is therefore the most efficiently replicating

one in the context of a specific host's genetics [55-57]. A grand variety of strains have been characterized thus far since the inception in the prion field of the concept of conformationally different protein strains. Strains derived from mink encephalopathies were shown to possess unique biochemical profile after proteinase K (PK) digestion [58] and differences in the relative amount of secondary structure among strains were reported [59]. Strains might therefore arise from many different conditions, all of which results in a specific conformation adapted by the misfolded protein. The genetic background of both the host species and the source of the pathogenic seed may alter the conformation, as well as post-translational modifications, physical and chemical condition of the micoenvironment in which the seeding-conversion process takes place. In recent years, the compelling heterogeneity of neurodegenerative diseases, together with the shared presence of insoluble, β-enriched proteinaceous aggregates, lead the researchers to speculate that other PMD-related proteins would behave like the prion protein, thus exhibiting different strains, enciphering different diseases [60, 61]. Both amyloid-β and Tau, the major constituent of Alazheimer's disease (AD) plaques and tangles, were indeed found to form different strains [62-64]. Moreover, tau strains would retain cell selectivity (neurons or glial cells) and spatial distribution of the pathology. Akin to taupathies and prion diseases, α-synuclein have been shown to adapt different structures which may account for the different clinical features of synucleinopathies. In the next chapter, α-synuclein biology and pathological aspects, as well as strain-typing, will be discussed in detail.

1.2 α-synuclein in physiology and pathology

1.2.1 Biology of α-synuclein

α-synuclein involvement in neurodegenerative diseases was originally identified in an attempt to characterize tau-derived paired helical filaments in AD [65]. The anti-Tau antibody developed by the researchers also labelled two cytosolic proteins owing an apparent molecular mass of 19 KDa. Additional purification steps lead to the identification of the two synaptic proteins [66], originally termed "perfectin" and "imperfectin" (α- and β-synuclein, respectively). Whereas early findings indicated that α-synuclein was an integral component of the amyloid plaques in AD, its role in PD was still unknown until genetic studies [67] conducted in a family with early onset of PD and autopsy-confir-

med Lewy pathology indicated a marker that segregated with disease in this family, mapping in the long arm of chromosome 4 (region q21-q23), where the SNCA gene maps. Subsequently, LBs and LNs were shown to display strong immunoreactivity for α-synuclein [68]. α-synuclein inclusions were also found to be characteristic of diseases caused by SNCA mutations [69] and the staining for α-synuclein was found to precede and to be more reliable than the unspecific staining for ubiquitin [70]. α-synuclein has a highly conserved and repeated N-terminal region, a hydrophobic central region and a less conserved, negatively charged C-terminal region [71]. The amino-terminal region is mostly composed of seven imperfect repeats of eleven aminoacids, owing a conserved core of a consensus sequence KTKEGV, spanning from residue 7 to residue 87 [72] (Figure 2).

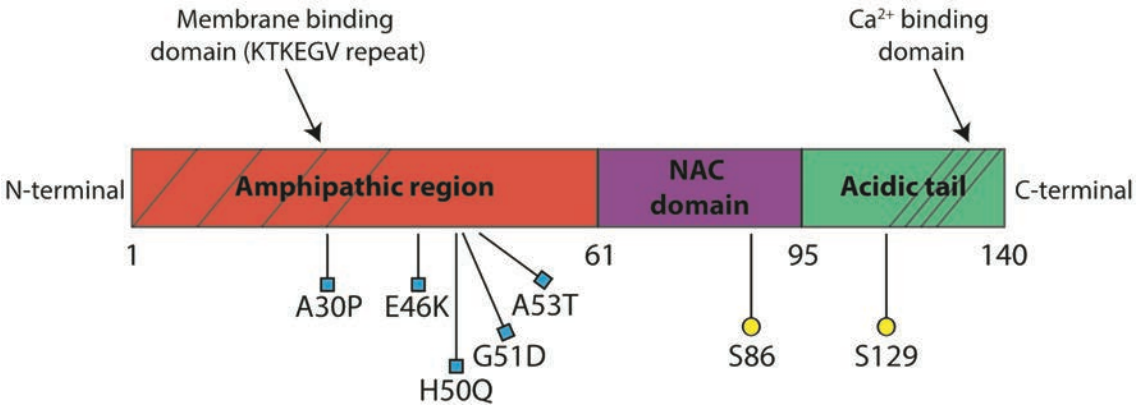

Figure 2. α-synuclein structure

Representative image of α-synuclein domains. Main mutations and phospho-sites involved in diseases are indicated [73].

The hydrophobic region (residues 61 to 95) of α-synuclein was termed non-Amyloid-β component (NAC) by Saitoh and co-workers [74], corresponding to the protein found by Spillantini's group using tau antibodies [75]. Furthermore, the precursor of the NAC was shown to be a natively unfolded protein [72]. Nonetheless, the amino-terminal region of α-synuclein was predicted to form an α-helix upon binding to membranes [76]. In depth structural analyses showed that α-synuclein adopts an 11/3 helix as predicted by its sequence, lying along the surface of the membrane, half-buried in the phospholipid bilayer [77]. It has been further suggested [78] that α-synuclein may adopt a helical tetrameric conformation in physiological conditions, although evidences for this state are not definitive [79]. Likewise, whereas the physiological role of α-synuclein has been studied in several different contexts [73, 79], the exact function of α-synuclein remains

yet unclear. Although α-synuclein is mostly expressed in nervous system, where it localizes in the nerve terminal and accounts for 0,1% of all pre-synaptic proteins [79], it has been shown that is expressed in other non-neural tissues [80]. Within the presynaptic bouton, α-synuclein has been found to co-localize with lipid raft markers [81], where it was suggested to influence lipid packing [82] and to promote the uptake of polyunsaturated fatty acids [83]. Due to its presynaptic localization and its interactions with the membrane, it was postulated that α-synuclein may play a role in neurotransmitter release [84]. Electrophysiological studies conducted on α-synuclein KO mice [85, 86] showed that α-synuclein is involved in dopamine vescicular release. Within the synaptic terminal, α-synuclein was reported to dilate the exocytic fusion pore [87], to function as a chaperone [88] and to interact with the SNARE complex [89]. Although the physiological role of α-synuclein has not been clarified yet, its central role in neurodegenerative diseases has been thoroughly and extensively investigated to such an extent that the numerous α-synuclein pathologies have been grouped together as α-synucleinopathies.

1.2.2 Clinical features of α-synucleinopathies

The defining feature of synucleinopathies is the presence of inclusions made up of aggregated α-synuclein, which appear as intraneuronal tangles termed Lewy bodies (LBs) and Lewy neurites (LNs) [90]. Besides AD, Lewy pathology, in the form of Dementia with Lewy Bodies (DLB), Parkinson's Disease (PD) and PD associated dementia (PD-D), is the most common cause of dementia in the elder population [91], comprising 1-2% of the total population aged above 65 years [92]. In the frame of parkinsonism symptoms, defined by the sum of extrapyramidal motor symptoms including tremor, bradykinesia, posture instability and rigidity, DLB and PD-D share a variety of clinical features, such as hallucination and cognitive impairments, with executive and visual-spatial dysfunction being the most prominent and overlapping features [93]. When cognitive symptoms appear before the motor impairments by at least one year, diagnosis of DLB is considered appropriate by general consensus, whereas PD-D is diagnosed when the motor pathology occurs at least one year before the cognitive symptoms [94]. Although DLB and PD-D are sometimes considered as opposing edges of the same pathological spectrum [92, 95, 96], marked differences have been reported [92], supporting the hypothesis that they are different, albeit similar, diseases. The differences between the two diseases are more marked in early and mid stages of the pathologies, but

tend to converge at later stages [94]. Cognitive symptoms, such as hallucinations [97] (related to grey matter loss in parietal, occipital and orbitofrontal cortices [98]) and the decline in attention, executive functions, episodic memory and constructive abilities have been reported to be greater and faster in decline in DLB [92]. REM sleep behaviour disorder (RBD) show high prevalence in DLB, and was suggested to precede the cognitive impairment by ten years [99]. Similarly, other prodromal symptoms, such as hyposmia, constipation and depression, have been proposed to be clinically useful in discriminating between PD-D and DLB [100-102]. The clinical differences between DLB and PD are also reflected in the selective impairment of neurotransmitter systems. Whereas PD shows impairments in subcortical regions related to dopaminergic [103] and cholinergic pathways [104, 105], DLB presents alteration in the cortical serotoninergic system [106]. Moreover, higher amyloid-β and tau pathology were found in DLB compared to PD-D [107-110]. Although DLB and PD-D are mainly sporadic pathologies, genetic factors have been shown be involved in the onset of the diseases, as heritability accounts for approximatively 30% of the DLB and PD-D cases [111].

Mutations in the α-synuclein gene SNCA [112], as well as locus duplications and triplications [113], have been found to cause PD, indicating a concentration-dependency of the assembly of α-synuclein. On the other hand, loss of the SNCA gene was shown to produce a phenotype without neurodegeneration [85]. Genome-wide association studies (GWAS) identified other genes that appear to influence the odds of occurrence of synucleinopathies [114], indicating that multiple biological pathways are compromised in α-synuclein associated diseases. [115-117]. α-synuclein over-expression was shown to disrupt the trafficking between the endoplasmatic reticulum and the Golgi, thus affecting the autophagic response [118, 119]. Moreover, α-synuclein aggregates were found to be implicated in a variety of cellular pathways, involving synaptic impairment [120, 121], disfunction in the organelle dynamic and axonal transport [122], mitochondrial fragmentation [123] and alteration of various transcription factors [124]. These pathways may be differentially involved in synucleinopathies, explaining the heterogeneity in the clinical symptoms and disease progression observed in different pathologies.

1.2.3 Spreading of α-synuclein

Due to the progressive nature of the disease, correlation between the topographic distribution of LBs and LNs and the clinical phenotype of the pathology, it has been proposed that synucleinopathies may be classified into stages of fixed anatomical pattern of inclusions, recapitulating the course of the disease [125-127]. According to the distribution of the Lewy pathology, DLB was originally divided in three subtypes: brainstem, limbic and neocortical [128]. The advent of α-synuclein antibodies [15] provided a more reliable tool for the assessment of Lewy pathology compared to the previously used methodologies (based on ubiquitin or hematoxylin-eosin staining [129]), allowing a more extensive neuropathological characterization. Based on α-synuclein immunoreactivity, Braak and co-workers [125] proposed a staging system for sporadic PD in which neuronal damage progresses along predictable routes, following the selective susceptibility of the neuronal populations. According to the Braak model, Lewy pathology may originate outside of the central nervous system (CNS) and being transported retrogradely through the vagal nerve [125]. Supporting this hypothesis, abundant α-synuclein aggregates have been detected in the peripheral autonomic nervous system [130, 131]. In stage I Lewy pathology can be detected in the dorsal IX/X motor nucleus in the medulla oblungata, in the intermediate reticular zone and in the anterior olfactory nucleus, with LNs being more represented than LBs. Stage II is defined by LBs and LNs in the caudal raphe nuclei and in the reticular formation. In incidental DLB cases (iDLB), LBs and LNs are found in the substantia nigra at early Braak stages (I-II), with no relationship between the α-synuclein burden and the neuronal loss [132]. The most characteristic lesion of stage III are found in the substantia nigra and in the magnocellular nuclei of the basal forebrain. At stage IV, the pars compacta of the substantia nigra appears markedly degenerated and depigmentation may be observed. LNs appear in the amygdala and in the hippocampus and LBs can be seen in the anteromedial temporal mesocortex. Lewy pathology spreads into the neocortex at stage V, whilst brainstem, olfactory bulb and substantia nigra worsen their burden of lesions. In stage VI, LNs and LBs are observed throughout the whole neocortex. Although the neuropathological diagnostic criteria managed to identify prodromal symptoms, such as anosmia and autonomic dysfunctions, the Braak staging was restricted for PD, therefore not predictable of DLB pathology. Moreover, it did not account for amygdala-predominant Lewy pathology, which was later proposed to be a separate form of synucleinopathy [133]. A similar sta-

ging system for Lewy pathology has been proposed by the DLB consortium for Lewy pathology, grouping PD-D and DLB together [134, 135] and including amygdala dominant cases. The two strategies for classifying the diseases were merged in a new protocol developed within the BrainNet Europe, in the attempt to increase the inter-observer agreement [134]. α-synucein aggregates have been found in other rarer synucleinopathies, such as pure autonomic failure, in which α-synuclein aggregates are mostly confined to the peripheral nervous system (PNS) [136], iDLB, in which LBs and LNs are found while no clinical symptom is manifested [137], and multiple system atrophy (MSA), the third most common synucleinopathy. In MSA, α-synuclein deposits are found in oligodendrocytes termed Papp-Lantos bodies or glial cytoplasmic inclusions [138, 139], and shows autonomic, cerebellar, and pyramidal impairments together with parkinsonism. Despite their vast heterogeneity, synucleinopathies share characteristic features and several overlapping aspects. By affecting the spreading of the disease, the aggregation of α-synuclein into different conformations, together with differences in the vulnerability of different populations of neurons toward α-synuclein aggregates, have been proposed as causative of the variety of clinical outcomes [140].

The spreading of α-synuclein inclusion is assumed to follow a caudo-rostral trajectory, although not straightforward, implying the neuron-to-neuron transfer of pathogenic α-synuclein [138]. This phenomenon was originally discovered when neuronal grafts were reported to develop Lewy pathology years after the surgical procedure [141-143]. The host-to-graft transmission was suggestive of a prion-like mechanism [144]. In this scenario, α-synuclein misfolded form is released by a neuron, either actively or after neuronal death, and uptaken by the neighbors [145]. The release appears to be exocytosis-mediated [146], whereas internalization follows the endocytic pathway [147]. The transfer on tunneling nanotubes, as well as passive diffusion due to α-synuclein interaction with the membrane were also proposed [148, 149]. α-synuclein spreading along axonal connections was demonstrated *in vivo* and *ex vivo* in various animal models. Fibrillar forms of α-synuclein were found to be transported anterogradely through the axon and taken up by the next neuron in mouse embryonic cultures [150], while *in vivo* studies conducted with rats showed the transneuronal spreading of fibrils from the olfactory bulb toward other non-olfactory regions [151]. Another study [152] reported the caudal to rostral pathway of spreading of α-synuclein aggregates injected in the MO of rats, supporting the spreading along interconnected regions. Lastly, PD pathology was suc-

cessfully passaged to non-human primates by administration of human PD-derived LBs. Animal models and neuropathological examinations allowed the identification of common routes in synucleiniopathies, such as the existence of a prodromal phase, but highlighted the differences as well, in terms of spreading route and selective neuronal vulnerability. Moreover, the original region developing α-synuclein pathology is still controversial [138]. The presence of different strains of α-synuclein, virtually owing different spreading properties and preferences toward neuronal subtypes, has been proposed as causative of the differences found among synucleinopathies.

1.2.4 α-synuclein strains

Akin to other proteins involved in PMDs, evidences from structural and kinetic studies converge in indicating the existence of strains as responsible of the heterogeneity observed in the clinical phenotype and pattern of lesions of α-synucleinopathies. As aforementioned, strains are defined by being different structural assemblies of the same starting protein. The shape influences the kinetics, in turn defining the route of spreading in other cells, which may possess different vulnerability towards the various strains. Being a natively unfolded protein [72], α-synuclein aggregation is ruled by thermodynamics [153], therefore the production of different strains depends either on physical and chemical conditions surrounding the site of the assembly or on variation in the primary aminoacidic sequence, which cause a slightly different folding of the protein (Fig.3). Outside of the influence of the temperature, critical roles in strain selection have been attributed to charged residues, salt concentration and surface water dynamics [155], all of which may affect the folding and aggregation of the NAC region, the core of the α-synuclein amyloid fibril [73].

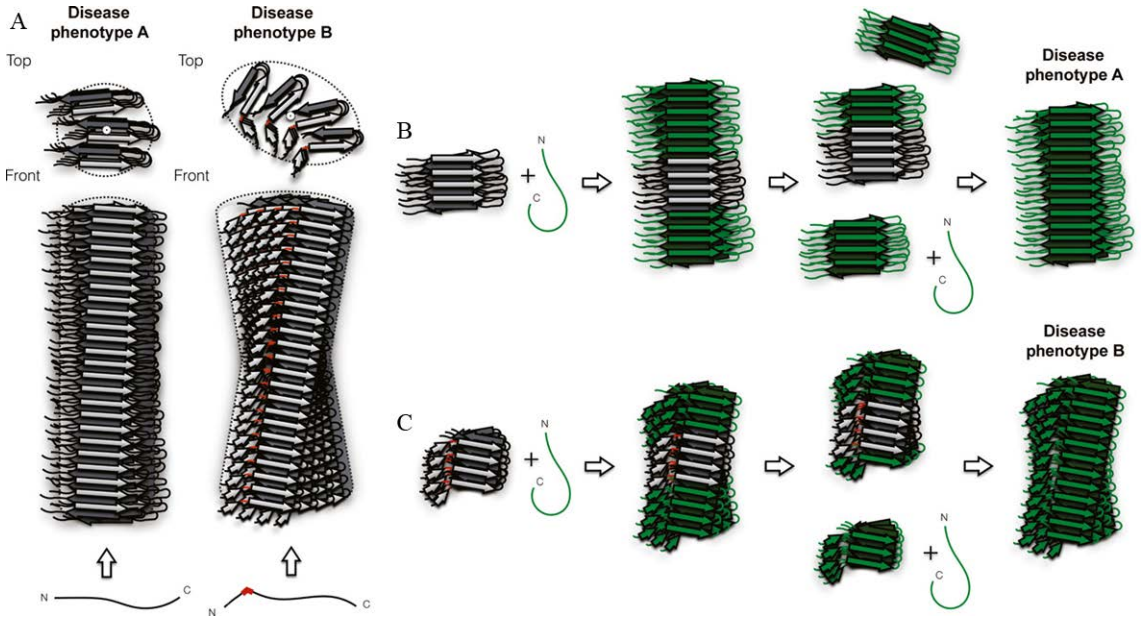

Figure 3. Strains selection

Illustrative example of strain selection. **A.** Small changes in the primary sequence, or in the physical and chemical conditions of the micro-environment of the reaction, may produce ribbon-like fibrils (Disease phenotype B), which differ from the classical cylindrical fibrils (Disease B). Upon breakage of the fibrils, different seeds are produced (**B, C**) which faithfully propagate their own conformation, resulting in strain variability [153].

The first event in the assembly of α-synuclein is believed to be dimerization [155], which initiates the production of aggregation-competent oligomers, which may encompass a wide variety of structures [156]. The structural conversion of the oligomers determines their toxicity and their ability to nucleate into longer fibrils [157]. The first evidence of the ability of α-synuclein aggregation to yield different strains was obtained by incubating monomeric α-synuclein into buffers at different salt concentration [158]. High salt (termed buffer A) resulted in assemblies formation within hours, whereas low salt buffer (buffer B) resulted in a longer lag phase before aggregation. However, aggregates from buffer A depolymerized when incubated at 4°C and re-polimerized upon eating at 37°C, whilst aggregates derived from incubation in buffer B were irreversible. Electron microscope analyses revealed differences in the structure of these aggregates, with assemblies from buffer A showing cylindrical aspect and those from buffer B being planar and often twisted. Due to their appearances, α-synuclein aggregates derived from buffer A were termed fibrils and those from buffer B ribbons. Fibrils and ribbons were shown to differ further for their PK banding profile, overall β-sheets content and ability to bind

thioflavin-T (ThT, a commonly used dye for detecting protein aggregates). Indeed, ribbons showed no binding to ThT, whereas fibrils did. From a structural point of view, the N-terminal structure of ribbons appears rigid and β-sheet enriched, whereas in fibrils is largely disordered [158]. Lastly, these two strains were further distinguished by their toxicity when administered to human neuroblastoma SH-SY5Y cell cultures, with fibrils causing more extensive cell deaths compared to ribbons. In a subsequent work [159], the same group reported that fibrils and ribbons bore pathogenic potential when injected in rats substantia nigra, although fibrils exhibited the highest toxic effect compared to ribbons or oligomers, indicating that strains can be further differentiated by their cytotoxic effects. A synthetic α-synuclein strain were reported to be produced upon serial sonication steps. Compared to *de novo* pre-formed fibrils (PFFs), sonication-generated aggregates displayed a lesser ability in seeding the aggregation of α-synuclein in neuronal cultures and in tau transgenic mice compared to PFFs, but a greater ability of seed tau aggregation [160]. Different conformations of α-synuclein fibrils were also observed between aggregates produced in presence or absence of lipopolysaccharide [161]. Evidences of α-synuclein strains derived from different synucleinopathies were discovered by injecting brain homogenates from MSA patients into hemizygous TgM83$^{+/-}$ mice [162]. This mouse line displayed the familial-PD associated mutation A53T but did not develop spontaneous Lewy pathology as the homozygous TgM83$^{+/+}$ did [163]. Researchers showed that, when intracerebrally inoculated with extracts from MSA brains, TgM83$^{+/-}$ rapidly developed signs of synucleinopathy and widespread deposition of Lewy bodies. On the other hand, α-synuclein fibrils extracted from TgM83$^{+/+}$ were not able to transmit the pathology when injected in TgM83$^{+/-}$ mice. In a follow-up study [164], the same group reported that, akin to the fibrils derived from TgM83$^{+/+}$ mice, brain homogenates from PD patients were not able to start the pathology when injected in hemizygous mice or in HEK cells with the same genetic background. These results indicated that different strains of α-synuclein underlie the differences observed in the clinical outcome of PD and MSA. Moreover, differences in the seeding activity between pathology-derived α-synuclein were found when injecting wild type mice with brain homogenates derived from DLB and MSA patients [165]. MSA-derived α-synuclein was found to strongly induce pathology in the recipient mice, whereas DLB-derived synuclein showed only rare appearance of Lewy bodies. Spreading of the two strains also differed. MSA synuclein was shown to spread efficiently in the entorhinal cortex, hip-

pocampus and the pyramidal layer of the piriform cortex, but affected mildly the motor cortex, which was more affected by PFFs and DLB-derived synuclein. Altogether, the evidences here reported favor the hypothesis that the differences observed among synucleinopathies may depend on the existence of different strains, each of them owing a unique structure, underlying different kinetics, responsible of the spreading of the disease and the selection of vulnerable cells. A grand number of methodologies have been developed to study the multi-faceted process of aggregation of prion-like proteins. The next chapter will present the techniques that allowed to investigate the formation and the architecture of the fibrils, their kinetic of aggregation, the strain variability of misfolded proteins and their potential application as diagnostic and drug-screening tools.

1.3 Methods in protein aggregation

1.3.1 Tinctorial properties of protein aggregates

The detection of amyloid fibrils was classically performed by means of direct dyes (such as Congo red, an industry-derived deep crimson dye, or methyl-violet) that displayed different tinctorial properties when bound to fibrils and non-fibrillar components. Although several other dyes were developed, their usage was often laborious and produced high background noise, resulting in poor reproducibility [166]. These hindrances were overcame by the discovery that the fluorescent probe ThT could bind to amyloid with high sensitivity and specificity, leading to an overall superior diagnosis of the presence of amyloids in a histological section [167]. Thioflavin-T is a benzothiazole molecule that shows a dramatic increase in fluorescent brightness when bound to amyloids, shifting its excitation maximum from 385 nm to 450 nm and its emission maximum from 445 nm to 482 nm [168, 169]. ThT has been shown to act as a molecular rotor, owing a benzylamine and a benzathiole rings freely rotating around their carbon-carbon bond, quenching the fluorescence emission of unbound ThT [170]. It has been proposed [166] that ThT recognizes β-sheet structures by inserting within channels formed by cross-strand ladders, a typical (but not exclusive [171-173]) architecture found in amyloid structures. The bound state causes the preservation of the excited state by locking the rotation, resulting in enhanced quantum yield. Outside of ThT, a variety of other extrinsic fluorescent dyes have been implemented, each with its own specific binding to structural features of amyloids [174]. 4-(dicyanovinyl)-julolidine (DCVJ) is

another molecular rotor which was described to bind with high affinity to early oligomers [175]; 1-anilinonapthalene-8-sulfonate (ANS) and its dimeric form (bis-ANS) exert their function by recognizing hydrophobic surfaces. Intrinsic fluorescence has also been deployed for the unbiased detection of amyloids, as it represents a label-free, quantitative parameter for the aggregation process [176]. Regardless the heterogeneity of the polypeptide chains forming aggregates, intrinsic fluorescence gave similar results in the lifetime and spectral signatures, as in the case of amyloid β, α-synuclein and tau fibrils [176]. The presence of aromatic residues (i.e., Triptophan and Tyrosine) also accounts for the intrinsic fluorescence displayed by protein aggregates [174]. Although these residues are normally buried within hydrophobic pockets in the core of the protein, upon the reorganization of the three-dimensional structure that occurs during misfolding and aggregation, they can alter their quantum yield of fluorescence, thus allowing the detection of the aggregation process.

1.3.2 Study of the architecture of protein aggregates

Whereas intrinsic fluorescence and the usage of extrinsic dyes have allowed the detection of aggregates in histological slides, they offer limited information on the structural features that characterizes the various types of protein aggregates. The study of the secondary structure have been historically carried out by spectroscopical analyses that take advantage of the optical properties of polypeptides such as circular dichroism [177]. Under a circularly polarized light, α-helices and β-sheets show a markedly different and characteristic spectral profile. Secondary structures have been also detected by Fourier-transformed infrared spectroscopy, which relies on infra-red absorption and emission spectra [178], and by Raman spectroscopy (and its surface-enhanced and tip-enhanced evolution [179, 180]). β-sheet structures typically result in a prominent band peaked at 1650 nm^{-1} termed Amide I, dependent on the C=O stretching vibration of the peptide backbone, which differs between β-sheets and α-helices. Beyond the study of the secondary structure, a various techniques have been developed to delve into the structure of protein aggregates at atomic resolution [181]. The precise arrangement of the residues that forms the cross-β ladder of amyloids have been dissected by means of solid state nuclear magnetic resonance, electron and cryo-electron micoscopy (EM and cryo-EM respectively), X-ray micro-crystallography and atomic force microscopy

(AFM). AFM provides a three-dimentional topographic map of a sample casted on a flat surface such as mica sheets. The scanning is performed byA tip with a radius in the nanometer range mounted on a cantilever, which oscillates until it touches the sample (contact mode) or within its resonance frequence (non-contact or tapping mode) [182]. These techniques allow the study of the morphology and aggregates at atomic level, providing details on the geometry of the assembly, the residues engaged and the differences among the various fibrillar species. By using these techniques, structural models various amyloids have been produced [182]. Although structural studies proved to be useful both in the diagnosis and in the characterization of pathology-related aggregates, the most crucial aspect of protein aggregation is the kinetic, which provides informations about the pace of production of amyloids, the intermediate species that are formed before the deposition of fibrillar structures and may discriminate among different strains.

1.3.3 Protein misfolding assays and The Real-Time Quaking-Induced conversion (RT-QuIC)

The emergence of the importance of the self-assembly properties in the onset of neurodegenerative diseases have lead the scientific community to investigate not just the structure of amyloid, but also the kinetic of the aggregation. Indeed, the normally slow aggregation process that takes place during the onset of the pathology can be mimicked *in vitro* and, under appropriate conditions, may occur several degree faster than under biological conditions. Outside of physical and chemical factors that accelerate the *in vitro* fibrillization process, the addition of an aggregation-prone molecule that act as a nucleus for the fibrillization, defined as seed, has helped to reduce the lag phase of the reaction, thus avoiding the possible denaturation of the monomers during the course of the process [174; 183]. The growth of the fibrils follows a sigmoidal curve, displaying a lag phase during which the nucleation process takes place, followed by an exponential phase that indicates the formation and the elongation of the fibrils. Once all the monomers have been converted into β-sheet enriched species, a plateau phase is observed, as shown in Figure 4.

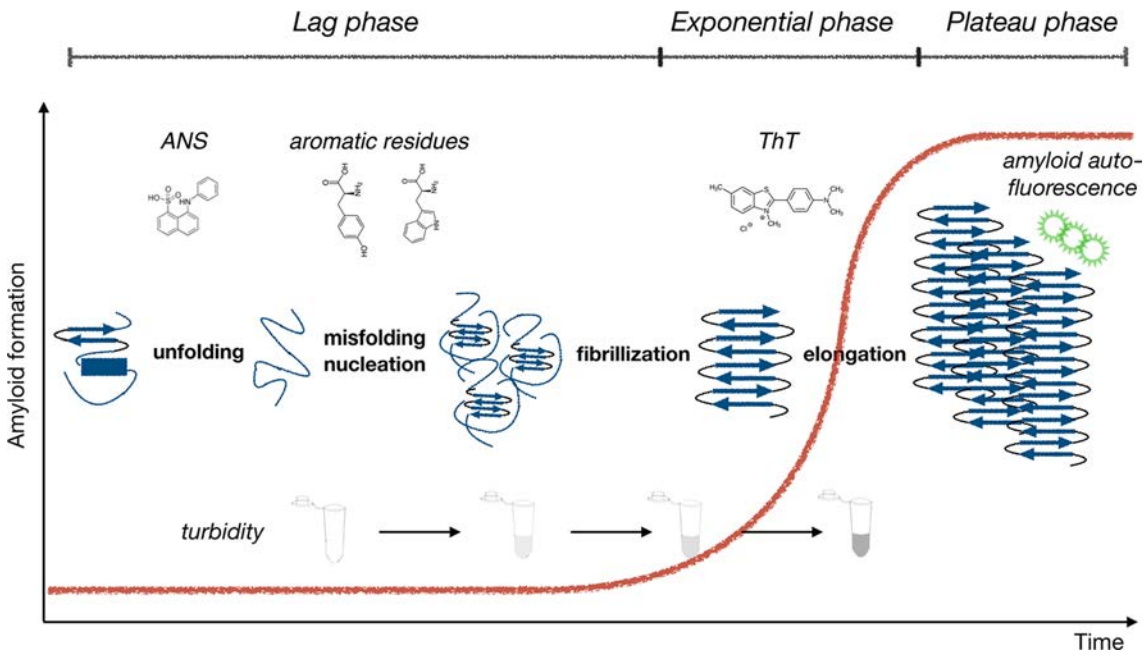

Figure 4. Kinetic of protein aggregation

Illustrative scheme showing the course of the aggregation and the various reporter system to follow it. During the lag phase, the protein undergoes the unfolding and the nucleation into an aggregation-competent structure. These steps can either be monitored by the intrinsic fluorescence of aromatic residues or by ANS. The vial in this phase appear as a clear liquid. During the exponential phase, fibrillization takes place, resulting in the elongation of the fibers. This step is recognized by ThT and the sample appears progressively more turbid. In the last phase, a plateau is observed, indicating that the fibril has incorporated all the available monomers. Auto-fluorescence may be detected. The vial results cloudy and turbid [174].

The usefulness of seeding assays, especially for the diagnosis of prion diseases, have prompted the research of faster and more reliable techniques to track the aggregation process. In this frame, a fundamental innovation was the development of the protein misfolding cyclic amplification (PMCA) [184]. The original study aimed to reproduce the replication and the conversion of the prion protein *in vitro*, starting from minute amounts of the misfolded form of the prion protein, which acted as a seed. Brain homogenates from scrapie infected hamsters were used as seed to trigger the aggregation of PrP^C found in healthy brain homogenates in a cyclic reaction. The PMCA reaction consisted in cycles of incubation, during which the seed is supposed to contact and convert its native counterpart and to form growing oligomers, followed by pulses of sonication that would break longer fibrils, increasing the number of seeding-competent species that would further the reaction. The detection of the end-products of the reaction was carried by Western blot after PK digestion. The technique was further improved by making it automated [185-187] and therefore suitable for high throughput, and by the usage of

biological fluids, such as blood, urine or the cerebrospinal fluid (CSF) as source of the seed, thus allowing PMCA to be applicable in diagnosis [188, 189]. Furthermore, PMCA was applied for the detection of prion contamination in surgical or biological materials. In recent years, PMCA was applied for the amplification of other neurodegenerative-related molecules using the CSF as source of the seed, as in the case of α-synuclein [190] and the amyloid-β peptide [191], providing a useful diagnostic tool for PD and AD, respectively. To overcome the inherent complications of the PMCA, (poor reproducibility, lack of consistency with different prion strains, the need of PK digestion and Western blot and infectivity of the end-product of the reaction [192]), other *in vitro*, cell-free assays have been developed starting from the original PMCA. A major advancement was the substitution of sonication, which was reported to be difficult to control, with shaking [193, 194], which produced the same output in a more controllable environment and, strikingly, resulted in a non-infectious end-products. Moreover, shaking is thought to cause the unfolding of prion protein by increasing the air-water interface, enhance the fragmentation of polymers and to favor the interaction between the seed and the substrate [195]. This novel assay, termed quaking induced conversion (QUIC), was further refined by the addition of ThT, allowing to monitor in real time the aggregation process. These advancements lead to the development of the real-time quaking induced conversion (RT-QuIC) [196, 197], a fully automated technique that was originally reported to be able to detect the seeding activity of various prion strains with 80% of sensitivity and 100% specificity using as seed either brain homogenates or CSF, underlying the possibility that RT-QuIC might be useful for diagnostic purposes. By adjusting the physical and chemical environment of the RT-QuIC reaction [198, 199], the RT-QuIC was further tuned for the detection of different prion strains [200, 201] and for the detection of the seeding activity from other biological fluids, such as blood [202], urine [203], skin [204] and nasal brushings [205], representing a less invasive source of the proteopathic seed. Besides the diagnostic potential, the RT-QuIC showed to be a promising technique as a pre-screening assay for therapeutic molecules [201]. Indeed, two studies [206, 207] reported the inhibition of the signal of the RT-QuIC by using compounds with known anti-prion activity, such as doxycycline. Lastly, similar to the PMCA, RT-QuIC was successfully applied for the detection of the seeding activity from other neurodegenerative diseases. Tau seeding activity was detected in brain homogenates and in the CSF of patients affected by Pick's disease [208], a tauopathy dependent

on the aggregation of the shortest tau isoform (0N3R). Recently, multiple reports [209-211] indicated that RT-QuIC is a suitable technique for the amplification of minute amounts of misfolded α-synuclein derived either from brain homogenates or CSF, although it failed in discriminating among synucleinopathies.

2. Aim of the project

Strain typing have been proposed to underlie the different course of similar diseases, explaining the differential vulnerability of various brain region toward conformers of the same protein. In this frame, the present work aims to take advantage of the RT-QuIC to exploit these differences by the detection of the seeding activity of brain homogenates (BH) derived from PD, DLB and non-neurodegenerative controls (Ctrl) cases in frontal cortex (FCx) and in the substantia nigra pars compacta (SNc), as these areas are differentially affected in the two diseases. The workflow is divided into three sections:

I. Establish the RT-QuIC for the detection and amplification of misfolded species of α-synuclein. To this aim, seeding-competent α-synuclein in the BH of PD and DLB patients will be isolated from factors that may interfere with the aggregation process. Kinetic parameters from the RT-QuIC will be used to exploit the putative differences between strains of α-synuclein.

II. The validation of the RT-QuIC products will be performed by means of biochemical analyses to determine whether the observed results are actually due to the amplification of α-synuclein seeds, since the RT-QuIC offers no indication of the species that cause the increase in the quantum yield of ThT. The RT-QuIC products will be compared to their counterpart before the RT-QuIC, indicating the reactions that did not undergo the RT-QuIC process.

III. Structural characterization of α-synuclein aggregates will be conducted to delve into the structural features of the aggregates. The secondary structure of the product of the reaction seeded with PD, DLB and Ctrl derived material will be investigated through Raman spectroscopy and compared among different brain regions and with their BQ counterparts. Likewise, the structural features will be elucidated by means of EM and AFM.

3. Methods

Consumables, antibodies and instrumentations used for this study are listed in table 1. Units of measurements follow the international system of units.

List of materials

	Abbreviation	Company
Instrumentation		
TissueLyser LT		Qiagen, USA
Meso Scale Discovery Sector Imager	MSD	MSD, USA
Amicon Ultra centrifugal 100 kDa filter		Merck-Millipore, IRL
Sealing tape		Thermo-Fisher Scientific, USA
black 96-well plate with bottom optic		Thermo-Fisher, USA
FLUOStar Omega fluorescent reader		BMG Labtech, USA
Trans-Blot Turbo transfer system		Bio-Rad, USA
ChemiDoc XRS+		Bio-Rad, USA
Perkin Elmer Wallac 1420 Victor microplate reader		GMI, USA
ProteOn XPR36 Protein Interaction Array system		Bio-Rad, USA
micro-Horiba Xplora		Horiba, IT
Gold mirror support		Thorlabs, UK
Formvar-coated copper EM-grid		Agar scientific, UK
LEO EM912 Omega electron microscope		Zeiss, DE
on-axis 2048x2048-CCD camera		TRS, DE
Consumables		
Phosphate buffered saline	PBS	Merck-Millipore, IRL
Protease Inhibitor		Roche Diagnostic GmbH, DE

List of materials

Phosphatase Inhibitor		Roche Diagnostic GmbH, DE
Stainless steel beads		Qiagen, USA
Sodium dodecyl sulfate	SDS	Sigma-Aldrich, USA
Tween		Sigma-Aldrich, USA
Bovine Serum Albumin	BSA	Roth GmbH, DE
Sodium chloride	NaCl	Sigma-Aldrich, USA
Sodium phosphate monobasic		Sigma-Aldrich, USA
Sodium phosphate dibasic		Sigma-Aldrich, USA
Ethylenediaminotetraedric acid	EDTA	Sigma-Aldrich, USA
Thioflavin-T	ThT	Sigma-Aldrich, USA
α-synuclein		rPeptide, USA
Proteinase K	PK	Sigma-Aldrich, USA
Loading Buffer		Roth GmbH, DE
Acrylamide		Roth GmbH, DE
Polyvinyldiene fluoride membrane	PVDF	Healthcare Life Sciences, DE
Methanol		Merk, DE
Tris		Roth GmbH, DE
Glycine		Roth GmbH, DE
Tris-HCl		Roth GmbH, DE
Dry milk		Roth GmbH, DE
glutaraldehyde		Science Services, DE
uranylacetate		Merck, DE
Antibodies		
MJFR1		AbCam, USA
SULFO-TAG labelled antibody Syn1		BD Biosciences, USA
secondary antibody HRP-conjugated goat anti-rabbit IgG antibody		Dianova GmbH, DE

List of materials

anti synuclein phospho S129 antibody		AbCam, USA
oligomeric synuclein-specific antibody		ADx, BE
Syn F-1		Biolegend, UK

Table 1. List of materials. Instrumentations, antibodies and consumables used for this work are listed.

3.1 *Patients*

DLB, PD and Ctrl FCx were obtained at autopsy from 10 patients per group. SNc was obtained from 8 DLB and 6 PD patients. Clinical features are listed in table 1.

Procedures for brain tissue extraction, processing and neuropathological classification had been published before [212, 213] Postmortem brain tissue was obtained from donors through a rapid neuropathological autopsy (mean postmortem interval = 5.5 hours). After brain removal, two symmetric brain halves were obtained through a mid-sagittal incision and the right hemibrain was flash-frozen by immersion in -60 ºC isopentane. The left hemibrain was fixed in 4% buffered formaldehyde for 3 weeks and processed for standard neuropathological examination. Assessment of Alzheimer's type pathology and commonly associated conditions, including Lewy type pathology, was performed according to current recommendations by the National Institute of Aging – Alzheimer's Association. Lewy type pathology was assessed according to following procedures and classifications.

ID	SEX	AGE AT DEATH	MAIN NEUROPATH. DIAGN.	COMBINED NEUROPATH. DIAGNOSES	BRAAK stage TAU	BRAAK stage α-syn	AGE OF ONSET *	TIME OF SURVIVAL *	DEMENTIA (YES/NO)
BCPA 667	M	80	PARKINSON'S	No	1	5			**NO**
BCPA 581	M	79	PARKINSON'S	No	3	4			**NO**
BCPA 572	F	79	PARKINSON'S	VASCULAR	2	5			**NO**
BCPA 396	M	65	PARKINSON'S	No	1	6			**NO**
BCPA 142	M	84	PARKINSON'S	No	1	4			**NO**

BCPA 060	**M**	**77**	**PARKINSON'S**	No	**2**	**6**	**67**	**10**	**YES**
BCPA 636	M	75	PARKINSON'S	ALZHEIMER, VASCULAR	5	6			**NO**
BCPA 500	F	76	PARKINSON'S	ALZHEIMER, VASCULAR	4	6			**YES**
BCPA 385	M	82	PARKINSON'S	VASCULAR	1	6	**74**	**8**	**YES**
BCPA 167	F	90	PARKINSON'S	VASCULAR	3	6	**75**	**15**	**YES**
BCPA 517	F	73	LEWY BODY DEMENTIA	ALZHEIMER	3	6	**68**	**5**	**YES**
BCPA 436	M	80	LEWY BODY DEMENTIA	No	3	6			**YES**
BCPA 348	F	71	LEWY BODY DEMENTIA	ALZHEIMER	3	6			**YES**
BCPA 283	M	77	LEWY BODY DEMENTIA	ALZHEIMER	3	6			**YES**
BCPA 258	F	88	LEWY BODY DEMENTIA	ALZHEIMER, HIPPOCAMP. SCLEROSIS	4	6	**83**	**5**	**YES**
BCPA 178	F	69	LEWY BODY DEMENTIA	ALZHEIMER, NORMAL PRESSURE HIDROCELPAH Y	3	6	**65**	**4**	**YES**
BCPA 174	M	75	LEWY BODY DEMENTIA	No	0	5			**YES**
BCPA 129	M	77	LEWY BODY DEMENTIA	No	2	5	**72**	**5**	**YES**
BCPA 121	M	70	LEWY BODY DEMENTIA	No	2	5	**64**	**6**	**YES**
BCPA 047	F	92	LEWY BODY DEMENTIA	ALZHEIMER	4	6	**90**	**2**	**YES**

Table 2. Clinical features. The table recapitulates the clinical features of the patients from which FCx samples were obtained (n = 10 for both DLB and PD). Sex, age of death, main neuropathological diagnosis, dementia features and co-pathologies are listed. Moreover, Braak stages of Lewy pathology and tau burden are shown. * Informations about age of onset and time of survival were not available for all the samples. When possible, they were included.

3.2 Isolation of α-synuclein seeding competent fraction

Brain tissues derived from FCx or SNc were homogenized with TissueLyser LT (Qiagen, USA) using 5 mm stainless steel beads (Qiagen, USA) at 10% weight/volume (w/V) in ice-cold Phosphate buffered saline (PBS, Merk-Millipore, IRL) at pH 7.0 with

protease and phosphatase inhibitors (Roche Diagnostic GmbH, DE). Samples were centrifuged at 850 x g for 10 minutes (min) at 4°C. The pellet was resuspended in 1 mL of PBS 7,0 and stored at -80 °C for further analysis. The supernatants were centrifuged at 5200 rpm (rounds per minute, equal to 2872 x g) for 10 min at 4°C and the soluble fraction was stored at -80 °C. The pellet was re-suspended in PBS containing 2% Sodium dodecyl sulfate (SDS, Sigma-Aldrich, USA), pH 7.0 and centrifuged for 20 min at 14000 x g, 4°C, using Amicon Ultra centrifugal 100 kDa filters (Merck-Millipore, IRL). In parallel, the re-suspended pellet was centrifuged at 14000 x g for 10 min at 4°C to analyse the SDS soluble and insoluble fractions. The fraction lower than 100 kDa was collected and subjected to RT-QuIC analysis. All the remaining fractions were tested as well to check their seeding activity. Only freshly prepared samples were used for the analysis.

3.3 Total α-synuclein ELISA

Detection of total α-synuclein in the fraction lower than 100 kDa was performed using electrochemiluminescence based detection system as previously described [214]. 3 µg/ml of MJFR1 (AbCam, USA) in PBS were used as capture antibody. After washings in PBST, containing 0.005% Tween (Sigma-Aldrich, USA), and blocking in 1%of bovine serum albumin (BSA, Roth GmbH, DE) in PBST for 1 h at room temperature with shaking at 300 rpm, 25 µl of five sample in duplicate, diluted 1:50 in 1% BSA in PBST were applied to the assay plate for 1 h, with shaking set at 700 rpm at room temperature. SULFO-TAG labelled antibody Syn1 (BD Biosciences, USA) diluted 1:1 in 1% BSA in PBST was used as detection antibodies. Measurements were obtained with a Meso Scale Discovery Sector Imager (MSD, USA) and light signal was detected at 620 nm.

3.4 Real Time-Quaking Induced Conversion

A recently published protocol [197] was modified for the detection of α-synuclein. 3 µl of the working fractions were added in 97 µl of converting buffer, containing 32 % of 5x PBS (0.64 M Sodium Chloride (NaCl, Sigma-Aldrich, USA), 57,5 mM sodium phosphate monobasic (Sigma-Aldrich, USA), 94,4 mM sodium phosphate dibasic (Sigma-Aldrich, USA), pH 8,4), 1 mM Ethylenediaminotetraedric acid (EDTA, Sigma-

Aldrich, USA), 170 mM NaCl, 10 µM ThT (Sigma Aldrich, USA) and 140 ng/µl of α-synuclein (rPeptide, USA).

Only freshly thawn α-synuclein was used as substrate. Reactions were prepared in a black 96-well plate with bottom optic covered with sealing tape (Thermo-Fisher Scientific, USA) and incubated at 37 °C using a FLUOStar Omega fluorescent reader (BMG Labtech, USA), with 60 seconds (s) of double orbital shaking at 600 rpm followed by 29 min break, after which fluorescent measurement (excitation 450 nm, emission 480 nm) were taken. The reaction was run for 120 cycles, corresponding to 60 hours (h). Each sample was run in triplicates and considered positive when at least two out of three replicates gave a positive seeding response (signal increase >50%). Reactions without seed or without substrate were run to evaluate self-aggregation of both species.

3.5 Proteinase K digestion and Western blotting

RT-QuIC products (labelled AQ, as in After RT-QuIC) and their counterpart (labelled as BQ, Before RT-QuIC, indicating the reaction that did not undergo the RT-QuIC process) were treated with 5 µg/mL of proteinase K (PK) (Sigma-Aldrich, USA) and incubated for 60 min at 37°C. PK was deactivated by a 30 min incubation step at 65°C.

Probes were analyzed by Western blotting. Briefly, the PK-digested products were mixed 1:1 with loading buffer (Roth GmbH, DE), boiled for 5 min at 95°C and deactivated by 10 min incubation in ice. The samples were next loaded into a 15% Acrylamide (Roth GmbH, DE) gel and run at 80-100 V for 2-3 hours. After the gel electrophoresis, proteins were transferred into a methanol activated Polyvinyldiene fluoride membrane (PVDF, GE Healthcare Life Science, DE) in a transfer buffer containing 20% methanol (Merk, DE), 48 mM Tris (Roth GmbH, DE), 39 mM Glycine (Roth GmbH, DE), 0.375% SDS using the Trans-Blot Turbo transfer system (Bio-Rad, USA) for 1h at 18 V. The membranes were blocked with 5% non-fat dry milk (Roth GmbH, DE) in Tris buffered saline plus Tween (TBST, containing 10mM Tris-HCl (Roth GmbH, DE), pH 7.8, 100 mM NaCl, 0.1% Tween-20) for 1 h at room temperature and incubated with the primary antibody anti-total α-synuclein MJFR1 (Abcam, USA) diluted either 1:1000 or 1:5000 in 2,5% non-fat dry milk in TBST. Dilution 1:5000 was used for the PK digested samples, while dilution 1:1000 was used for the detection of the total amount of α-synuclein in the fraction lower than 100 kDa, which were run in a 12% acrylamide gel. The secondary antibody HRP-conjugated goat anti-rabbit IgG antibody (Dianova GmbH,

DE) was diluted 1:1000 in 2.5% non-fat dry milk in TBST. Detection was carried with the molecular imager ChemiDoc XRS+ (Bio-Rad, USA) using enhanced chemiluminescence.

3.6 Oligomeric α-synuclein ELISA

Detection of oligomeric α-synuclein was performed on the RT-QuIC products by using an oligomeric synuclein-specific assay and following manufacturer's instruction (ADx, BE). Briefly, the wells were coated with 20 µl of biotin solution and incubated with 80 µl of either BQ or AQ reactions over night at 4°C. Each sample was run in duplicate. After five washings, 100 µl of peroxidase labeled streptavidin were applied in each well and incubated for 30 min at room temperature. After five washings, 100 µl of chromogen solution were added and incubated at room temperature for 30 min in the dark. Absorbance at 450 nm was taken shortly after adding 100 µl of stop solution using a Perkin Elmer Wallac 1420 Victor microplate reader (GMI, USA).

3.7 Dot Blot

For the analysis of the fractions, 5 µL of n=3 patients per group had been spotted onto a nitrocellulose membrane. Membranes were incubated over night at 4°C with MJFR1 antibody (raised against total α-synuclein), phospho-S129 antibody (both Abcam, USA) and with SynF-1 antibody (Biolegend, UK) (raised against fibrillary α-synuclein). All antibodies were applied in a dilution of 1:1000.

For the RT-QuIC products, nitrocellulose membrane was spotted with 3 µl of AQ RT-QuIC products and BQ reactions and blocked in 5% dry milk in TBST. Membranes were incubated over night at 4°C with MJFR1 antibody 1:5000 against total α-synuclein or with SynF-1 (Biolegend, UK) diluted 1:1000 against aggregated, fibrillar α-synuclein. The day after, the membranes were washed in TBST and incubated 1h at room temperature with the appropriate HRP-conjugated secondary antibody and developed with the molecular imager ChemiDoc XRS+ (Bio-Rad, USA) using enhanced chemiluminescence.

3.8 Surface-Plasmon Resonance

Interaction studies were performed by using the ProteOn XPR36 Protein Interaction Array system (Bio-Rad, USA). Recombinant protein was immobilized according to manufacturer's protocols on a GLH sensor chip by amino-coupling with a final immobilization level of ~12500 RU. Analytes were diluted in PBST as running buffer. Samples were injected with a flow rate of 50µl/min for 2 min. For referencing a ligand surface without any bound protein was used. Data correction was done by subtracting the blank chip surface from the protein bound surface to remove contribution of unspecific compounds on the chip surface. For obtaining the corresponding association and dissociation rate constants the 1:1 interaction model (ProteOn analysis software) was used for fitting the sensorgrams.

3.9 Raman spectroscopy

Raman spectra of drop-casted sample solutions were recorded using a micro-Horiba Xplora (Horiba, IT) coupled to a 785 nm wavelength laser with a 1200 grooves/mm grating. The backscattered light was collected by a 100× microscope objective with 0.9 NA, which generates a 1 µm laser beam waist and a laser power at the sample of 40 mW. The acquisition time of each spectrum was 20 s with 10 accumulations. The samples for Raman analysis were prepared by repeating the standard RT-QuIC protocol without the addition of ThT in order to avoid any signal interference [158]. A 5 µl drop from either AQ RT-QuIC products or BQ reactions was deposited onto a gold mirror support (Thorlabs, UK), followed by air drying for 20 minutes and acquisition of Raman spectra from the outer ring of the dried drop. A schematic workflow of the procedure is illustrated in figure 5.

Specifically, Raman acquisitions from the central region of the ring showing the maximum signal intensity were considered for the analysis. Five measurements per sample from n = 3 patients per type (DLB, PD, Ctrl) were collected and averaged. The spectra were baseline corrected. A multi-peak Lorentzian fit was performed over the 1580 – 1705 cm^{-1} amide I region of the Raman spectrum. The fitting procedure provides a semiquantitative estimate of the secondary structure composition. Specifically, amide I band results from the convolution of structures centered at: 1635 cm^{1} disordered struc-

tures, 1655 cm^{1} α-helices, 1670 cm^{1} organized β-sheets, 1687 cm^{-1} loose *β*-strands / *β*-turns, [215]. The integrated area value of each fit component was collected and the component band peaked at 1670 cm^{-1} mainly ascribed to the β-sheet content of cross-β peptide assemblies [30].

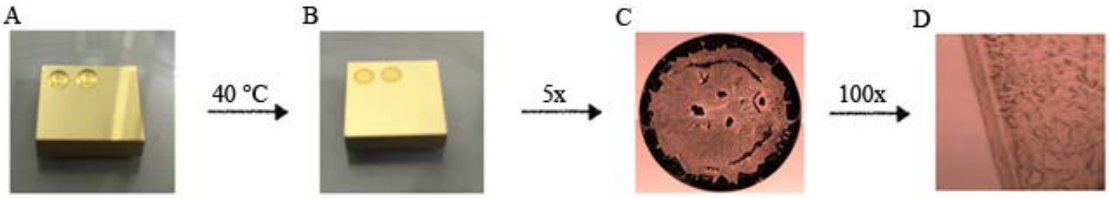

Figure 5. Schematic workflow for Raman spectroscopy.
A. A drop of 5 µl of sample was casted onto a gold mirror and let dry for 20 minutes at 40 °C. **B.** The drying procedure of the drop caused the drifting of the proteins towards the edge of the drop, producing a typical “"coffee-ring"” structure. **C**. At 4x magnification, crystal structures, most probably sedimented salts, are visible at the center of the drop. **D.** The thin annular structure of the drifted proteins is clearly visible at 100x magnification.

3.10 Transmission Electron Microscopy

BQ and AQ RT-QuIC products were analyzed by negative staining under a transmission electron microscope (TEM). A Formvar-coated copper EM-grid (Agar scientific, UK) was floated on 10 µl of sample solution to which 10 µl of 0.25% glutaraldehyde (Science Services, DE) were added. After 1 min the grid was briefly washed on 3 droplets of water and then incubated with 2% uranylacetate (Merck, DE) in water for 30-60 s. The grid was removed from the droplet und excess fluid was blotted by touching the grid vertically with a piece of filter paper. After drying the negative stained samples were imaged at using a LEO EM912 Omega electron microscope (Zeiss, DE). Digital micrographs were obtained with an on-axis 2048x2048-CCD camera (TRS, DE).

3.11 AFM analysis

The morphology of the samples was inspected by tapping mode AFM. An aliquot of sample solution (10 µl) was dried on top of freshly cleaved mica substrates at room temperature for 20 min followed by rinsing in MQ water to remove salts and debris and drying under a gentle nitrogen steam. The samples were immediately imaged using a JPK NanoWizard III Sense scanning probe microscope operated in AFM mode (maximum scan size 15 µm). Single beam uncoated silicon cantilevers (µMash HQ:NSC15

Cr-Au BS) were used. The drive frequency was between 250 and 300 kHz and the scan rate was 0.5 Hz.

3.12 Statistical analysis

The area under the curve (AUC) was extracted from each RT-QuIC run and normality was established by Kolmogorov-Smirnov test with Dallal-Wilkinson-Lillefor P value. Once validated that samples were normally distributed, data were analyzed by one-way ANOVA with multiple comparisons followed by Brown-Forsythe test. The normality test was conducted for densitometry values, obtained with the software ImageJ 1.47v, derived from Dot blot, Western blot, ELISA and Raman spectroscopy. Likewise, one-way ANOVA with multiple comparisons, as performed for the RT-QuIC, was also done for these experiments. All the analyses were performed using GraphPad Prism 7.

3.13 Ethical issues

All brain tissue samples from Banco de Tejidos CIEN (BT-CIEN) were obtained from brain donors of the biobank in compliance with Spanish national regulation for the use of human biological samples for research. Accordingly, all tissue donations were received under informed consent by the donor or, for donors unable to give consent, by the legal guardian or the next of kin, either ante mortem or post mortem, following the procedure established by the external research ethical committee of the biobank (Research Ethics and Animal Welfare Committee, Instituto de Salud Carlos III, Ministry of Health). The BT-CIEN biobank is registered at the National Registry of Biobanks (Reg. No. 741) and is a member of the National Network of Biobanks.

4. Results

4.1. Validation of the Lewy pathology and α-synuclein aggregation by RT-QuIC

In the first set of experiments, we confirmed the presence of Lewy pathology in the FCx and SNc of our cohort of sample. Next, we developed a fractionation protocol aimed to enrich the misfolded α-synuclein and to remove factors that may influence the aggregation process. The presence of α-synuclein was biochemically validated, while the seeding activity of each of the produced fraction was determined by RT-QuIC. Next, we tested whether these fractions could amplify recombinant α-synuclein during the RT-QuIC. We determined whether self-aggregation may bias our analysis. Since α-synuclein aggregates in PD are mainly found in subcortical region [145], the seed for the reaction was taken from FCx and SNc, as the latter is a critical region for the development and the progression of PD [104, 125-127]. Furthermore, sensitivity and specificity for the RT-QuIC analysis were assessed, defined as the occurrence of false negative and false positive results, respectively.

4.1.1 Histochemical profile of the Lewy pathology do not differ between DLB and PD

Immunohistochemistry (IHC) was conducted on paraffin-embedded sections from FCx (Fig. 6A) and SNc (Fig. 6B) of DLB and PD cases. No significant differences were observed in the occurrence or distribution of the Lewy pathology among PD and DLB cases in both the brain regions examined, independent of the presence of co-pathology..

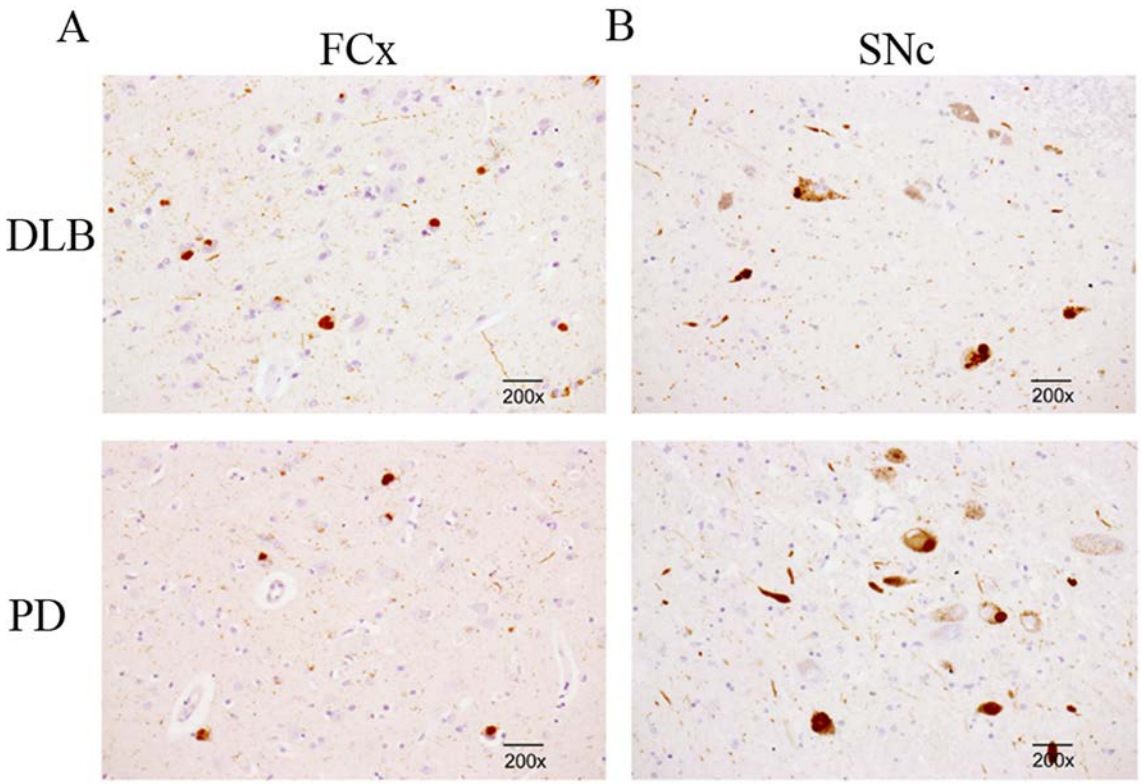

Figure 6. Paraffin embedded histological sections of FCx and SNc of DLB and PD samples. Neither the amount, nor the distribution of Lewy bodies in either region shows a significant difference between the two pathologies both in FCx (A) and SNc (B). Scalebar is set at 200 µm.

4.1.2 Enrichment of the α-synuclein-containing fraction

Due to the high structural variability of α-synuclein, various biological components in the brain homogenates may alter the aggregation process. Therefore, we developed a serial centrifugation protocol aimed to exclude the factors that may bias the RT-QuIC response. A schematic overview of the protocol is showed in Figure 7. A 10% w/V BH was produced from both FCx and SNc and subsequently spun to remove the nuclear fractions. The soluble part was centrifuged to let aggregates and other heavy molecules deposit. This fraction was next re-suspended in 2% SDS in PBS (pH 7,0) and further centrifuged by applying a 100 kDa filter to separate the components according to their molecular weight and their solubility in SDS. 3 µl of each of the produced fractions from three different samples was tested in duplicates for their ability to seed the aggregation of recombinant α-synuclein in the RT-QuIC (Figure 7A). Each soluble and insoluble DLB and PD derived fractions were tested in triplicates by dot blot for the presence of total, phosphorylated and aggregated α-synuclein, showing no significant differences between DLB and PD patients (Figure 7B).

All fractions showed no seeding activity, with the exception of the indiscriminate signal derived from the fraction upper than 100 kDa. Larger α-synuclein aggregates, most probably generated by self-aggregation of the substrate, caused an unspecific seeding reaction. Likewise control derived fractions (data not shown) showed a false positive RT-QuIC signal response supporting this assumption. Therefore, we excluded **these** fractions from the analysis and proceeded with the fraction lower than 100 kDa, referred from hereon as α-synuclein seeding-competent fraction (α-syn-SCF).

This result indicates that the seeding-competent α-synuclein can be separated from other molecules that can interfere with the aggregation process during the RT-QuIC, either by inhibiting or by promoting the conversion.

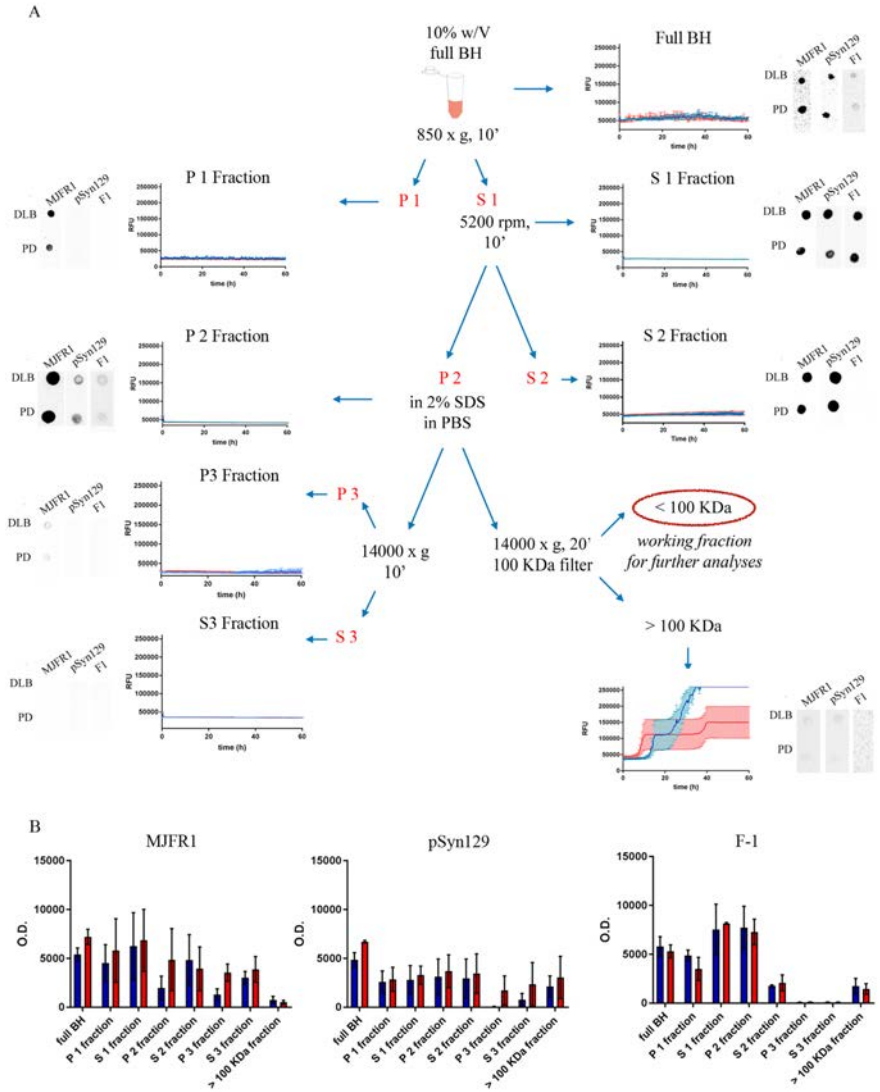

Figure 7. Seeding activity of α-synuclein in different isolated fractions. A. Schematic representation of the protocol developed to enrich the fraction containing seeding-competent α-synuclein. Seeding activity from FCx from DLB (blue) and PD (red) fractions was assayed from each fraction by RT-QuIC (n = 3 for

each group, in duplicates). No seeding activity could be detected in each of the isolated fractions, except for the fraction upper than 100 kDa, which shows seeding activity from each group, indicating a possible self-aggregation of the samples. For all fractions, dot blot were conducted for the detection of total α-synuclein (MJFR1), phosphorylated α-synuclein (pSyn129) and fibrillar α-synuclein (F-1). The final fraction, lower than 100 kDa (encircled in red) represents the oligomeric α-synuclein containing fraction, defined as α-synuclein-seeding-competent fraction (α-syn-SCF). B. Statistical analysis conducted on the Dot blot after densitometry shows no significan differences for all α-synuclein forms in each fraction.

4.1.3 The α-syn-SCFs contain equal level of α-synuclein among groups

In order to rule out self-aggregation of α-synuclein by concentration effects, we performed Western blot analyses of the α-syn-SCFs derived from five samples from FCx and SNc of PD, DLB and Ctrl cases (Figure 8A, B). MJFR1 antibody detected single band of an apparent molecular weight of approximately 18 kDa, coherent with the molecular weight of α-synuclein, in each condition tested. The densitometric analysis (Figure 8C, D) indicated that equal amounts of α-synuclein are found within the same brain region. Overall, the amount of α-synuclein appeared to be lower in the SNc compared to FCx, in line with the higher total amount of proteins in the latter.

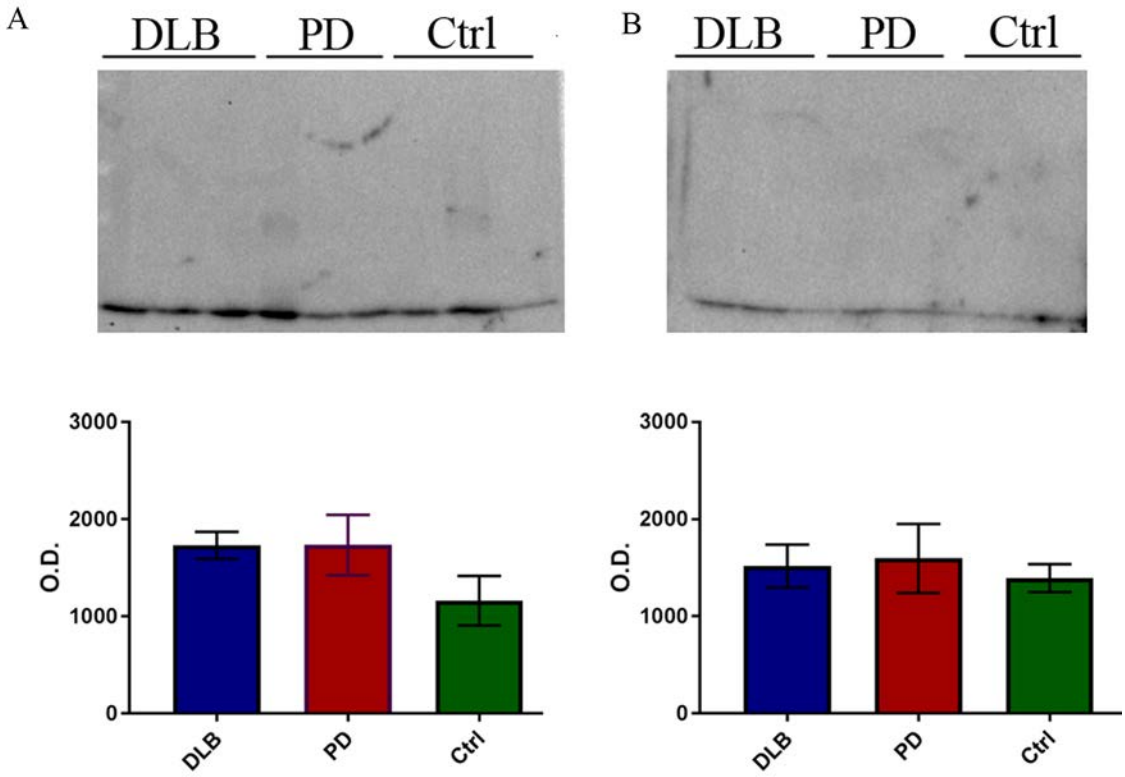

Figure 8. Detection of α-synuclein in the α-syn-SCF. Western blot analyses were conducted on the α-syn-SCFs of DLB, PD and Ctrl derived from FCx (A) and SNc (B). Densitometric analysis of representa-

tive immunoblot of monomeric α-synuclein in the α-syn-SCF from FCx and SNc revealed no significant (n.s) differences between DLB (blue), PD (red) and controls (green).

To further validate that the α-syn-SCF extracted from different pathological contexts (i.e., DLB and PD) would show no differences in the total amount of α-synuclein, we performed an ELISA using electrochemiluminescence detection system (Figure 9). This method allows a more precise quantification and result in higher signal-to-noise ratio compared to the classic ELISA. MJFR1 was used to the detection of the total amount of α-synuclein.

In line with the Western blot results, no significant differences could be observed among DLB, PD and Ctrl samples in both FCx and SNc derived α-syn-SCFs. Moreover, ELISA validated the higher amount in the FCx α-syn-SCF compared to the SNc α-syn-SCF, with the former showing a two-fold higher concentration compared to the latter.

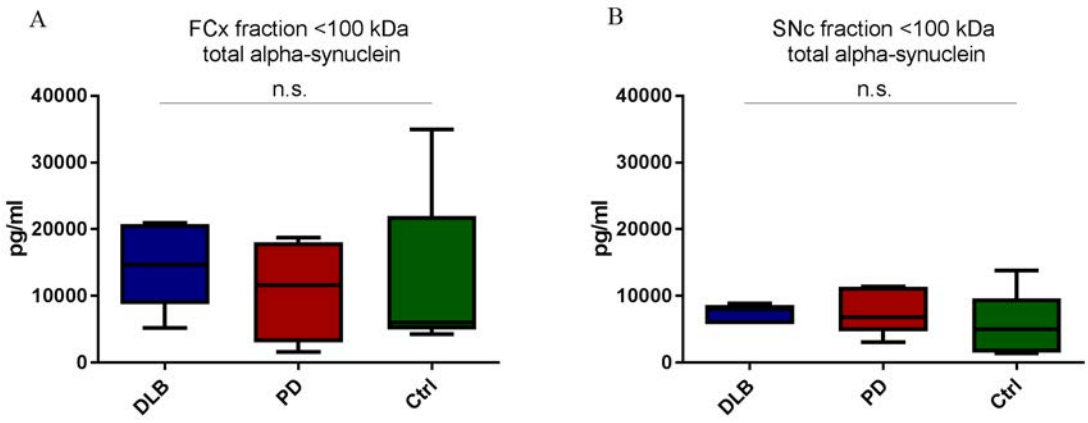

Figure 9. Confirmation of the α-synuclein amount among samples. Electrochemiluminescence ELISA analyses on the α-syn-SCFs of DLB, PD and Ctrl derived from FCx (A) and SNc (B) confirmed that the concentration of α-synuclein in the α-syn-SCFs is comparable among groups.

Taken together, these results indicate that the amount of α-synuclein is comparable among DLB, PD and Ctrl samples within the same brain region, thus ruling out that variations in the concentration may bias the analysis.

4.1.4 Ruling out self-aggregation

Before proceeding with the seeded RT-QuIC reactions, we assayed whether the RT-QuIC produced self-aggregation derived from the seed or from the substrate. To this aim, five reactions either devoid of the seed or devoid of the substrate were run in tripli-

cate. Figure 10 shows that neither reactions displayed a positive signal, indicating that self-aggregation from these species can be excluded as a factor influencing the RT-QuIC.

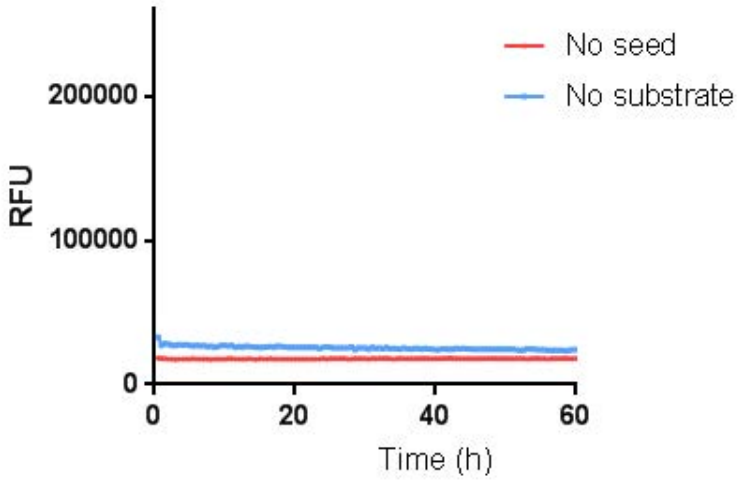

Figure 10. Self-aggregation of α-synuclein in the RT-QuIC assay. Five reactions devoid of either the seed (orange) or the substrate (light blue) were run in triplicates for 60 h in the RT-QuIC. No seeding activity could be detected, excluding the possibility that these species may aggregate by themselves.

4.1.5 DLB-seeded, but not PD-seeded reactions, promote the conversion of α-synuclein during the RT-QuIC

The α-syn-SCFs were tested by RT-QuIC for their ability to seed the aggregation of recombinant α-synuclein. α-syn-SCFs were obtained from FCx of ten patients of each group (n = 10), in triplicates, and were run in parallel. After 60 h, the increase in ThT could be detected exclusively from DLB seeded reactions, while PD and Ctrl seeded reactions showed no increase in the ThT signal. As shown in Figure 11A, the DLB seeded reaction resulted in the typical sigmoidal curve, which reflects the kinetics of the process of aggregation. One-way ANOVA with multiple comparisons followed by Brown-Forsythe test was used to compare the AUCs of the reactions, indicating a significant difference (** $p < 0.01$) between DLB and PD and DLB and Ctrl seeded reactions (Figure 11B).

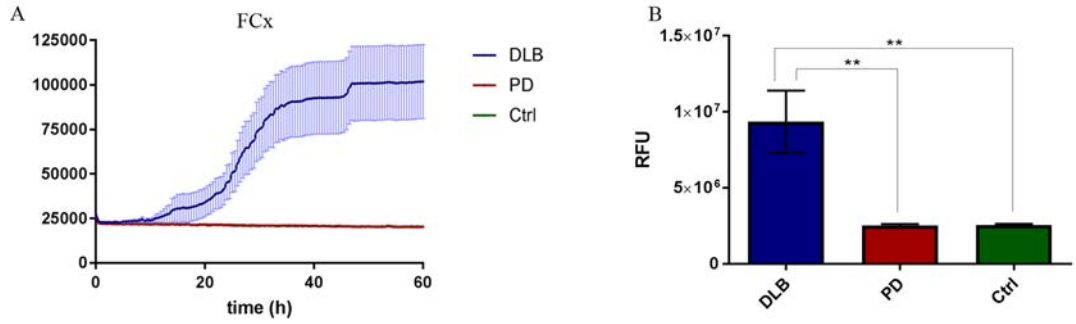

Figure 11. RT-QuIC seeded with FCx derived material. A. Seeding activity from α-synuclein could be observed only when the reactions were seeded with α-syn-SCF from DLB patients (blue, n=10), while no signal could be detected from PD and control cases (red and green respectively, n = 10). B. The area under the curve (AUC) recapitulates the differences observed in the kinetic curve. Statistical analysis was performed by one-way ANOVA with multiple comparisons followed by Brown-Forsythe test (**, $p < 0.01$).

The same analysis has been conducted on reactions seeded with SNc derived material, as SNc is central in the PD pathogenesis but results to be less affected in DLB. A-syn-SCFs from 8 DLB samples, 6 PD and 5 controls were used as seed for the conversion of α-synuclein in the RT-QuIC. Similarly to FCx seeded reactions, the experiment was run for 60 h, after which the seeding activity could be detected exclusively when DLB α-syn-SCFs were used to trigger the aggregation. As shown in Figure 12, the kinetic resembles the one observed in FCx seeded reactions, although the differences between DLB and PD were less prominent according to the statistical analysis of the AUC (* $p < 0.05$). The AUC value of DLB seeded reactions was one order of magnitude lower in SNc compared to FCx, probably reflecting the lower amount of total α-synuclein in SNc compared to FCx.

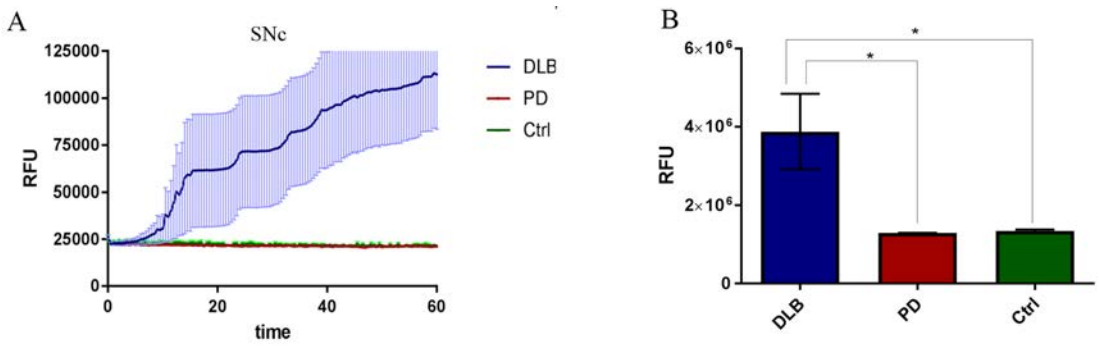

Figure 12. RT-QuIC seeded with SNc derived material. A. Seeding activity from α-synuclein could be observed only when the reactions were seeded with the α-syn-SCF from DLB patients (blue, n=8), while no signal could be detected from PD and control cases (red and green, n = 6 and n = 5 respectively). The Ctrl curve is hidden behind the PD curve. B. The area under the curve (AUC) indicates the differences observed in the kinetic curve. Statistical analysis was performed by one-way ANOVA with multiple comparisons followed by Brown-Forsythe test (*, $p < 0.05$).

As recapitulated in table 3, the RT-QuIC analysis resulted positive in 7 out of 10 DLB samples when seeded with FCx derived material, while only 1 reaction of 20 was positive when seeded either with PD or Ctrl derived α-syn-SCFs. Therefore, the RT-QuIC owned 70% of sensitivity and 95% of specificity when the reactions were seeded with FCx derived material. When the α-syn-SCFs were produced starting from the SNc, 6 out of 8 DLB samples resulted positive and neither PD nor Ctrl reactions showed an increase in the ThT signal, implying 75% of sensitivity and 100% of specificity.

Diagnosis	Combined pathology	Number of FCx samples	Sex FCx	FCx RT-QuIC pos.	Number of SNc samples	Sex SNc	SNc RT-QuIC pos.
DLB	none	4	4 M	3/4	2	2 M	2/2
	AD	6	1 M, 5F	4/6	6	1 M, 5 F	4/6
	total	10	5M, 5F	7/10	8	3 M, 5 F	6/8
				70% sensitivity			75% sensitivity
PD	none	5	5 M	1/5	2	2 M	0/2
	AD	2	1 M, 1F	0/2	2	1 M, 1F	0/2
	VD	3	1 M, 2 F	0/3	2	2 F	0/2
	total	10	7 M, 3 F	1/10	6	3 M, 3 F	0/6
Controls	None	10	7 M, 3 F	0/10	5	2 M, 3 F	0/5
				95% specificity			100% specificity

Table 3. Overview of diagnostic accuracy. The table recapitulates the RT-QuIC results in DLB, PD and controls in FCx and SNc, matching the results for combined pathologies and sex.

Specificity and sensitivity underlie the suitability of the RT-QuIC for the detection of seeding-competent α-synuclein in DLB brain homogenates, showing a lag-phase below 10 h and a signal increase of more than 50%. In addition, the positive seeding response was independent from the kind of brain region and from the presence of co-pathologies. Non-significant seeding activity, when present, was obtained from PD and control derived α-syn-SCFs. Together, our observations demonstrated that the seeding-reactive α-synuclein species in DLB patients revealed an RT-QuIC seeding response.

4.2 Biochemical validation of the RT-QuIC products

Although the RT-QuIC recognizes cross-β structures found in amyloid structures, it offers no information about the biological species that are responsible of the formation of the aggregates. Therefore, the biochemical characterization of the RT-QuIC products appear to be a necessary step. Here we took advantage of widely applied biochemical tools, such as PK digestion and Western blot, Dot blot and ELISA to investigate whether the observed increase in ThT from DLB seeded reaction is actually due to α-synuclein.

4.2.1 Detection of PK resistant α-synuclein in in DLB seeded RT-QuIC reactions

Resistance to PK treatment is a common feature of misfolded proteins commonly found in neurodegenerative diseases [216]. To explore whether converted and aggregated α-synuclein in DLB brain seeded RT-QuIC reactions underwent structural changes in a more stable and β-sheet enriched state conformation, we treated the AQ products with 5 μg/mL of PK. BQ reactions, identical to the AQ reaction but not subjected to the RT-QuIC procedure, were also treated with the same conditions. Immunoblot analysis conducted on five samples using anti-MJFR1 (Fig. 13A) for total α-synuclein revealed PK-resistant bands in the AQ reactions seeded with the α-syn-SCF derived from DLB FCx, migrating through the acrylamide gel with an apparent molecular weight spanning between 10 kDa and 18 kDa. The statistical analysis was conducted on the band exhibiting a molecular weight of 10 kDa, showing significative differences among groups (Fig. 13B). The strong signal observed in the BQ reactions is consistent with the presence in excess of monomeric α-synuclein that serves as substrate for the RT-QuIC reaction. However, BQ reactions were completely digested by PK, indicating that before RT-QuIC the reaction is devoid of amyloid structures.

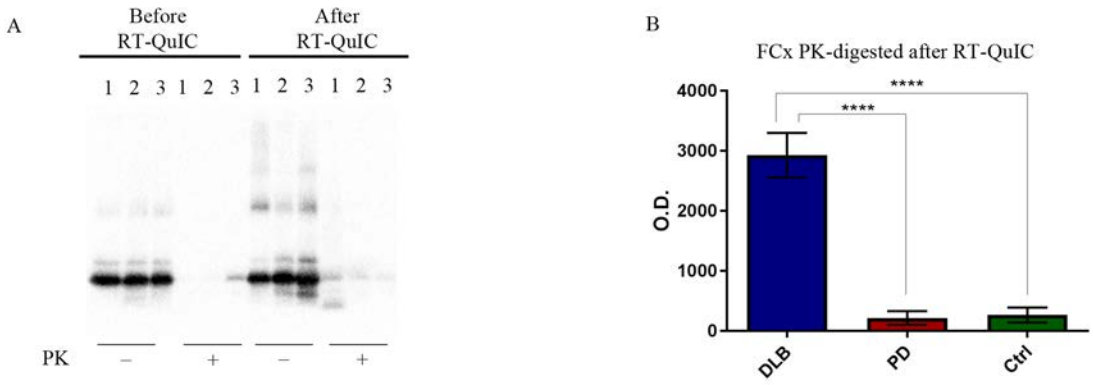

Figure 13. Detection of PK-resistant α-synuclein fragments in FCx seeded RT-QuIC samples. RT-QuIC products (n = 5 for each group: 1 = DLB; 2 = PD; 3 = Ctrl) were treated with PK (5 µg/ml). **A.** Resistant α-synuclein fragments in the 10 to 18 kDa range were detectable after RT-QuIC by immunoblotting only in reactions seeded with DLB α-syn-SCF. **B**. The densitometric analysis was performed on the band at 10 kDa, showing a significative difference after one-way ANOVA with multiple comparisons followed by Brown-Forsythe test (**** $p < 0.0001$).

In line with the results obtained with FCx samples, when the same analysis was performed on SNc derived reactions, DLB AQ products were the only ones to show the presence of PK resistant fragment. However, a different banding profile of PK resistance was observed, as a single band at approximately 10 kDa emerged after PK treatment (Fig. 14A). Differences among samples were significative ($p < 0.0001$, Fig. 14B).

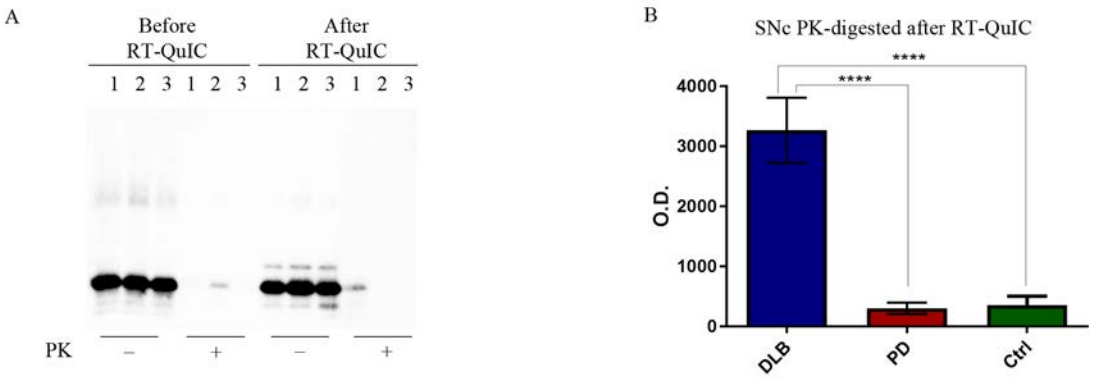

Figure 14. Detection of PK-resistant α-synuclein fragments in SNc seeded RT-QuIC samples. RT-QuIC products (n = 5 for each group: 1 = DLB; 2 = PD; 3 = Ctrl) were treated with PK (5 µg/ml). **A.** Resistant α-synuclein fragments migrating at a molecular weight of approximately 10 kDa could be detected in the AQ products by immunoblotting only in reactions seeded with DLB α-syn-SCF. **B**. The densitometric analysis showed a significative difference after one-way ANOVA with multiple comparisons followed by Brown-Forsythe test (**** $p < 0.0001$).

This analysis demonstrated that, after the RT-QuIC, DLB-seeded products show partial partial PK resistant bands which are detected by the antibody MJFR1 raised against total α-synuclein, while the BQ counterpart was completely digested after PK treatment.

4.2.2 Monomeric α-synuclein is reduced after the RT-QuIC in DLB seeded reactions

During the RT-QuIC process, aggregates are supposed to be produced by the addition of monomers to growing structures, which are subsequently broken by shaking and let grow again during the next incubation phase, until all the monomers are incorporated into aggregates. To elucidate whether monomeric α-synuclein is incorporated into fibrillar species, we performed a Dot blot to compare the total amount of α-synuclein in the BQ and AQ reactions. 5 µl of BQ and AQ reactions seeded with FCx derived α-syn-SCFs were casted on a nitrocellulose membrane and incubated with the MJFR1 antibody (Fig. 15A, B). The optical density of the spots was acquired and expressed as a ratio of the optical density expressed by 3 µl of recombinant monomeric α-synuclein at a concentration of 1g/L (Fig. 15C).

The results showed a reduction in the amount of monomeric α-synuclein in the AQ DLB seeded reaction when compared to its BQ counterpart, indicating that α-synuclein monomers are consumed during the RT-QuIC, possibly being incorporated into bigger structures that are not sensitive to MJFR1 antibody. A similar result was obtained for SNc derived samples (Fig. 15D, E), although the results were less significative.

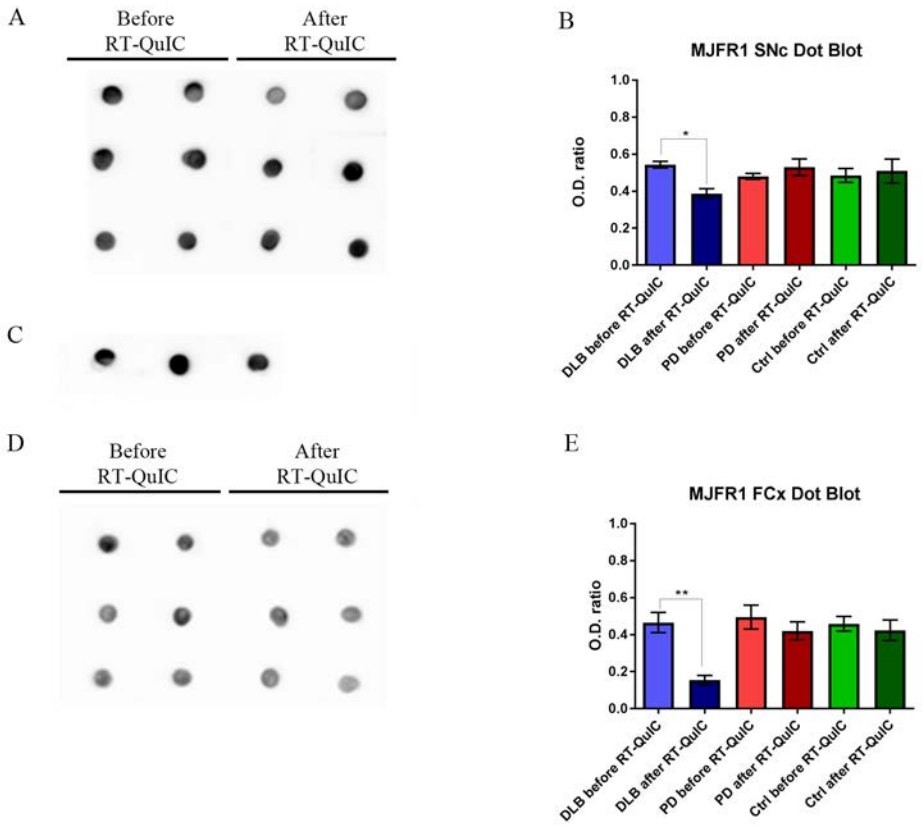

Figure 15. Detection of monomeric α-synuclein before and after the RT-QuIC. **A.** Total α-synuclein level in FCx of DLB, PD and Ctrl samples was detected by Dot blot by using MJFR1 antibody. **B.** The densitometry of the spots were divided by the densitometric value of monomeric α-synuclein and expressed as a ratio. Light colors indicates the BQ reaction (light blue for DLB, light red for PD and light green for Ctrl). One-way ANOVA and multiple comparisons followed by Brown-Forsythe test showed a significant reduction (** $p < 0.001$ of the amount of total α-synuclein in the AQ DLB seeded reaction when compared with its BQ counterpart. **C.** Representative Dot blot on of monomeric α-synuclein used to produce the ratio for the analysis. **D, E**. Dot blot was conduced on SNc derived α-syn-SCF as well. The graphic owns the same color code as the one made for FCx. One-way ANOVA with multiple comparisons followed by Brown-Forsythe test showed a significant difference between BQ and AQ of DLB seeded reactions (*, $p < 0.05$).

4.2.3 Fibrillar and oligomeric α-synuclein species are generated during RT-QuIC in DLB seeded reactions

We proceeded in analyzing whether fibrillar or oligomeric species are produced. To this aim, we performed a Dot blot using the antibody F1, which specifically recognizes fibrils of α-synuclein. The specificity of the antibody towards this structure was demonstrated by Surface plasmon resonance (SPR). This methodology allows the determination of the affinity parameters between a ligand (the antibody) and an analyte (α-synuclein fibrils) through their equilibrium dissociation constant (KD). Figure 16 shows that this antibody displays a preferential binding toward aggregated α-synuclein, while no binding was observed when tested against monomeric α-synuclein.

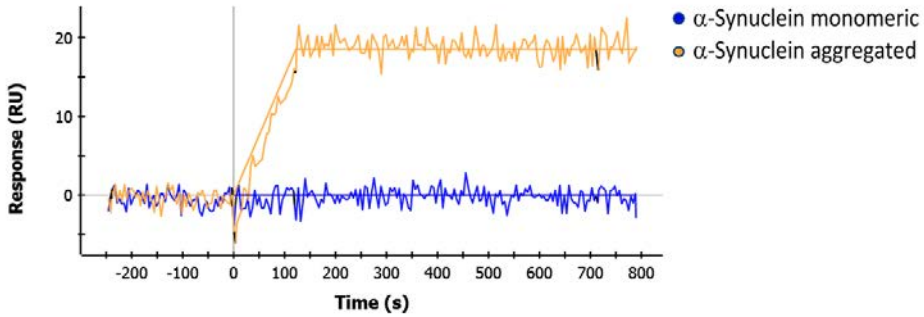

Analyte	Ligand	ka(1Ms)	kd(1/s)	KD (M)	Rmax (RU) grouped
α-Synuclein monomeric	AKF1	8.85E+03	7.14E-01	8.07E-05	1.44E-13
α-Synuclein aggregated	AKF1	1.63E+01	4.40E-09	2.70E-10	1.00E+06

Figure 16. Surface Plasmon Resonance. The affinity of the fibrillar F1 antibody (AKF1) was assessed by SPR. Binding was observed when the antibody was analyzed in combination with RT-QuIC products aggregated α-synuclein (yellow curve), while no binding was observed when monomeric α-synuclein was applied as analyte (blue curve). The table also reports the values for the association and dissociation constants (ka and kd, respectively) as well as and the equilibrium dissociation constant between the antibody and its antigen (KD) and the maximum signal (Rmax).

After demonstrating the affinity of the F1 antibody toward aggregated α-synuclein, we spotted 5 µl of five samples (either BQ or AQ) on a nitrocellulose membrane to perform the Dot blot. We found that fibrillar α-synuclein can be specifically and significantly detected only in DLB seeded reactions from FCx (Fig. 17A, B) and SNc (Fig. 17C, D).

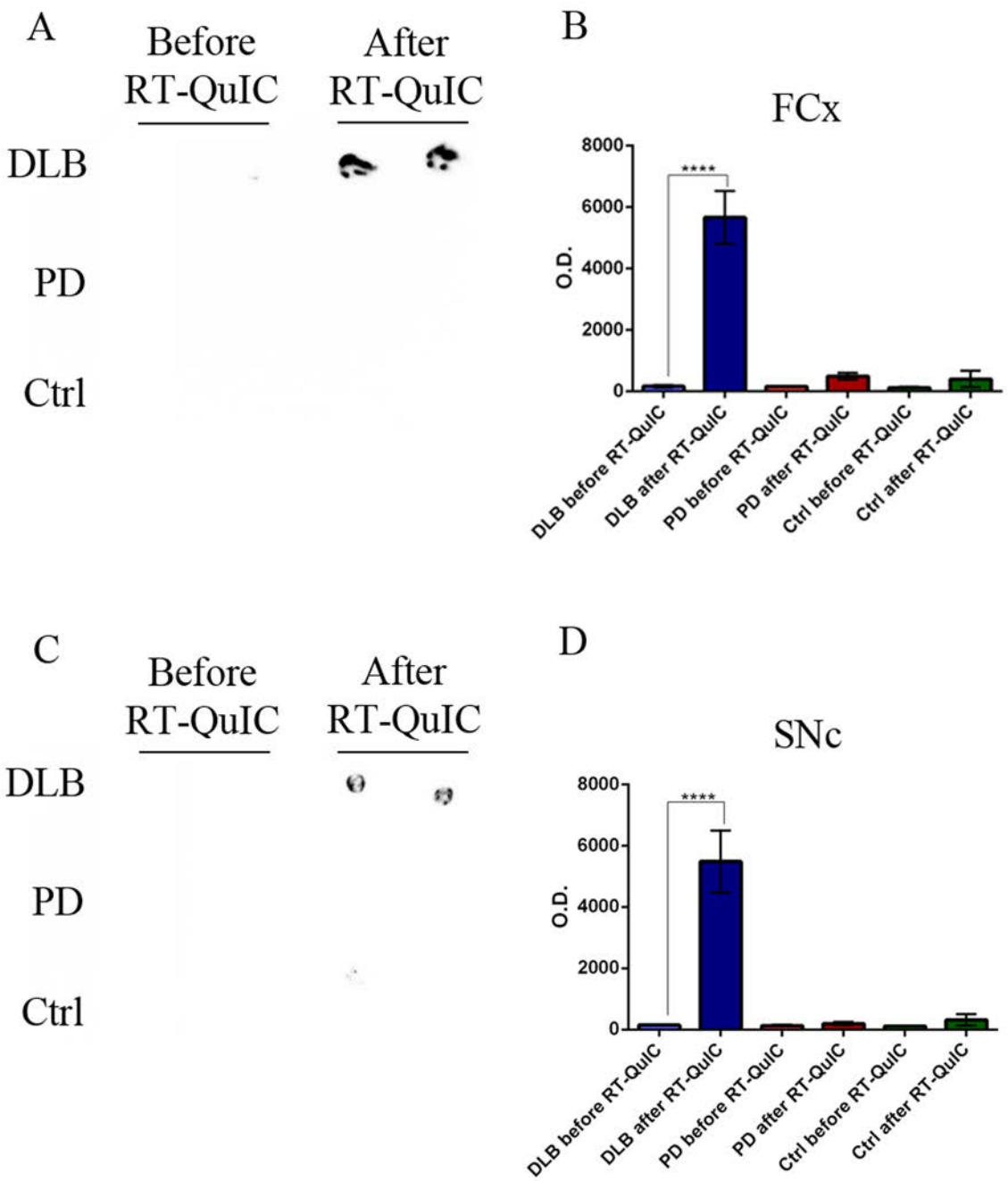

Figure 17. Detection of fibrillar α-synuclein before and after the RT-QuIC. A, B. Fibrillar α-synuclein was detected by means of Dot blot in five DLB seeded reactions (dark blue) from FCx, while no signal could be detected neither from PD and Ctrl AQ reaction nor from any BQ reactions. One way ANOVA with multiple comparisons followed by Brown-Forsythe test showed a significant difference between BQ and AQ in the DLB seeded reactions (**** $p < 0.0001$), indicating the formation of fibrillar species of α-synuclein. C, D. In SNc seeded reactions, the same pattern could be observed.

These results indicate that, together with the reduction of monomeric α-synuclein after RT-QuIC, the intermittent shaking and incubation process causes the formation of fibrillar species of α-synuclein by the conversion of monomers. Importantly, thhis effect was

comparable between FCx and SNc DLB seeded reactions. Lastly, we wondered whether oligomeric α-synuclein could be produced by the RT-QuIC, along with the formation of fibrils, as these two species should not be mutually exclusive. We therefore took advantage of antibodies that could specifically detect oligomeric forms of α-synuclein. In both FCx and SNc (Fig. 18A, B) oligomeric species of α-synuclein could be found only when the reactions were seeded with DLB α-syn-SCFs, while minimal signal was observed from all other conditions.

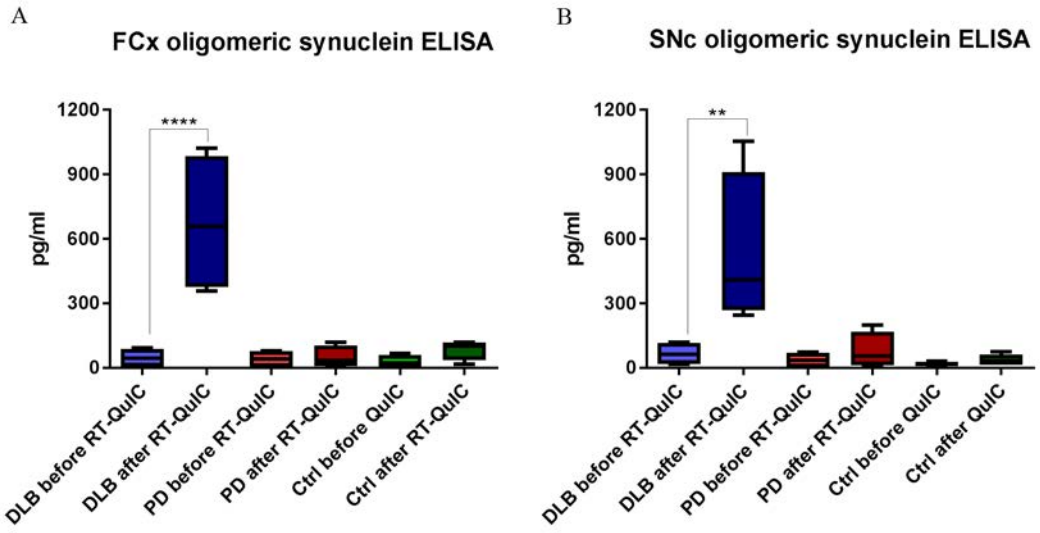

Figure 18. Detection of oligomeric α-synuclein before and after the RT-QuIC.

A. Five FCx derived BQ and AQ reactions, in duplicate, were tested for the presence of oligomeric α-synuclein by means of ELISA. A significant increase (**** $p < 0.0001$) in the amount of oligomeric α-synuclein could be observed in DLB seeded reactions when compared to its BQ counterpart. B. Similar results were obtained when SNc derived reactions were assayed. Statistical significance was assessed by one-way ANOVA with multiple comparisons followed by Brown-Forsythe test (** $p < 0.001$).

Together, the biochemical analyses we conducted on the RT-QuIC products clearly indicate that, during the course of the reaction, the monomeric α-synuclein deployed as substrate is incorporated into larger structures only by the DLB derived seed and forms both oligomeric and fibrillar species, which are resistant to PK treatment. These results were irrespective of the brain region out of which the α-syn-SCF was produced, although FCx derived α-syn-SCFs showed a stronger seeding activity and higher response when tested with immuno-based detection systems such as Dot blot and ELISA.

4.3 Structural analysis of α-synuclein aggregates generated by RT-QuIC

The results so far presented show that the α-syn-SCF derived from DLB FCx and SNc are able to seed the conversion of monomeric α-synuclein, which owns the characteristic features of protein aggregates when assessed biochemically. In our last set of experiments, we sought to characterize the structural properties of the RT-QuIC products. Similarly to the biochemical analyses, we confronted the AQ reactions with their BQ counterpart, in order to exploit the effects produced by the RT-QuIC protocol. The relative amount of secondary structures were characterized by Raman spectroscopy, while the architecture of the aggregates was observed by TEM and AFM.

4.3.1 Analysis of the background noise in Raman spectroscopy

Raman spectroscopy analysis allows to track local structural characteristics which mirror the relative content of secondary structures and the surface exposition of aromatic residues. However, this methodology is particularly sensitive to the microenvironment of the reaction. Firstly, we probed different Raman supports for their background noise (Fig. 19). Specifically, Aluminium crucible (Al crucible), Polytetrafluoroethylene (PTFE, most commonly known with its commercial name Teflon) and gold mirror (Au mirror) were chosen as candidates for the analysis.

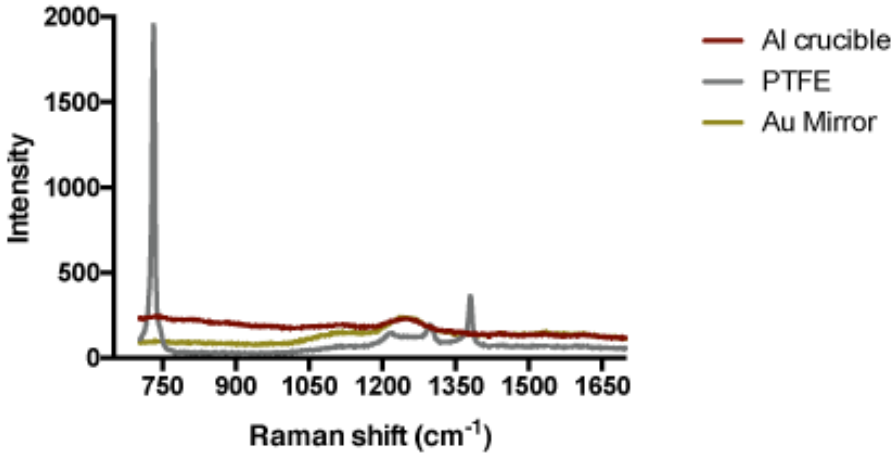

Figure 19. Background signals from different Raman supports. Al crucible (brown line), PTFE (silver line) and gold mirror (gold line) were tested as candidate suports for the Raman analysis. Whereas a high baseline noise was detected from the Al crucible and a double spike at approximately 750 cm^{-1} and 1370

cm^{-1} was detected from PTFE, minimal background noise was detected from the gold mirror.

According to the analysis of the background noise of the substrates, the gold mirror was selected as most suitable support for the Raman spectroscopy, as it showed minimal response compared to the other substrates tested.

Next, we analyzed how the solution in which the RT-QuIC reaction is produced (i.e., the RT-QuIC mix) would respond when assayed for its Raman scattering, as well as the PBS, as the salt amount may cause interference in the measurements (Figure 20). The RT-QuIC mix here tested is devoid of the seed, the substrate and of ThT, as the latter is known to show a high signal when tested by Raman spectroscopy [217].

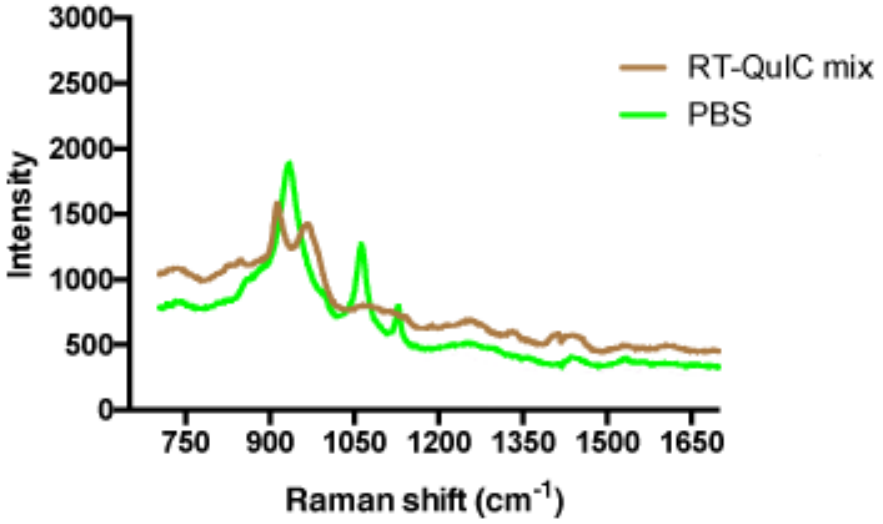

Figure 20. Background signals from the components of the RT-QuIC reactions. RT-QuIC mix without seed, substrate and ThT (brown line) and PBS alone (light green line) showed an increase in the Raman intensity with bands spanning between 880 cm^{-1} and 1050 cm^{-1} approximately.

Although a background band could be detected in the region between 850 cm^{-1} and 1050 cm^{-1}, this region of the spectrum does not provide informations of the secondary structures. Therefore, we concluded that Raman spectroscopy may be helpful in determining the relative amount of secondary structure in the samples.

As further preliminary analysis, we tested different concentrations of α-synuclein to detect the Raman shift caused by the substrate alone. Different concentrations were tested (Figure 21) in order to evaluate whether the local increase of protein concentration caused by the formation of the "coffee-ring" would have biased the analysis.

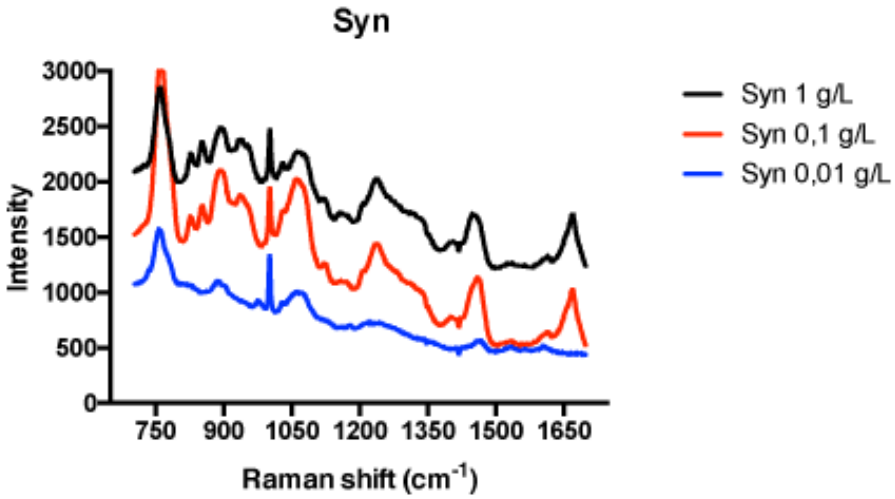

Figure 21. Raman shift of α-synuclein as a function of concentration. Three different concentrations of α-synuclein (1 g/L, black line; 0.1 g/L, red line; 0.01 g/L, blue line) were tested for their Raman shift. The leftmost peak (approximately 780 cm^{-1}) is indicative of the total amount of the protein as it depends on the presence of phenylalanine (Phe) found in position 4 and 104 in the primary sequence of α-synuclein. The amount of secondary structure is reflected by the Amide I band, peaked at 1670 cm^{-1}.

A minimal secondary structure is to be expected from the BQ reactions, as the concentration of the substrate in the RT-QuIC reaction is close to 0.1 g/L, represented by the red curve in Figure 21. The results show that, by increasing the concentration, α-synuclein displays an increase in the amount of secondary structures, as reflected by the increase in the Amide I band peaked at 1670 cm^{-1}.

4.3.2 Analysis of the Raman intensity along the coffee-ring

After evaluating the background noise that the component of the solutions and the substrates may produce, we sought to analyze the RT-QuIC products and the BQ reactions. We first determined the most suitable region of the "coffee-ring" out of which the analysis could be performed (Figure 22), as the protein concentration, and hence the signal, is not constant along the radius of the annulus.

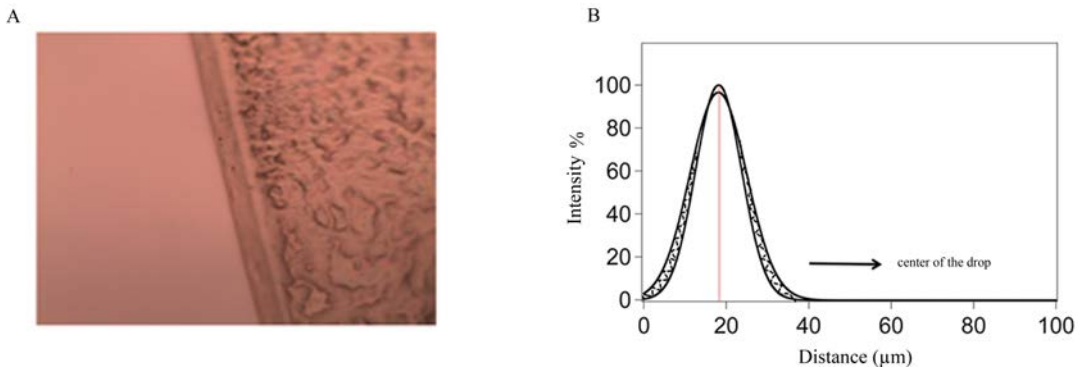

Figure 22. Raman signal along the radius of the "coffee-ring". A. section of the "coffee-ring" at 100x magnification under light microscope. B. Raman shift intensity of the Phe peak at 780 cm^{-1} plotted as a function of the distance from the border.

This analysis shows that the maximum amount of proteins, as reflected by the Phe peak, is found at the centre of the annulus at approximately 20 μm from the border. The intensity profile outlines a 40 μm large annulus corresponding to the coffee-ring deposit including the protein content of the deposited sample. The intensity decreases in the proximal regions and completely disappear going toward the centre of the drop, indicating the most of the protein content is indeed found in the "coffee-ring".

This result indicates that the region showing the highest intensity of the Raman shift is the middle part of the "coffee-ring". Therefore, we chose this part of the annulus as reference region for performing the analysis of the β-sheet content of the BQ and AQ reactions.

4.3.3 Detection of β-sheet structures in DLB-seeded RT-QuIC reactions by Raman spectroscopy

In order to inspect changes to *α*-synuclein secondary structure Raman spectroscopy analyses were conducted on the BQ and AQ reactions.

Minimal secondary structure elements were observed from BQ reactions either containing FCx or SNc derived α-syn-SCFs (Figure 23), in line with the mild increase observed in the monomeric α-synuclein (Figure 23, black curve) as a function of its concentration.

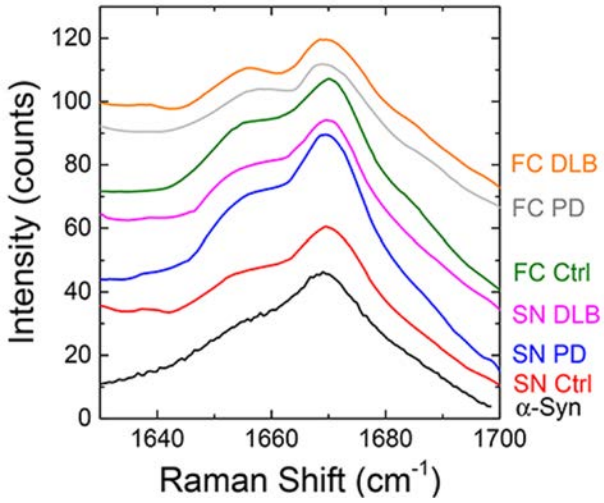

Figure 23. Raman spectra of the amide I band region of the samples before RT-QuIC processing. The spectrum of a deposited aqueous solution of *α*-synuclein at the concentration value used in RT-QuIC experiments (*α*-syn, 140 ng/µL) is reported (black) for comparison. BQ samples from FCx are depicted in yellow (DLB), grey (PD) and green (Ctrl). SNc BQ reactions are illustrated in purple (DLB), blue (PD) and red (Ctrl). For the sake of clarity, the spectra were offset.

The analysis was next performed on AQ samples. Since the amide I band results from the sum of four contributes, namely disordered structures peaked at 1635 cm^{-1}, α-helices at 1655 cm^{-1}, organized β-sheets at 1670 cm^{-1} and loose β-strands and β-turn at 1687 cm^{-1}, the band was deconvoluted by multi-Lorentzian fit to unravel the relative contributions of these structures to the Amide I signal (Figure 24).

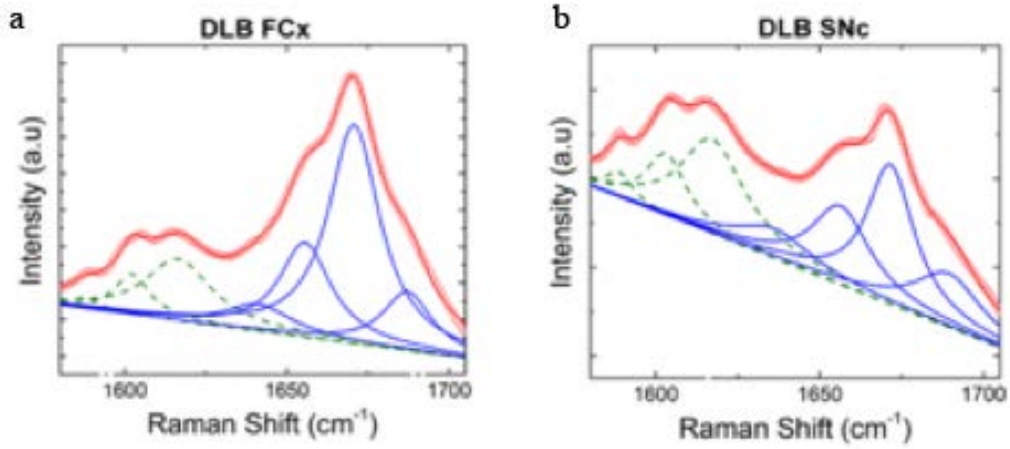

Figure 24. Deconvolution of the Amide I band. Exemplary multi-peak fit of Raman spectra over the 1580-1705 cm^{-1} amide I region applied to the DLB seeded products from DLB (**A**) and SNc (**B**). The convolution of the fitting Lorentzian curves (blue curves), indicating the relative contributions of secondary structures, accurately reproduce raw data (red lines), providing an R-square ≥ 0.995. Green lines indicate contributions from other, non-secondary structures.

As shown in Figure 25, an overall increase in the 1670 cm^{-1} component ascribed to organized β-sheets was apparent in DLB FCx and SNc seeded RT-QuIC products while was not detected in PD- and Ctrl-seeded products, which displayed a profile comparable to the BQ samples. Importantly, these reactions were run in absence of ThT, ruling out the possibility that ThT binding would have favored the aggregation process.

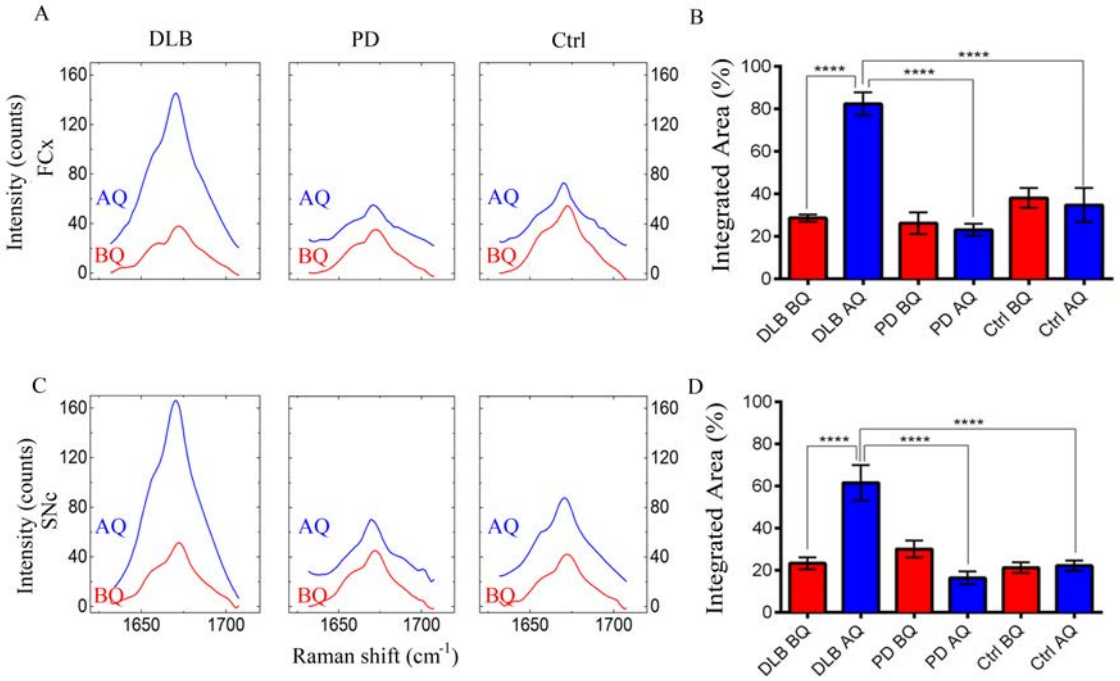

Figure 25. Raman spectra of AQ and BQ samples. A. The 1670 cm^{-1} Raman band in DLB FCx seeded reactions (after RT-QuIC, AQ) underwent an overall increase in intensity e as compared to the initial batches (before-QuIC, BQ). These changes could be not observed in PD and Ctrl-seeded reactions. B. The integrated area amplitudes was normalized to the maximum value found in DLB samples and expressed in % ± SEM) of this band and statistically analyzed by one-way ANOVA with multiple comparisons followed by Brown-Forsythe test (**** $p < 0.0001$). C, D. Similar results were obtained when samples were derived from SNc α-syn-SCFs.

Together, Raman spectroscopy results provide a further validation to the RT-QuIC that supports the biochemical data, indicating that the amount of β-sheet structures are enriched after RT-QuIC when the seed for the aggregation was derived from DLB seeds, while minimal structural features were found in both PD and Ctrl seeded reactions.

4.3.4 Fibrillar structures are detected by EM and AFM

To visualize the fibrillary structures, we performed imaging analyses by means of TEM and AFM in order to delve into the structural of the fibrils formed by RT-QuIC. Both

techniques provide informations on the three-dimensional features at nanometric range, thus allowing to exploit the architecture of the aggregates.

The analysis of the BQ samples revealed that no overt protein aggregates could be detected neither by AFM (Figure 26) nor by TEM (Figure 27), regardless of the brain region from which the α-syn-SCF was produced. Under AFM, all the BQ samples appear as < 4 nm size globular seeds, scribed to small clusters of monomers likely, induced by spontaneous protein aggregation during the handling of the samples. The height, in nanometers, of the globular structures is rendered in a false color gradient, from brown (0 nm) to light yellow (15 nm). Under TEM, similar results could be found, with no clear aggregates in any of the tested samples.

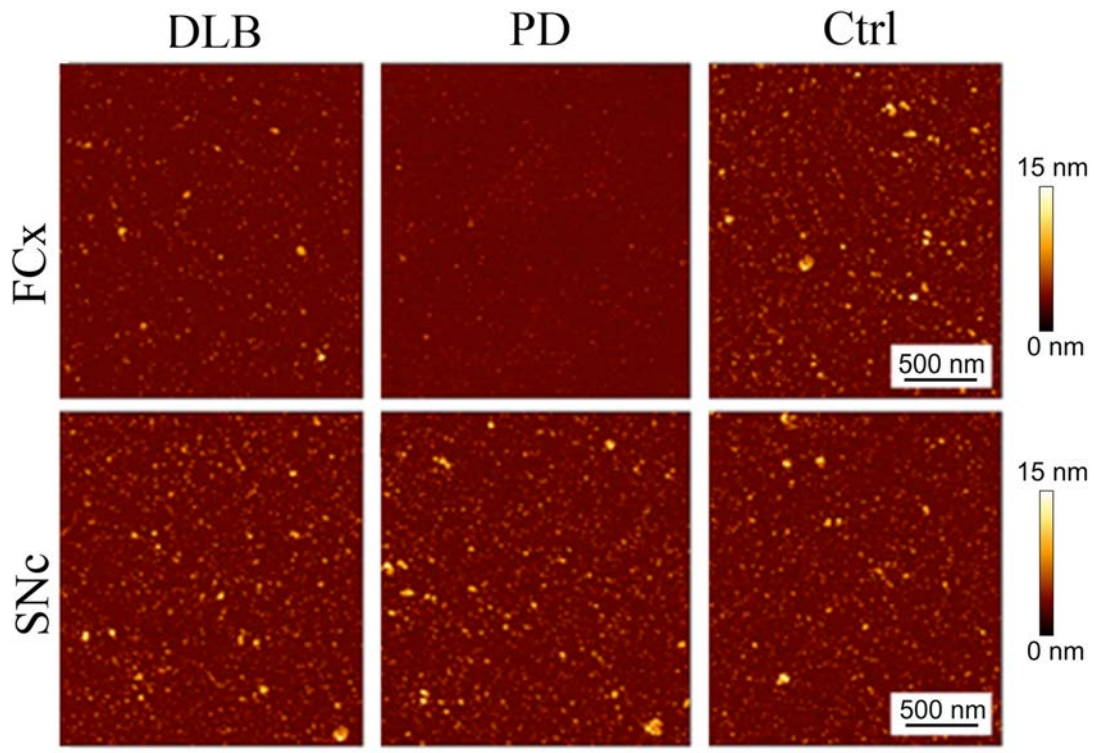

Figure 26. AFM on BQ samples. Tapping mode of AFM conducted on DLB, PD and Ctrl derived α-syn-SCFs from either Fcx and SNc before the RT-QuIC processing. The analysis revealed globular seeds of 4 ± 2 nm size irrespective of sample type. Scalebar was set at 500 nm in lenght. False colors (brown to yellow) indicates the height of the particles in the sample.

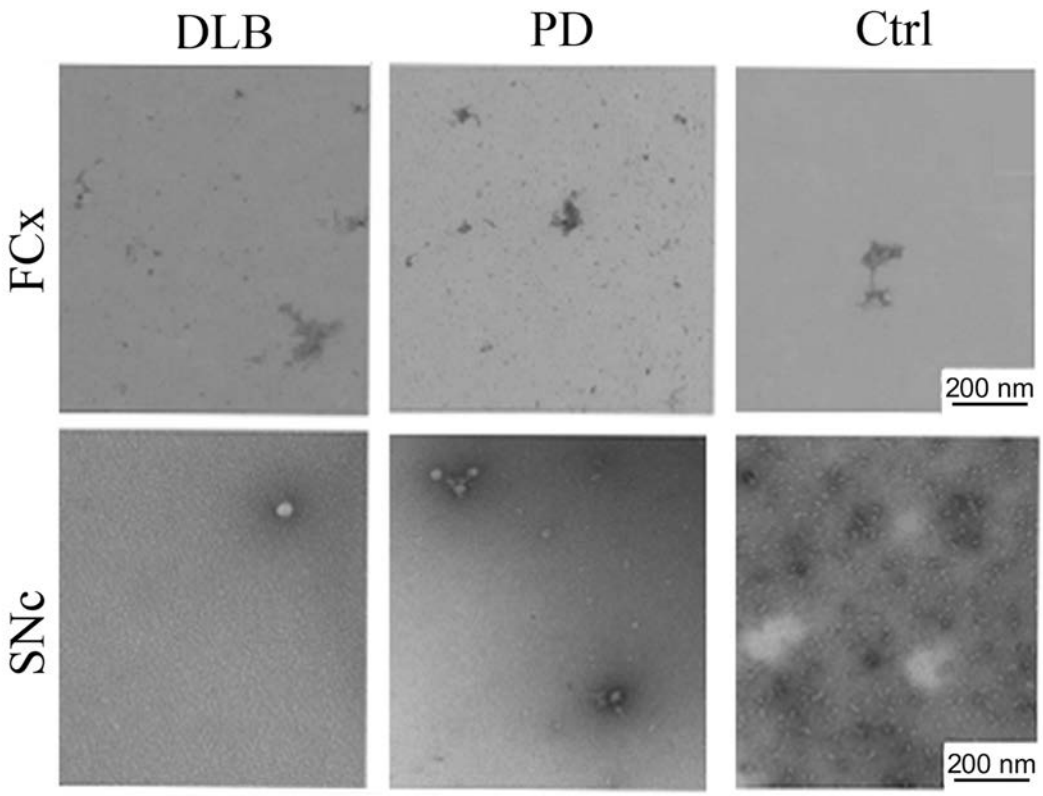

Figure 27. TEM on BQ samples. Negative staining of the BQ reactions derived from FCx and SNc from either DLB, PD or Ctrl cases observed by transmission electron microscope, showing small seeds irrespective of the sample type and no clear aggregated or fibrillary structure, comparable to the AFM results. Scalebar was set at 200 nm.

When the micrographs were taken from AQ samples by AFM (Figure 28) or TEM (Figure 29), the appearance of pre-fibrillar aggregates as protofilaments of approximately 120 nm in length for DLB FCx was observed, whilst amorphous aggregates spanning between 50 nm and 200 nm could be detected for DLB SNc. These changes could not be observed in PD and control samples. TEM analyses validated the results obtained by AFM, showing the presence of large α-synuclein fibrils only in DLB-seeded RT-QuIC reactions. The size and the compactness of rod-shaped α-synuclein fibrils were variable between different brain regions (FCx and SNC); in SNc the clustering of single fibrils to larger aggregates was less pronounced.

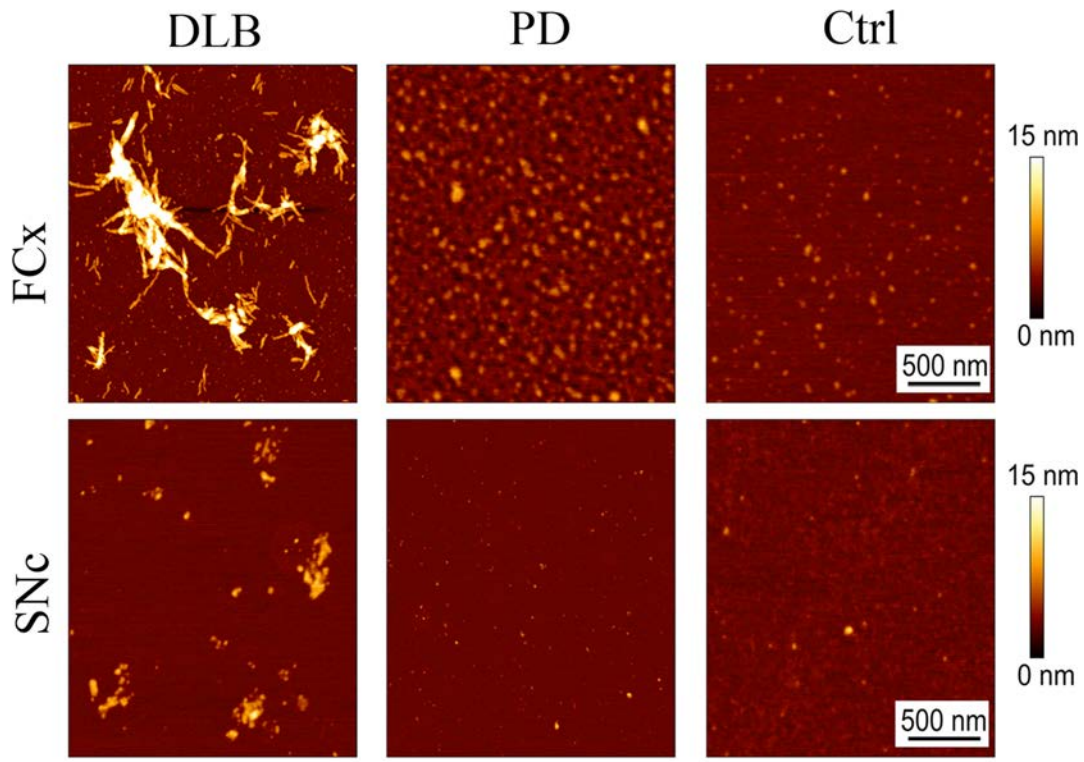

Figure 28. Morphological characterization of the RT-QuIC products under AFM. Tapping mode AFM was used to detect aggregated α-synuclein structures in the AQ reactions. Fibrillar aggregates could be detected when the reactions were seeded with α-syn-SCFs from FCx of DLB patients, while amorphous aggregates were produced using SNc derived seeds from DLB samples. No conspicuous structures could be observed when reactions were seeded with either PD or Ctrl derived material.

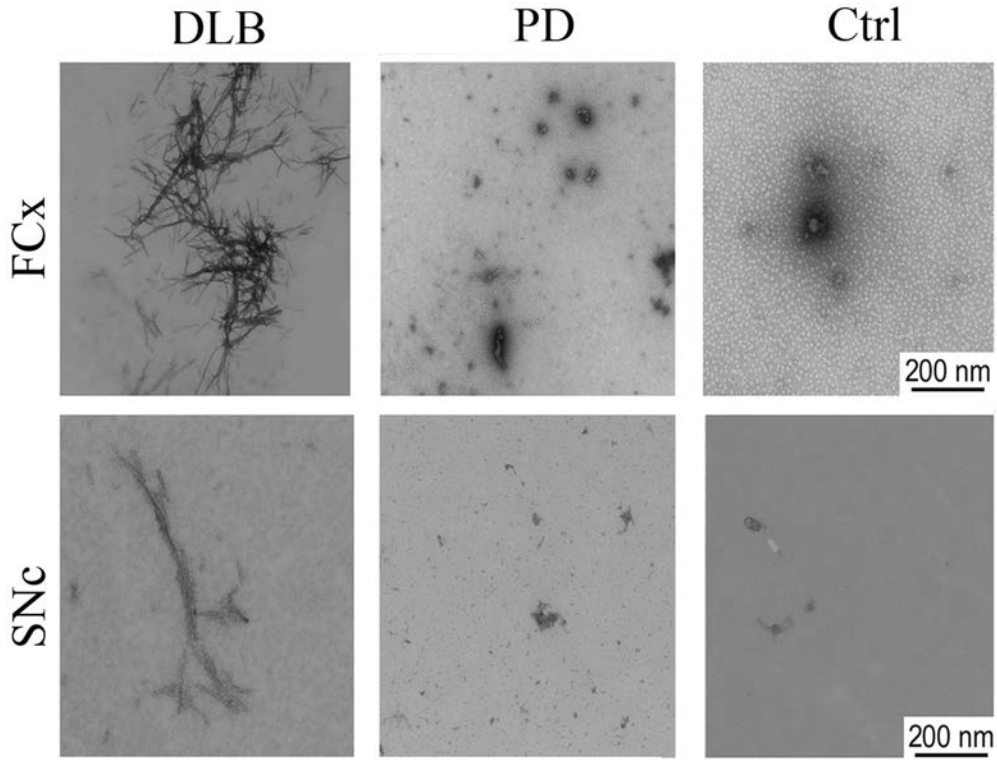

Figure 29. Morphological characterization of the RT-QuIC products under TEM. Coherently with the AFM images, Micrographs obtained in negative staining under TEM show the presence of fibrillar structures of AQ products seeded with DLB derived α-syn-SCFs from both FCx and SNc.

5. Discussion

By analogy to prion diseases, variable clinical and pathological features in α-synucleinopathies[9,10] may correlate with the presence of conformationally different fibrillar inclusions. Prion-like behaviour of α-synuclein has been reported by demonstrating the transmissibility of the MSA α-synuclein strains [162] and evidences of graft-to-host spreading of α-synuclein aggregates further corroborate the hypothesis that α-synuclein acts as a prion-like molecule [141-143]. However, whether DLB and PD depend on different spatial conformations of the pathogenic α-synuclein seed that may account for the different onset and clinical course of the two pathologies still needs to be clarified [96].
In the present study, we were interested in studying the seeding capacity of α-synuclein in DLB and PD brains and distinguish them according to their seeding characteristics in the RT-QuIC. We hypothesize that the existence of α-synuclein conformation variability in DLB and PD patients may influence the seeding conversion and the signal kinetic, as already shown for prion protein [200]. Different brain regions have been postulated to own different sensitivity towards α-synuclein aggregates, possibly depending on the types of neurons found in different brain areas [125]. Therefore, to exclude potential brain region-dependent effects on the seeding of α-synuclein, we run our analyses by testing both brain regions, FCx and SNc.

5.1 Isolation of an α-synuclein containing, seeding-prone fraction

α-synuclein aggregation is a process dominated by the rules of thermodynamics. Heterotypic interactions with other biomolecules, therefore, may cause the misfolding of α-synuclein by the exposure of the hydrophobic core, thus favoring the aggregation
α-synuclein aggregation may be influenced by various biological components, such as nucleic acids [42], phospholipids [218] and high molecular weight structures such as proteoglycans [219]. Cross-seeding with other proteins prone to misfold, such as tau [160] has been reported as well as a factor that may trigger α-synuclein seeding. To reduce the factors that may reult in unspecific RT-QuIC signals, and to increase the purity and concentration of the reactive α-synuclein-seeds, we developed a novel fractionation protocol by enriching α-synuclein seeding competent fractions by serial centrifugation step. The brain homogenates were centrifuged at low speed to remove cellular debris

and, importantly, the nuclear fraction [220]. The supernatant was further centrifuged to allow the sedimentation of α-synuclein aggregates [221] and their separation from soluble proteins, whose might as well interfere with the aggregation process. Partial denaturation of the fibrils was performed by SDS treatment before the application of a molecular weight filter at 100 kDa. This last step was aimed to separate small oligomers of α-synuclein and misfolded monomers from larger aggregates and other high molecular weight compounds which may contain β-sheet structures and therefore affect the aggregation of α-synuclein [219]. β-sheet enriched molecules may further bind to ThT, thus biasing the RT-QuIC analysis by producing false positive results. Indeed, ThT positive signals could be indiscriminately observed from the fraction upper than 100 kDa. Since Ctrl seeded reactions gave positive results as well, it is unlikely that α-synuclein aggregates are causative of the increase in the ThT emission, but may rather be attributed to the presence of molecules that may have caused self aggregation of α-synuclein. Notably, no seeding activity could be detected in any other fractions. The relative amount of total, phosphorylated and fibrillary α-synuclein in each fraction had been estimated by dot blot analysis, indicating no significant differences between DLB and PD patients and control cases. We therefore defined the fraction lower than 100 kDa as our starting working material and termed it α-synuclein seeding competent fraction (α-syn-SCF). Various species at different molecular weights may be contained in the α-syn-SCF, as the energetic landscape of α-synuclein indicates the existence of several energetic minima before the aggregation into larger and more stable aggregates [153]. However, the analysis of the total α-synuclein content in the α-syn-SCF by Western blot using the antibody MJFR1 against total α-synuclein failed to detect any band that could be suggestive of the presence of oligomeric structures of α-synuclein. It is tempting to speculate that the handling and processing required for the Western blot, such as denaturation and boiling, could have dismantled the oligomers, thus resulting in the lone appearance of the monomeric band of α-synuclein at 17 kDa. Outside of biological compounds, concentration have in fact been indicated as a factor that may promote α-synuclein aggregation, even without the presence of a pathogenic seed [113]. Therefore, we ensured that the presence of equal amounts of total α-synuclein in the α-syn-SCFs, and that the number and structure of Lewy bodies as observed by IHC were not significantly different in our selected DLB and PD brain samples, ruling out the odds of observing positive si-

gnals due to concentration effects that may cause self-aggregation of α-synuclein.

5.2 Seeding of α-synuclein in DLB and PD patients

For our approach and goals, we omitted any pre-analytical steps that could potentially affect its seeding characteristics and structure, such as adding a preformed seed, adding beads or using a mutated α-synuclein substrate in the RT-QuIC reaction [210]. We used recombinant α-synuclein with a wild type sequence to maintain the conformation characteristics of the pathologic seed. Self aggregation of α-synuclein is yet another factor to take into account when working with the RT-QuIC. Repeated cycles of freezing and thawing of both the seed and the substrate required for the RT-QuIC might cause them to aggregate and thus produce a positive signal. Therefore, only freshly prepared seed and freshly re-suspended α-synuclein have been used for this analysis. Reactions ran without the seed or the substrate produced no positive RT-QuIC signals, indicating that self-aggregation can be ruled out as potential factor affecting the reaction. Remarkably, our main finding was that RT-QuIC analyses of the α-syn-SCFs revealed a positive signal response specifically in reactions seeded with FCx and SNc brain tissue from DLB patients, whereas PD and controls showed negative RT-QuIC seeding responses. The seeding-reactive α-synuclein oligomeric species in DLB patients had a relative short lag-phase (<10 h) both in FCx and SNc. Importantly, the results were not influenced by the type of co-pathology (see Table 2), indicating that the presence of other proteinaceous aggregates does not significantly influence the course of the reaction. We interpreted our observation that DLB brains contain a pathogenic, oligomeric α-synuclein seed whose seeding reactivity is significantly different from α-synuclein seed in PD patients. Since the levels of total α-synuclein were equal, we propose that the folding and structure of the oligomeric α-synuclein seeds is markedly different in DLB compared to PD patients or controls. In particular, DLB patients exhibit a reactive prion-like α-synuclein seed promoting the conversion of monomeric α-synuclein substrates in the RT-QuIC (Figure 30).

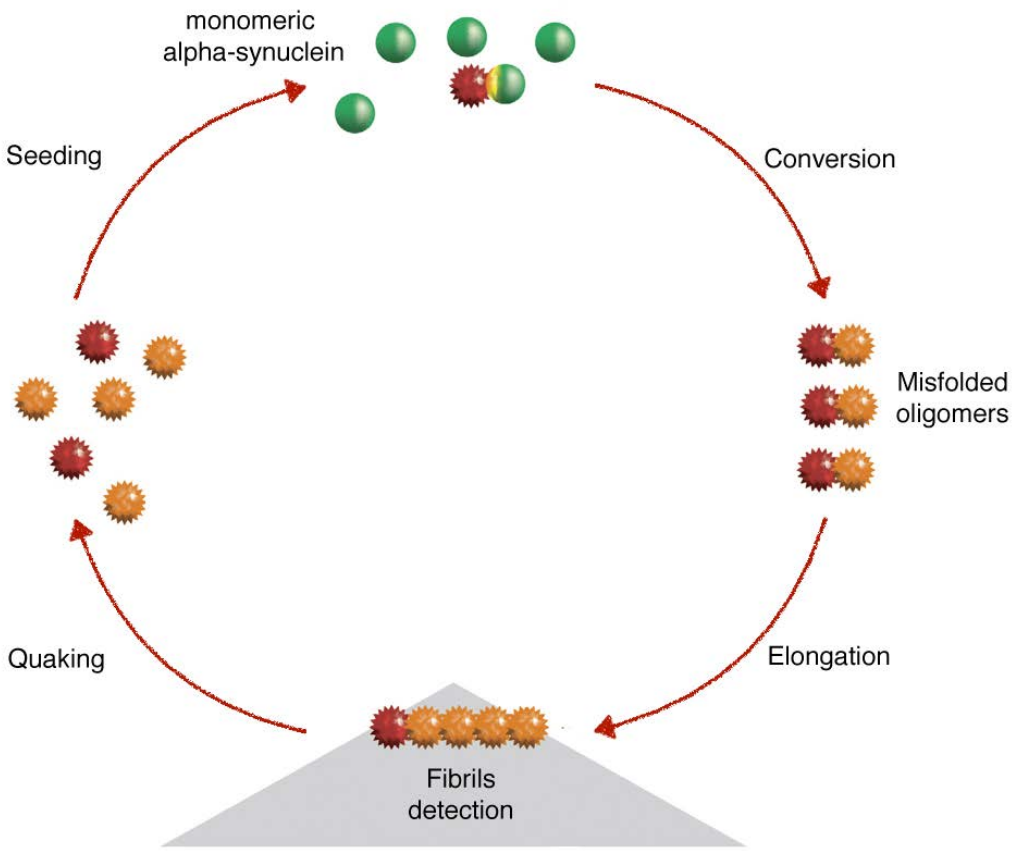

Figure 30. α-synuclein seeding-conversion mechanism. Illustrative diagram of the potential seeding-conversion mechanism of α-synuclein during the RT-QuIC. The α-syn-SCF works as a seed (in red) for the aggregation of monomeric α-synuclein (substrate, in green). The conversion causes the conformational modification into misfolded oligomers that elongates into fibrils. After the detection of fibrils, a quaking event breaks the longer fibrils into shorter, reactive oligomers, that further seed the convesion of monomeric α-synuclein. Modified from [197].

5.3 Biochemical evidences of α-synuclein aggregates in DLB-seeded RT-QuIC reactions

Although the RT-QuIC is a suitable technique to detect the seeding activity and the aggregation kinetics of a biological specimen, its measurements relies on ThT fluorescence, which recognize cross-β structures [166-170]. Therefore, RT-QuIC does not provide informations about the proteins involved in the formation of such structures.

To validate the conversion of monomeric α-synuclein into higher order structures during the RT-QuIC, we analysed the end-product of aggregates generated from DLB, PD and control seeded reactions. Resistance to proteinase K (PK) treatment is a common feature of protein aggregates found in neurodegenerative diseases. Mild PK-treatment of the RT-QuIC products revealed that the ThT stained aggregated material in the RT-QuIC is

at least partial resistant to PK, similar to PrP^{Sc} in prion diseases [216]. The Western blot banding profile showed the occurrence of N-terminal truncated PK undigested α-synuclein fragments (between 18 kDa and 10 kDa) in DLB FCx tissue. A comparable pattern of PK resistant α-synuclein fragments in DLB patients could be already observed in a previous study in DLB brain tissue [164], indicating that mild PK-resistant characteristics in DLB patients were maintained during the RT-QuIC analysis. Moreover, our observation of a single PK-undigested α-synuclein specific band in DLB SNc tissue compared to a cleavage of α-synuclein into smaller fragments in DLB FCx indicates the DLB-SNc seeded reactions may result in a more stable and compact end-product. Further analyses conducted by Dot blot and ELISA corroborated this result, showing the formation of both oligomeric and fibrillar species of α-synuclein. We proposed that the differences in α-synuclein seeds in both brain regions may depend either on different vulnerability of these structures [140] or on the intracellular medium in both tissues, which seems to be relevant for the occurrence for the α-synuclein conformation in α-synucleinopathies [165].

5.4 Structural evidences of α-synuclein aggregates in DLB-seeded RT-QuIC reactions

In order to detect the formation of secondary structures in the RT-QuIC products, we analyzed our samples by Raman spectroscopy. The minimal secondary structure found in the reaction before RT-QuIC, which is a frequent feature of natively unfolded proteins, including α-synuclein [217]. The increase in secondary structures in the samples before RT-QuIC may also be due to an artificial increase in the local concentration after the formation of the "coffee-ring", which might have caused the partial folding of α-synuclein. After RT-QuIC, an overall increase in β-sheet signals from DLB-seeded RT-QuIC reactions indicates the formation of cross-β peptide assemblies, which was not apparent in PD- and control-seeded reactions. This result supports the formation of aggregates enriched in β-sheets only in DLB-seeded reactions, which is in accordance with the positive seeding response of the RT-QuIC. The observed increase in the β-sheets content mirrors the RT-QuIC results, providing an unbiased validation of the formation of aggregates during the course of the reaction. Lastly, morphological studies, conducted by AFM and TEM, showed that DLB-seeded reactions may generate rod-shaped

amyloid-fibrils of different sizes and structures which differ from other α-synuclein fibrils (exhibiting a more circular and compact appearance), generated via RT-QuIC [210]. Fibril compactness and size is increased in FCx seeded reactions, which is in line with our observation that DLB-SNc seeded reactions may result in a smaller sized RT-QuIC product. Evidences that the RT-QuIC seeding responses from DLB and PD patients may be influenced by the average size of α-synuclein seeds could be neither confirmed by our Western blot nor the dot blot analysis with conformation specific α-synuclein antibodies. Therefore, we consider size variances of α-synuclein seeds in DLB and PD as less decisive for the observed differences in our RT-QuIC analyses; however, we cannot fully exclude them. Putative explanations are the usage of a different substrate (substrate contained the S129A mutation to block phosphorylation), and the application of different seed material, such as a preformed aggregated α-synuclein seed [209-211].

5.5 Structural variability underlies potential α-synuclein strain typing

The fractionation protocol was introduced to avoid the possibility that various biological molecules may have jeopardized the experiments by affecting the aggregation process. Although PD-derived α-syn-SCFs showed the same level of total α-synuclein and the assessment Lewy pathology in the brains revealed no overt differences, RT-QuIC failed to amplify the PD-derived seed. The biochemical and structural analyses we conducted confirmed the RT-QuIC findings, indicating that the RT-QuIC products of PD-seeded reactions could not produce the signatures of the aggregation process that were detected in the DLB-seeded reactions. Taken together, our results are suggestive of a potential strain difference between DLB and PD derived α-syn-SCF, which may be the characteristics of different strains, the former having seeding-conversion activity when tested in the RT-QuIC and showing the presence of aggregated forms of α-synuclein (oligomers and fibrils) by different biochemical and structural methodologies, while the latter showed no signal in this system and no structural nor biochemical hallmark for the presence of fibrillar species. In our setting, specificity was 95% for FCx derived material and 100% for SNc derived material, whilst sensitivity was 70% for FCx seeded reactions and 75% for SNc seeded reactions.

These results are in line with those of Prusiner's group [164], in which brain homogenates derived from MSA patients could drive the onset of α-synucleinopathy in recipient

mice, while PD material could not produce any sign of infectivity, pointing towards the existence of different α-synuclein strains between MSA and PD. In both Prusiner's work and ours, PD-derived material showed no ability of seeding the aggregation of α-synuclein, which is reflected in the lack of the onset of pathology in their system and in the lack of seeding activity in the RT-QuIC in our experiments. Although DLB and PD are often referred as variants of the same spectrum of disease [91-93], we could produce aggregated forms of α-synuclein by RT-QuIC only from DLB cases, indicating that, similarly to the differences observed between MSA and PD, a strain difference might exist between DLB and PD as well. The evidences here reported, however, do not exclude that PD-derived α-synuclein own no seeding activity.

In recent years, It has been indeed demonstrated that PD-derived α-synuclein possess the ability to amplify recombinant α-synuclein in vitro with different methodologies. α-synuclein aggregates were successfully detected by Shahnawaz and co-workers [190] using PMCA seeded with CSF derived from PD samples with a sensitivity of 88% and a specificity of 97%. Their PMCA system provided results that correlated with the severity of the disease and was able to detect two control cases that later on developed PD, indicating the possibility of applying this detection system to prodromal stages of the pathology as well. As stated by the authors, the PMCA assay was not able to distinguish among different forms of synucleinopathies. They provided no biochemical validations, affecting the reliability of the assay.

Likewise, Fairfoul and co-workers [209] were able to detect the seeding activity of α-synuclein seeds derived from both BH and CSF in the RT-QuIC by adding zirconia/silica beads to the reaction with a specificity of 100% and 92% and 95% of sensitivity for DLB and PD, respectively. The authors reported also the ability of their system to detect prodromal stages of DLB, by obtaining a positive RT-QuIC signal from control cases affected by RBD, hallmark of the prodromal stage of DLB. However, this work reported no biochemical validations of the RT-QuIC and displayed low sensitivity (65%) for reactions seeded with CSF derived from DLB combined with mixed pathologies, whereas our protocol appears to be irrespective of the presence of co-pathologies along with the main synucleinopathy diagnosis.

A thorough characterization of the RT-QuIC products was conducted by Sano and co-workers [210] in reactions seeded with DLB derived brain homogenates, which resulted in 100% specificity, 92% of sensitivity for DLB and 95% sensitivity for PD. Here, the

usage of mutated recombinant α-synuclein might have been critical for the experiments. A common feature in Lewy bodies is the presence of α-synuclein phosphorylated at residue 129. By inducing a point mutation (S129A), the researcher reduced the ability of α-synuclein to form aggregates and forced their production by RT-QuIC, avoiding in this way the possibility of producing false positives. Consistent with our reports, they showed that the presence of other protein aggregates does not influence the course of the reaction.

Lastly, Groveman and co-workers [211] reported a successful amplification of monomeric α-synuclein when seeded with BH and CSF from PD and DLB patients. Similarly to Sano's work, Groveman's experiments were carried out using mutated α-synuclein (K23Q, which displays lower self-aggregation), yielding 100% of specificity and 93% of sensitivity towards α-synucleinopathies (DLB and PD grouped together). Interestingly, their work suggested a possible difference between DLB and PD, with the former showing a greater ability in seeding the aggregation compared to PD seeded reactions. However, the difference between the two was not statistically significant. Although the three studies here summarized were all able to detect, in some extent, the seeding activity of pathogenic α-synuclein, the protocols applied differed widely for physical and chemical conditions of the reaction and, more importantly, for the starting seed and substrate used for the reaction. In table 4, the differences among these protocols and the one we developed here are reported. Specificity and sensitivity of the protocols are listed as well.

Comparison among RT-QuIC protocols

	Seed	sub.	shaking/ Incubation	T	pH	SDS	beads	Spec.	Sens.
Fairfoul et al. (2016)	5-15 µl CSF; 2 µL BH 1:20000 in PBS	0.1 g/L human full length α-synuclein (Stratech , UK)	1 min double orbital, 200 rpm / 15 min	30 °C	8,2	No	37± 3 mg zirconia/ silica	100%	DLB 92% PD 95%
Sano et al. (2017)	5 µl 10% w/ V BH in PBS	0.10-0.15 g/L S129A α-synuclein	40 s circular, 432 rpm/ 140 s	40 °C	7,5	No	No	100%	DLB 92% PD 95%
Groveman et al. (2018)	2 µl 10% w/ V BH in PBS; 15 µl CSF	0.1 g/L filtered human full length α-synuclein (Stratech , UK); 0.1 g/L K23Q α-synuclein	1 min double orbital, 400 rpm/ 1 min	42 °C	8,0	0.00 15% for CSF	6 glass or silica, 1 mm diameter	100%	DLB + PD 93%
Candelise et al. (*submitted in 2018)*	3 µl enriched fraction form 10% w/ V BH	human full length α-synuclein (rPeptide , UK)	1 min double orbital, 600 rpm/29 min	37 °C	8,4	No	No	FCx 95% SNc 100%	FCx 70% SNc 75%

Table 4. Comparison among α-synuclein RT-QuIC protocols. The table summarizes the differences in the protocols so far developed, including the one presented in this work, followed to detect α-synuclein seeding activity in the RT-QuIC.

It is therefore apparent that multiple ways may be exploited to detect α-synuclein seeding activity. A different micro-environment of the reaction, a different physical conditions for the aggregation, a different source for the seed or the usage of a different substrate, and any combinations of these factors, may hence lead to the detection of α-synuclein seeding activity from various pathologies. Whereas previous protocols could not discriminate among α-synucleinopathies (at least not statistically), our methods was

able to exploit the differences in seeding activity of DLB and PD, in line with the trend observed by Grovemann and co-workers and coherent with the reported inability of PD derived material to produce Lewy pathology in recipient mice [164]. We suggest that the enrichment protocol we followed was critical for the exploitation of the differences in seeding activity. During the fractionation, PD-derived α-synuclein may dissociate from other compounds that could have allowed the detection of the seeding activity. Alternatively, DLB-derived α-synuclein aggregates may be more resistant to SDS treatment, generating aggregation-prone fragments, while PD-derived may be less resistant to this treatment and hence lose the ability to promote the conversion of α-synuclein during the RT-QuIC reaction. We speculate that DLB and PD are characterized by different strains possessing different structural and biochemical profiles, therefore accounting for the differences in the spreading and symptomatology of these diseases.

5.6 Considerations on selective vulnerability

The clinical features that underlie PD and DLB differ significantly in the sequence of occurrence of the symptomatology [125, 133], which in turn reflects putative differences in the route of spreading of pathogenic species of α-synuclein in the two pathologies [101]. Neuronal loss, moreover, diverges significantly not only between diseases, but also in the neuronal population and subpopulation affected (e.g., hippocampal glutamatergic neurons and dentate gyrus glutamatergic neurons [222]). Since the presence of α-synuclein aggregates in FCx is indicative of cognitive dysfunctions in patients, and therefore most prominent in DLB, whilst α-synuclein aggregates in SNc would account for the motor symptoms, characteristic of PD and affecting DLB only at a later stage [153], we sought to compare the seeding activity from FCx and SNc, as dopaminergic neurons in the SNc appear to be selectively more affected in PD compared to DLB. In this scenario, a specific increase in the quantum yield of ThT would have been expected from SNc derived PD seeds, while FCx from DLB would have been enhanced compared to PD. However, we could surprisingly detect seeding activity only in DLB seeded reaction regardless the brain region considered. This result could be either explained by a concentration effect, or by a different sensitivity of FCx and SNc towards α-synuclein aggregation. In order to rule out the first option, we ran a two-way ANOVA to delve into the differences between DLB samples from FCx and SNc, as reported in table 5.

Two-Way ANOVA

	FCx BQ vs SNc BQ		FCx AQ vs SNc AQ	
	p value	**Significance**	**p value**	**significance**
WB BQ	> 0.99	n.s.		
ELISA BQ	0.583	n.s.		
RT-QuIC AUC			0.8	**
OligoSyn ELISA	> 0.99	n.s.	0.96	n.s.
PK-WB AQ			0.489	n.s.
F1 Dot Blot	> 0.99	n.s.	> 0.99	n.s.
MJFR1 Dot blot	0.98	n.s.	0.08	n.s.
Raman Spectr.	> 0.99	n.s.	0.984	n.s.

Table 5. Recapitulatory table of the two-way ANOVA. Two-way ANOVA was run along all the experiments reported in this work to detect differences between FCx and SNc from DLB patients. p-value and significance are listed for the comparison of the BQ fraction and the AQ products.

No significant differences could be detected in the analyses conducted on the α-syn-SCFs (Western blot and ELISA). Nonetheless, a significant difference was revealed in the AUC of the RT-QuIC reactions, with DLB derived, SNc seeded reactions showing a lower degree of aggregation based on the AUC of the kinetic curves. This result might suggest a greater ability of the FCx derived seed to promote the aggregation when compared to the SNc derived seed. The downstream biochemical analyses, as
well as the spectroscopic examination, did not yield the same significance, indicating an equal amount of aggregated α-synuclein structures and comparable levels of cross-β structures. These observations may indicate that α-synuclein oligomers and fibrils produced in the RT-QuIC from SNc derived samples differs from those produced from FCx derived seeds, owing a lower ability to bind ThT. The structural analyses conducted by AFM and EM show subtle differences in the appearances of these aggregates, thus supporting the selective vulnerability of different brain regions toward the same strain of α-synuclein. In this scenario, the neuronal subpopulations in the FCx (mainly glutamatergic and GABAergic neurons), would be more sensitive toward DLB strains of α-synuclein, while dopaminergic and cholinergic neurons within the SNc would result to be less affected by this strain, although they could still seed the RT-QuIC reaction. This

hypothesis reflects the clinical manifestation of DLB, showing cognitive symptoms, related to cortical activity, before the onset of the motor symptoms, dependent on the nigrostriatal pathway.

In conclusion, the present work propose the existence of two strains that account for the differences in the seeding activity and underlie the structural variability of DLB and PD, recapitulating the differences observed in the symptomatology of the two synucleinopathies.

6. Summary and Conclusions

Since the introduction of the concept of self-propagating proteins as common causative feature in neurodegenerative diseases, whether different conformations of pathogenic proteinaceous material might underlie similar diseases and might be indicators for strains has been a long lasting conundrum. Although heterotypic seeding has been commonly detected in most neurodegenerative diseases, “pure” α-synucleinopathies strikingly differ for their clinical manifestation, route of spreading and prodromic phase of the disease. Three synucleinopathies have been classically defined, namely DLB, PD and MSA. Whereas MSA was set apart from DLB and PD by showing oligodendroglial aggregates rather than the neuronal Lewy bodies and neurites found in PD and DLB, the discrimination between these two latter pathologies poses greater difficulties, as in later stages of disease they show a dramatic overlapping in the symptomatology and topology of the lesions.

In this frame, the work here presented aimed to discriminate between DLB and PD by exploiting the seeding activity of α-synuclein derived from brain homogenates of patients diagnosed with either DLB or PD. We first applied a novel fractionation protocol to selectively remove factors that may bias the aggregation process and next assayed the seeding activity of the working material, which we termed “seeding-competent fraction”, for its ability to amplify monomeric α-synuclein in the RT-QuIC reaction. Due to the putative selective vulnerability of different brain areas toward α-synuclein aggregates, we ran in parallel the enriched fractions derived from frontal cortex (mostly affected in DLB) and substantia nigra pars compacta (mostly affected in PD). In our system, we could detect seeding activity specifically from DLB patients regardless the brain region analyzed. Subsequent biochemical and structural analyses showed that the increase in the quantum yield observed in the RT-QuIC is actually due to α-synuclein forming larger structures (i.e., oligomers and fibrils, as seen by EM and AFM) that show the typical biochemical profile of protein aggregates, such resistance to proteinase K, selective binding to fibrillar and oligomeric antibodies and increased beta-sheet content (as seen by Raman spectroscopy).

Together, our work provides further evidence for the existence of a strain difference that underlies the observed differences in the clinical and histopathological features of the two pathologies. A better understanding of the structural differences of α-synuclein pa-

thogenic forms will help to identify factors which trigger the pathology in these conditions and pave the way for the development of specific therapeutic approaches in the future.

7. Bibliography

[1] Soto C (2001). Protein misfolding and disease; protein refolding and therapy. FEBS Lett. 498(2-3): 204-207.

[2] Soto C (2003). Unfolding protein misfolding in neurodegenerative diseases. Nat Rev Neurosci. 4(1): 49-60.

[3] Foit L, Morgan GJ, Kern MJ, Steimer LR, von Hacht AA, Titchmarsh J, Warriner SL, Radford SE, Bradwell JCA (2009). Optimizing protein stability in vivo. Mol Cell. 36(5): 861-871.

[4] Schönfelder J , Alonso-Caballero A , De Sancho D, Perez-Jimenez R (2018). The life of proteins under mechanical force. Chem Soc Rev. 47(10): 3558-3573.

[5] Balchin D, Hayer-Hartl M, Hartl FU (2016). In vivo aspects of protein folding and quality control. Science 353(6294): acc4354.

[6] Eisenberg D, Jucker M (2012). The amyloid state of proteins in human diseases. Cell 148(6): 1188-1203.

[7] Carrell RW, Gooptu B (1998). Conformational changes and disease—Serpins, prions and Alzheimer's. Curr Opin Struct Biol. 8(6): 799-809.

[8] Frantzmann T, Alberti S (2018). Prion-like low-complexity equences: key regulators of protein solubility and phase behavior. J Biol Chem. pii: jbc.TM118.001190.

[9] Dobson CM (1999). protein misfolding, evolution and disease. Trends Biochem Sci. 24(9): 329-332.

[10] Skrabana R, Sevcik J, Novak M (2006). Intrinsically disordered proteins in the neurodegenerative processes: formation of tau protein paired helical filaments and their analysis. Cell Mol Neurobiol. 26(7-8). 1085-1097.

[11] Uversky VN, Oldfield CJ, Midic U, Xie H, Xue B, Vucetic S, Iakoucheva LM, Obradovic Z, Dunker AK (2006). Unfoldomics of human diseases: linking protein intrinsic disorder with diseases. BMC Genomics. 10 Suppl 1:S7.

[12] Levine ZA, Larini L, LaPointe NE, Feinstein SC, Shea JE (2015). Regulation and aggregation of intrinsically disordered peptides. Proc Natl Acad Sci U.S.A. 112(9): 2758-2763.

[13] Hegy H, Tompa P (2008). Intrinsically Disordered Proteins Display No Preference for Chaperone Binding In Vivo. PloS Comput Biol. 4(3): e1000017.

[14] Prusiner SB (1982). Novel proteinaceous infectious particles cause scrapie. Science 216(4542): 36-144.

[15] Spillantini MG, Schmidt ML, Lee VM, Trojanowski JQ, Jakes R, Goedert M (1997). Alpha-synuclein in Lewy bodies. Nature 388(6645): 839-840.

[16] Bruijn LI, Houseweart MK, Kato S, Anderson KL, Anderson SD, Ohama E, Reaume AG, Scott RW, Cleveland DW (1998). Aggregation and motor neuron toxicity of an ALS-linked SOD1 mutant independent from wild-type SOD1. Science 281(5384): 1851-1854.

[17] Sorarú G, Orsetti V, Buratti E, Baralle F, Cima V, Volpe M, D'ascenzo C, Palmieri A, Koutsikos K, Pegoraro E, Angelini C (2010). TDP-43 in skeletal muscle of patients affected with amyotrophic lateral sclerosis. Amyotroph Lateral Scler. 11(1-2): 240-243.

[18] Li SH, Li XJ (1998). Aggregation of N-terminal huntingtin is dependent on the length of its glutamine repeats. Hum Mol Genet. 7(5): 777-782.

[19] Robakis NK, Wisniewski HM, Jenkins EC, Devine-Gage EA, Houck GE, Yao XL, Ramakrishna N, Wolfe G, Silverman WP, Brown WT (1987). Chromosome 21q21 sublocalisation of gene encoding beta-amyloid peptide in cerebral vessels and neuritic (senile) plaques of people with Alzheimer disease and Down syndrome. Lancet. 1(8529): 384-385.

[20] Grundke-Iqbal I, Iqbal K, Quinlan M, Tung YC, Zaidi MS, Wisniewski HM (1986). Microtubule-associated protein tau. A component of Alzheimer paired helical filaments. J Chem Biol. 261(13): 6084-6089.

[21] Gao YL, Wang N, Sun FR, Cao XP, Zhang W, Yu JT (2018). Tau in neurodegenerative disease. Ann transl Med 6(10): 165.

[22] Prusiner SB, McKinley MP, Bowman KA, Bolton DC, Bendheim PE, Groth DF, Glenner GG (1983). Scrapie prions aggregate to form amyloid-like birefringent rods. Cell 35 (2 pt.1): 349-358.

[23] Buell AK, Dobson CM, Knowles TP (2014). The physical chemistry of the amyloid phenomenon: thermodynamics and kinetics of filamentous protein aggregation. Essays Biochem. 56, 11-39.

[24] Amm I, Sommer T, Wolf DH (2014). Protein quality control and elimination of protein waste: the role of the ubiquitin-proteasome system. Biochim Biophys Acta 1843(1): 182-196.

[25] Dill KA (1990). Dominant foces in protein folding. Biochemistry 29(31): 7133-7155.

[26] Glenner GG, Page D, Isersky C, Harada M, Cuatrecasas P, Eanes ED, DeLellis RA, Bladen HA, Keiser HR (1971). Murine amyloid fibril protein: isolation, purification and characterization. J Histochem Cytochem. 19(1): 16-28.

[27] Harada M, Isersky C, Cuatrecasas P, Page D, Bladen HA, Eanes ED, Keiser HR, Glenner GG (1971). Human amyloid protein: chemical variability and homogeneity. J Histochem Cytochem. 19(1): 1-15.

[28] Lu JX, Qiang W, Yau WM, Schwieters CD, Meredith SC, Tycko R (2013). Molecular structure of β-amyloid fibrils in Alzheimer's disease brain tissue. Cell 154(6): 1257-1268.

[29] Kirschner DA, Abraham C, Selkoe DJ (1986). X-ray diffraction from intraneuronal paired helical filaments and extraneuronal amyloid fibers in Alzheimer disease indicates cross-beta conformation. Proc Natl Acad Sci U.S.A. 83(2): 503-507.

[30] Kisilevsky R, Raimondi S, Bellotti V (2016). Historical and Current Concepts of Fibrillogenesis and In vivo Amyloidogenesis: Implications of Amyloid Tissue Targeting. Front Mol Biosci. 3:17.

[31] Jarrett JT, Lansbury PT Jr. (1993). Seeding "one-dimensional crystallization" of amyloid: a pathogenic mechanism in Alzheimer's disease and scrapie? Cell 73(6): 1055-1058.

[32] Lomakin A, Teplow DB, Kirschner DA, Benedek GB (1997). Kinetic theory of fibrillogenesis of amyloid beta-protein. Proc Natl Acad Sci U.S.A. 94(15): 7942-7947.

[33] Cohen FE, Prusiner Sb (1998). Pathologic conformations of prion proteins. Annu Rev Biochem. 67: 793-819.

[34] Prusiner SB (1998). Prions. Proc Natl Acad Sci U.S.A. 95(23): 13363-13383.

[35] Naiki H, Nagai H (2009). Molecular pathogenesis of protein misfolding diseases: pathological molecular environments versus quality control systems against misfolded proteins. J Biochem. 146(6): 751-756.

[36] Buell AK, Galvagnion C, Gaspar R, Sparr E, Vendruscolo M, Knowles TP, Linse S3, Dobson CM (2014). Solution conditions determine the relative importance of nucleation and growth processes in α-synuclein aggregation. Proc Natl Acad Sci U.S.A. 111(21): 7671-7676.

[37] Naiki H, Yamamoto S, Hasegawa K, Yamaguchi I, Goto Y, Gejyo F (2005). Molecular interactions in the formation and deposition of beta2-microglobulin-related amyloid fibrils.
Amyloid 12(1): 15-25.
[38] Grey M, Linse S, Nilsson H, Brundin P, Sparr E (2011). Membrane interaction of alpha-synuclein in different aggregation states. J Parkinsons Dis. 1(4): 359-371.
[39] Liu C, Zhang Y (2011). Nucleic acid-mediated protein aggregation and assembly. Acta Protein ChemStruct Biol. 84:1-40.
[40] Cordeiro Y, Silva JL (2005). The hypothesis of the catalytic action of nuclei acid on the conversion of prion protein. Protein Pept Lett 12: 251-255.
[41] Yin J, Chen R, Liu C (2009). Nucleic acid induced protein aggregation and its role in biology and pathology. Front Biosci (Landmark Ed). 14: 5084-5106.
[42] Hegde ML, Vasudevaraju P, Rao KJ (2010). DNA induced folding/fibrillation of alpha-synuclein: new insights in Parkinson's disease. Front Biosci (Landmark Ed) 15: 418-436.
[43] Cordeiro Y, Macedo B, Silva JL, Gomes MPB (2014). Pathological implications of nucleic acid interactions with proteins associated with neurodegenerative diseases. Biophys Rev 6(1): 97-110.
[44] Gorobenko GP, Kinnunen KJ (2006). The role of lipid-protein interactions in amyloid-type protein fibril formation. Chem Phys Lipids. 141(1-2): 72-82.
[45] Prusiner SB (1994). Biology and genetics of prion diseases. Annu Rev Microbiol. 48: 655-686.
[46] Prusiner SB (1984). Prions: novel infectious pathogens. Adv virus Res.29: 1-56.
[47] Medori R, Tritschler HJ, LeBlanc A, VillaZhure F, Manetto V, Chen HY, Xue R, Leal S, Montagna P, Cortelli P, Tinuper P, Avoni P, Mochi M, Baruzzi A, Hauw JJ, Ott J, Lugaresi E, Autilio-Gambetti L, Gambetti P (1992). Fatal familial insomnia, a prion disease with a mutation at codon 178 of the prion protein gene. N Engl J Med.326(7): 444-449.
[48] Pan KM, Baldwin M, Nguyen J, Gasset M, Serban A, Groth D, Mehlhorn I, Huang Z, Fletterick RJ, Cohen FE, Prusiner SB (1993). Conversion of alpha-helices into beta-sheets features in the formation of the scrapie prion proteins. Proc Natl Acad Sci U.S.A. 90(23): 10962-10966.

[49] Wemheuer WM, Wrede A, Schulz-Schaeffer WJ (2017). Types and Strains: Their Essential Role in Understanding Protein Aggregation in Neurodegenerative Diseases. Front Aging Neurosci. 9: 187.

[50] Cuillé J, Chell PL (1936). La maladie dite tramblante du mouton est-ell inoculable? C.R. Acad. Sci.208: 1552-1554.

[51] Pattison IH, Millson GC (1961). Scrapie produced experimentally in goats with special reference to the clinical syndrome. J Comp Pathol. 71: 101-109.

[52] Gajdusek (1977). Unconventional viruses and the origin and disappearance of kuru. Science 197(4307): 943-960.

[53] Dickinson AG, Meikle VM, Frazer H (1968). Identification of a gene which controls the incubation period of some strains of scrapie agent in mice. J Comp Pathol. 78(3): 293-299.

[54] Chandler RL (1961). Encephalopathy in mice produced by inoculation with scrapie brain material. Lancet 1(7191): 1378-1379.

[55] Kimberlin RH, Walker CA (1978a). Evidence that the transmission of one source of scrapie agent to hamsters involves separation of agent strains from a mixture. J Gen Virol. 39(3): 487-496.

[56] Kimberlin RH, Walker CA (1978b). Pathogenesis of mouse scrapie: effect of route of inoculation on infectivity titres and dose-response curves. J Comp Pathol. 88(1): 39-47.

[57] Bruce ME(1993). Scrapie strain variation and mutation. Br Med Bull. 49(4): 822-838.

[58] Bessen RA, Kocisko DA, Raymond GJ, Nandan S, Lansbury P, Caughey B (1995). Non-genetic propagation of strain-specific properties of scrapie prion protein. Nature 475(6533): 698-700.

[59] Safar J, Wille H, Itri V, Groth D, Serban H, Torchia M, Cohen FE, Prusiner SB (1998). Eight prion strains have PrP(Sc) molecules with different conformations. Nat Med 4(10): 1157-1165.

[60] Sanders DW, Kaufman SK, Holmes BB, Diamond MI (2016). prions and protein assemblies that convey biological information in health and disease. Neuron 89(3): 433-448.

[61] Lemarre P, Pujo-Menjouet L, Sindi SS (2018). Generalizing a mathematical model of prion aggregation allows strain coexistence and co-stability by including a novel misfolded species. J Math Biol. doi: 10.1007/s00285-018-1280-4.

[62] Watts JC, Condello C, Stöhr J, Oehler A, Lee J, DeArmond SJ, Lannfelt L, Ingelsson M, Giles K, Prusiner SB (2014). Serial propagation of distinct strains of Aβ prions from Alzheimer's disease patients. Proc Natl Acad Sci U.S.A. 111(28): 10323-10328.

[63] Narasimhan S, Guo JL, Changolkar L, Stieber A, McBride JD, Silva LV, He Z, Zhang B, Gathagan RJ, Trojanowski JQ, Lee VMY (2017). Pathological Tau Strains from Human Brains Recapitulate the Diversity of Tauopathies in Nontransgenic Mouse Brain. J Neurosci. 37(47): 11406-11423.

[64] Sowade RF, Jahn TR (2017). Seed-induced acceleration of amyloid-β mediated neurotoxicity in vivo. Nat Commun. 8(1): 512.

[65] Wischik CM, Novak M, Edwards PC, Klug A, Tichelaar W, Crowther RA (1988). Structural characterization of the core of the paired helical filament of Alzheimer disease. Proc Natl Acad Sci U.S.A. 85(13): 4884-4888.

[66] Maroteaux L, Campanelli JT, Scheller RH (1988). Synuclein: a neuron-specific protein localized to the nucleus and presynaptic nerve terminal. J Neurosci. 8(8): 2804-2815.

[67] Polymeropoulos MH, Higgins JJ, Golbe LI, Johnson WG, Ide SE, Di Iorio G, Sanges G, Stenroos ES, Pho LT, Schaffer AA, Lazzarini AM, Nussbaum RL, Duvoisin RC (1996). Mapping of a gene for Parkinson's disease to chromosome 4q21-q23. Science 274(5290): 1197-1199.

[68] Spillantini MG, Schmidt ML, Lee VM, Trojanowski JQ, Jakes R, Goedert M (1997). Alpha-synuclein in Lewy bodies. Nature 388(6645): 839-840.

[69] Spira PJ, Sharpe DM, Halliday G, Cavanagh J, Nicholson GA (2001). Clinical and pathological features of a Parkinsonian syndrome in a family with an Ala53Thr alpha-synuclein mutation. Ann Neurol. 49(3): 313-319.

[70] Sampathu DM, Giasson BI, Pawlyk AC, Trojanowski JQ, Lee VM (2003). Ubiquitination of alpha-synuclein is not required for formation of pathological inclusions in alpha-synucleinopathies. Am J Pathol. 163(1): 91-100.

[71] Weinreb PH, Zhen W, Poon AW, Conway KA, Lansbury PT Jr (1996). NACP, a protein implicated in Alzheimer's disease and learning, is natively unfolded. Biochemistry 35(43): 13709-13715.

[72] Goedert M, Jakes R, Spillantini MG (2017). The Synucleinopathies: Twenty Years On. J Parkinsons Dis. 7(s1): S51-S69.

[73] Emanuele M, Chiaregatti E (2015). Mechanisms of alpha-synuclein action on neurotransmission: cell-autonomous and non-cell autonomous role. Biomolecules 5(2): 865-892.

[74] Uéda K, Fukushima H, Masliah E, Xia Y, Iwai A, Yoshimoto M, Otero DA, Kondo J, Ihara Y, Saitoh T (1993). Molecular cloning of cDNA encoding an unrecognized component of amyloid in Alzheimer disease. Proc Natl Acad Sci U.S.A. 90(23): 11282-11286.

[75] Jakes R, Spillantini MG, Goedert M (1994). Identification of two distinct synucleins from human brain. FEBS Lett. 345(1): 27-32.

[76] Davidson WS, Jonas A, Clayton DF, George JM (1998). Stabilization of alpha-synuclein secondary structure upon binding to synthetic membranes. J Biol Chem. 273(16): 9443-9449.

[77] Jao CC, Der-Sarkissian A, Chen J, Langen R (2004). Structure of membrane-bound alpha-synuclein studied by site-directed spin labeling. Proc Natl Acad Sci U.S.A. 101(22): 8331-8336.

[78] Bartels T, Choi JG, Selkoe DJ (2011). α-Synuclein occurs physiologically as a helically folded tetramer that resists aggregation. Nature 477(7362): 107-110.

[79] Bendor JT, Logan TP, Edwards RH (2013). The function of α-synuclein. Neuron 79(6): 1044-1066.

[80] Barbour R, Kling K, Anderson JP, Banducci K, Cole T, Diep L, Fox M, Goldstein JM, Soriano F, Seubert P, Chilcote TJ (2008). Red blood cells are the major source of alpha-synuclein in blood. Neurodegener Dis. 5(2): 55-59.

[81] Fortin DL, Troyer MD, Nakamura K, Kubo S, Anthony MD, Edwards RH (2004). Lipid rafts mediate the synaptic localization of alpha-synuclein. J Neurosci 24(30): 6715-6723.

[82] Parton RG, del Pozo MA (2013). Caveolae as plasma membrane sensors, protectors and organizers. Nat Rev Mol Cell Biol. 14(2): 98-112.

[83] Sharon R, Goldberg MS, Bar-Josef I, Betensky RA, Shen J, Selkoe DJ (2001). alpha-Synuclein occurs in lipid-rich high molecular weight complexes, binds fatty acids, and shows homology to the fatty acid-binding proteins. Proc Natl Acad Sci U.S.A. 98(16): 9110-9115.

[84] Murphy DD, Rueter SM, Trojanowski JQ, Lee VM (2000). Synucleins are developmentally expressed, and alpha-synuclein regulates the size of the presynaptic vesicular pool in primary hippocampal neurons. J Neurosci. 20(9): 3214-3220.

[85] Abeliovich A, Schmitz Y, Fariñas I, Choi-Lundberg D, Ho WH, Castillo PE, Shinsky N, Verdugo JM, Armanini M, Ryan A, Hynes M, Phillips H, Sulzer D, Rosenthal A (2000). Mice lacking alpha-synuclein display functional deficits in the nigrostriatal dopamine system. Neuron 25(1): 239-252.

[86] Yavich L, Tanila H, Vepsäläinen S, Jäkälä P (2004). Role of alpha-synuclein in presynaptic dopamine recruitment. J Neurosci. 24(49): 1165-1170.

[87] Logan T, Bendor J, Toupin C, Thorn K, Edwards RH (2017). α-Synuclein promotes dilation of the exocytotic fusion pore. Nat Neurosci. 20(5): 681-689.

[88] Chandra S, Fornai F, Kwon HB, Yazdani U, Atasoy D, Liu X, Hammer RE, Battaglia G, German DC, Castillo PE, Südhof TC (2004). Double-knockout mice for alpha- and beta-synucleins: effect on synaptic functions. Proc Natl Acad Sci U.S.A. 101(41): 14966-14971.

[89] Burré J, Sharma M, Tsetsenis T, Buchman V, Etherton MR, Südhof TC (2010). Alpha-synuclein promotes SNARE-complex assembly in vivo and in vitro. Science 329(5999): 1663-1667.

[90] Lewy F (1912). Paralysis agitans. I. Pathologische Anatomie. In Hanbuch der Neurologie Vol 3, Lewandowsky M, Abelsdorff G, eds. Springer Verlag, Berlin, pp. 920-933.

[91] McKeith I, Mintzer J, Aarsland D, Burn D, Chiu H, Cohen-Mansfield J, Dickson D, Dubois B, Duda JE, Feldman H, Gauthier S, Halliday G, Lawlor B, Lippa C, Lopez OL, Carlos Machado J, O'Brien J, Playfer J, Reid W; International Psychogeriatric Association Expert Meeting on DLB (2004). Dementia with Lewy bodies. Lancet Neurol. 3(1): 19-28.

[92] Jellinger KA, Korczyn AD (2018). Are dementia with Lewy bodies and Parkinson's disease dementia the same disease? BMC Med. 16(1): 34.

[93] Lippa CF, Duda JE, Grossman M, Hurtig HI, Aarsland D, Boeve BF, Brooks DJ, Dickson DW, Dubois B, Emre M, Fahn S, Farmer JM, Galasko D, Galvin JE, Goetz CG, Growdon JH, Gwinn-Hardy KA, Hardy J, Heutink P, Iwatsubo T, Kosaka K, Lee VM, Leverenz JB, Masliah E, McKeith IG, Nussbaum RL, Olanow CW, Ravina BM, Singleton AB, Tanner CM, Trojanowski JQ, Wszolek ZK; DLB/PDD Working Group

(2007). DLB and PDD boundary issues: diagnosis, treatment, molecular pathology, and biomarkers. Neurology 68(11): 812-819.

[94] Emre M, Aarsland D, Brown R, Burn DJ, Duyckaerts C, Mizuno Y, Broe GA, Cummings J, Dickson DW, Gauthier S, Goldman J, Goetz C, Korczyn A, Lees A, Levy R, Litvan I, McKeith I, Olanow W, Poewe W, Quinn N, Sampaio C, Tolosa E, Dubois B (2007). Clinical diagnostic criteria for dementia associated with Parkinson's disease. Mov Disord. 22(12): 1689-1707.

[95] Burn DJ, McKeith IG (2003). Current treatment of dementia with Lewy bodies and dementia associated with Parkinson's disease. Mov Disord. 18 Suppl 6: S72-S79.

[96] Weil RS, Lashley TL, Bras J, Schrag AE, Schott JM (2017). Current concepts and controversies in the pathogenesis of Parkinson's disease dementia and Dementia with Lewy Bodies. F1000Res. 6:1604.

[97] Fénelon G, Goetz CG, Karenberg A (2006). Hallucinations in Parkinson disease in the prelevodopa era. Neurology 66(1): 93-98.

[98] Beyer MK, Larsen JP, Aarsland D (2007). Gray matter atrophy in Parkinson disease with dementia and dementia with Lewy bodies. Neurology 69(8): 747-754.

[99] Ferman TJ, Boeve BF, Smith GE, Lin SC, Silber MH, Pedraza O, Wszolek Z, Graff-Radford NR, Uitti R, Van Gerpen J, Pao W, Knopman D, Pankratz VS, Kantarci K, Boot B, Parisi JE, Dugger BN, Fujishiro H, Petersen RC, Dickson DW (2011). Inclusion of RBD improves the diagnostic classification of dementia with Lewy bodies. Neurology 77(9): 875-882.

[100] Donaghy PC, McKeith IG (2014). The clinical characteristics of dementia with Lewy bodies and a consideration of prodromal diagnosis. Alzheimers Res Ther. 6(4): 46.

[101] Takemoto M, Sato K, Hatanaka N, Yamashita T, Ohta Y, Hishikawa N, Abe K (2016). Different Clinical and Neuroimaging Characteristics in Early Stage Parkinson's Disease with Dementia and Dementia with Lewy Bodies. J Alzheimers Dis 52(1): 205-211.

[102] Wong YC, Krainc D (2017). α-synuclein toxicity in neurodegeneration: mechanism and therapeutic strategies. Nat Med. 23(2): 1-13.

[103] Colloby SJ, McParland S, O'Brien JT, Attems J (2012). Neuropathological correlates of dopaminergic imaging in Alzheimer's disease and Lewy body dementias. Brain 135(pt. 9): 2798-2808.
[104] Del Tredici K, Braak H (2013). Dysfunction of the locus coeruleus-norepinephrine system and related circuitry in Parkinson's disease-related dementia. J Neurol Neurosug Psychiatry 84(7): 774-783.
[105] Hall H, Reyes S, Landeck N, Bye C, Leanza G, Double K, Thompson L, Halliday G, Kirik D (2014). Hippocampal Lewy pathology and cholinergic dysfunction are associated with dementia in Parkinson's disease. Brain 137(pt. 9): 2493-2508.
[106] Francis PT, Perry EK (2007). Cholinergic and other neurotransmitter mechanisms in Parkinson's disease, Parkinson's disease dementia, and dementia with Lewy bodies. Mov Disord. Suppl. 17: S351-S357.
[107] Gomperts SN, Locascio JJ, Makaretz SJ, Schultz A, Caso C, Vasdev N, Sperling R, Growdon JH, Dickerson BC, Johnson K (2016). Tau Positron Emission Tomographic Imaging in the Lewy Body Diseases. JAMA Neurol. 73(11): 1334-1341.
[108] Brooks DJ (2009). Imaging amyloid in Parkinson's disease dementia and dementia with Lewy bodies with positron emission tomography. Mov Disord. 24 Suppl. 2: S742-747.
[109] Compta Y, Parkkinen L, O'Sullivan SS, Vandrovcova J, Holton JL, Collins C, Lashley T, Kallis C, Williams DR, de Silva R, Lees AJ, Revesz T (2011). Lewy- and Alzheimer-type pathologies in Parkinson's disease dementia: which is more important? Brain 134(pt. 5): 1493-1505.
[110] Halliday GM, Song YJ, Harding AJ (2011). Striatal β-amyloid in dementia with Lewy bodies but not Parkinson's disease. J Neural Transm (Vienna). 118(5): 713-719.
[111] Guerreiro R, Escott-Price V, Darwent L, Parkkinen L, Ansorge O, Hernandez DG, Nalls MA, Clark L, Honig L, Marder K, van der Flier W8, Holstege H, Louwersheimer E, Lemstra A, Scheltens P, Rogaeva E, St George-Hyslop P, Londos E, Zetterberg H, Ortega-Cubero S, Pastor P, Ferman TJ, Graff-Radford NR, Ross OA, Barber I, Braae A18, Brown K, Morgan K, Maetzler W19, Berg D, Troakes C, Al-Sarraj S, Lashley T, Compta Y, Revesz T, Lees A, Cairns NJ, Halliday GM, Mann D, Pickering-Brown S, Powell J, Lunnon K, Lupton MK; International Parkinson's Disease Genomics Consortium (IPDGC), Dickson D, Hardy J, Singleton A, Bras J (2016). Genome-wide analysis

of genetic correlation in dementia with Lewy bodies, Parkinson's and Alzheimer's diseases. Neurobiol Aging. 38(214): e7-e214.

[112] Spillantini MG, Goedert M (2018). Neurodegeneration and the ordered assembly of α-synuclein. Cell tissue Res 373(1): 137-148.

[113] Singleton AB, Farrer M, Johnson J, Singleton A, Hague S, Kachergus J, Hulihan M, Peuralinna T, Dutra A, Nussbaum R, Lincoln S, Crawley A, Hanson M, Maraganore D, Adler C, Cookson MR, Muenter M, Baptista M, Miller D, Blancato J, Hardy J, Gwinn-Hardy K (2003). alpha-Synuclein locus triplication causes Parkinson's disease. Science 302(5646): 841.

[114] Walton RL, Soto-Ortolaza AI, Murray ME, Lorenzo-Betancor O, Ogaki K, Heckman MG, Rayaprolu S, Rademakers R, Ertekin-Taner N, Uitti RJ, van Gerpen JA, Wszolek ZK, Smith GE, Kantarci K, Lowe VJ, Parisi JE, Jones DT, Savica R, Graff-Radford J, Knopman DS, Petersen RC, Graff-Radford NR, Ferman TJ, Dickson DW, Boeve BF, Ross OA, Labbé C (2016). TREM2 p.R47H substitution is not associated with dementia with Lewy bodies. Neurol Genet. 2(4): e85.

[115] Srivatsal S, Cholerton B, Leverenz JB, Wszolek ZK, Uitti RJ, Dickson DW, Weintraub D, Trojanowski JQ, Van Deerlin VM, Quinn JF, Chung KA, Peterson AL, Factor SA, Wood-Siverio C, Goldman JG, Stebbins GT, Bernard B, Ritz B, Rausch R, Espay AJ, Revilla FJ, Devoto J, Rosenthal LS, Dawson TM, Albert MS, Mata IF, Hu SC, Montine KS, Johnson C, Montine TJ, Edwards KL, Zhang J, Zabetian CP (2015). Cognitive profile of LRRK2-related Parkinson's disease. Mov Disord. 30(5): 728-733.

[116] Tsuang D, Leverenz JB, Lopez OL, Hamilton RL, Bennett DA, Schneider JA, Buchman AS, Larson EB, Crane PK, Kaye JA, Kramer P, Woltjer R, Trojanowski JQ, Weintraub D, Chen-Plotkin AS, Irwin DJ, Rick J, Schellenberg GD, Watson GS, Kukull W, Nelson PT, Jicha GA, Neltner JH, Galasko D, Masliah E, Quinn JF, Chung KA, Yearout D, Mata IF, Wan JY, Edwards KL, Montine TJ, Zabetian CP (2013). APOE ε4 increases risk for dementia in pure synucleinopathies. JAMA Neurol. 70(2): 223-228.

[117] Deng HX, Shi Y, Yang Y, Ahmeti KB, Miller N, Huang C, Cheng L, Zhai H, Deng S, Nuytemans K, Corbett NJ, Kim MJ, Deng H, Tang B, Yang Z, Xu Y, Chan P, Huang B, Gao XP, Song Z, Liu Z, Fecto F, Siddique N, Foroud T, Jankovic J, Ghetti B, Nicholson DA, Krainc D, Melen O, Vance JM, Pericak-Vance MA, Ma YC, Rajput AH, Siddique T (2016). Identification of TMEM230 mutations in familial Parkinson's disease. Nat Genet. 48(7): 733-739.

[118] Shachar T, Lo Bianco C, Recchia A, Wiessner C, Raas-Rothschild A, Futerman AH (2011). Lysosomal storage disorders and Parkinson's disease: Gaucher disease and beyond. Mov Disord. 26(9): 1593-1604.

[119] Winslow AR, Chen CW, Corrochano S, Acevedo-Arozena A, Gordon DE, Peden AA, Lichtenberg M, Menzies FM, Ravikumar B, Imarisio S, Brown S, O'Kane CJ, Rubinsztein DC (2010). α-Synuclein impairs macroautophagy: implications for Parkinson's disease. J Cell Biol. 190(6): 1023-1037.

[120] Choi BK, Choi MG, Kim JY, Yang Y, Lai Y, Kweon DH, Lee NK, Shin YK (2013). Large α-synuclein oligomers inhibit neuronal SNARE-mediated vesicle docking. Proc Natl Acad Sci U.S.A. 110(10): 4087-4092.

[121] Wang L, Das U, Scott DA, Tang Y, McLean PJ, Roy S (2014). α-synuclein multimers cluster synaptic vesicles and attenuate recycling. Curr Biol. 24(19): 2319-2326.

[122] Tilve S, Difato F, Chieregatti E (2015). Cofilin 1 activation prevents the defects in axon elongation and guidance induced by extracellular alpha-synuclein. Sci Rep. 5: 16524.

[123] Calì T, Ottolini D, Negro A, Brini M (2012). α-Synuclein controls mitochondrial calcium homeostasis by enhancing endoplasmic reticulum-mitochondria interactions. J Biol Chem. 287(22): 17914-17929.

[124] Kontopoulos E, Parvin JD, Feany MB (2006). Alpha-synuclein acts in the nucleus to inhibit histone acetylation and promote neurotoxicity. Hum Mol Genet. 15(20): 3012-3023.

[125] Braak H, Del Tredici K, Rüb U, de Vos RA, Jansen Steur EN, Braak E (2013). Staging of brain pathology related to sporadic Parkinson's disease. Neurobiol Aging. 24(2): 197-211.

[126] McKeith IG, Boeve BF, Dickson DW, Halliday G, Taylor JP, Weintraub D, Aarsland D, Galvin J, Attems J, Ballard CG, Bayston A, Beach TG, Blanc F, Bohnen N, Bonanni L, Bras J, Brundin P, Burn D, Chen-Plotkin A, Duda JE, El-Agnaf O, Feldman H, Ferman TJ, Ffytche D, Fujishiro H, Galasko D, Goldman JG, Gomperts SN, Graff-Radford NR, Honig LS, Iranzo A, Kantarci K, Kaufer D, Kukull W, Lee VMY, Leverenz JB, Lewis S, Lippa C, Lunde A, Masellis M, Masliah E, McLean P, Mollenhauer B, Montine TJ, Moreno E, Mori E, Murray M, O'Brien JT, Orimo S, Postuma RB, Ramaswamy S, Ross OA, Salmon DP, Singleton A, Taylor A, Thomas A, Tiraboschi P, Toledo JB, Trojanowski JQ, Tsuang D, Walker Z, Yamada M, Kosaka K (2017). Diagnosis and

management of dementia with Lewy bodies: Fourth consensus report of the DLB Consortium. Neurology 89(1): 88-100.

[127] Alafuzoff I, Ince PG, Arzberger T, Al-Sarraj S, Bell J, Bodi I, Bogdanovic N, Bugiani O, Ferrer I, Gelpi E, Gentleman S, Giaccone G, Ironside JW, Kavantzas N, King A, Korkolopoulou P, Kovács GG, Meyronet D, Monoranu C, Parchi P, Parkkinen L, Patsouris E, Roggendorf W, Rozemuller A, Stadelmann-Nessler C, Streichenberger N, Thal DR, Kretzschmar H (2009). Staging/typing of Lewy body related alpha-synuclein pathology: a study of the BrainNet Europe Consortium. Acta Neuropathol. 117(6): 635-652.

[128] Kosaka K, Yoshimura M, Ikeda K, Budka H (1984). Diffuse type of Lewy body disease: progressive dementia with abundant cortical Lewy bodies and senile changes of varying degree--a new disease? Clin Neuropathol. 3(5): 185-192.

[129] Kuzuhara S, Mori H, Izumiyama N, Yoshimura M, Ihara Y (1988). Lewy bodies are ubiquitinated. A light and electron microscopic immunocytochemical study. Acta Neuropathol. 75(4): 345-353.

[130] Gelpi E, Navarro-Otano J, Tolosa E, Gaig C, Compta Y, Rey MJ, Martí MJ, Hernández I, Valldeoriola F, Reñé R, Ribalta T (2014). Multiple organ involvement by alpha-synuclein pathology in Lewy body disorders. Mov Disord. 29(8): 1010-1018.

[131] Navarro-Otano J, Gelpi E, Mestres CA, Quintana E, Rauek S, Ribalta T, Santiago V, Tolosa E (2013). Alpha-synuclein aggregates in epicardial fat tissue in living subjects without parkinsonism. Parkinsonism Relat Disord. 19(1): 27-31.

[132] Dijkstra AA, Voorn P, Berendse HW, Groenewegen HJ; Netherlands Brain Bank, Rozemuller AJ, van de Berg WD (2014). Stage-dependent nigral neuronal loss in incidental Lewy body and Parkinson's disease. Mov Disord. 29(10): 244-1251.

[133] Braak H, Del Tredici K (2017). Neuropathological Staging of Brain Pathology in Sporadic Parkinson's disease: Separating the Wheat from the Chaff. J Parkinsons Dis. 7(s1): S71-S85.

[134] McKeith IG, Dickson DW, Lowe J, Emre M, O'Brien JT, Feldman H, Cummings J, Duda JE, Lippa C, Perry EK, Aarsland D, Arai H, Ballard CG, Boeve B, Burn DJ, Costa D, Del Ser T, Dubois B, Galasko D, Gauthier S, Goetz CG, Gomez-Tortosa E, Halliday G, Hansen LA, Hardy J, Iwatsubo T, Kalaria RN, Kaufer D, Kenny RA, Korczyn A, Kosaka K, Lee VM, Lees A, Litvan I, Londos E, Lopez OL, Minoshima S, Mizuno Y, Molina JA, Mukaetova-Ladinska EB, Pasquier F, Perry RH, Schulz JB, Troja-

nowski JQ, Yamada M; Consortium on DLB (2005). Diagnosis and management of dementia with Lewy bodies: third report of the DLB Consortium. Neurology 65(12): 1863-1872.

[135] Leverenz JB, Hamilton R, Tsuang DW, Schantz A, Vavrek D, Larson EB, Kukull WA, Lopez O, Galasko D, Masliah E, Kaye J, Woltjer R, Clark C, Trojanowski JQ, Montine TJ (2008). Empiric refinement of the pathologic assessment of Lewy-related pathology in the dementia patient. Brain Pathol. 18(2): 220-224.

[136] Arai K, Kato N, Kashiwado K, Hattori T (2000). Pure autonomic failure in association with human alpha-synucleinopathy. Neurosci Lett. 296(2-3): 171-173.

[137] Dickson DW, Fujishiro H, DelleDonne A, Menke J, Ahmed Z, Klos KJ, Josephs KA, Frigerio R, Burnett M, Parisi JE, Ahlskog JE (2008). Evidence that incidental Lewy body disease is pre-symptomatic Parkinson's disease. Acta Neuropathol. 115(4): 437-444.

[138] Papp MI, Kahn JE, Lantos PL (1989). Glial cytoplasmic inclusions in the CNS of patients with multiple system atrophy (striatonigral degeneration, olivopontocerebellar atrophy and Shy-Drager syndrome). J Neurol Sci. 94(1-3): 79-100.

[139] Quinn N (2015). A short clinical history of multiple system atrophy. Clin Auton Res. 25(1): 3-7.

[140] Sulzer D, Surmeier DJ (2013). Neuronal vulnerability, pathogenesis, and Parkinson's disease. Mov Disord. 28(6): 715-724.

[141] Kordower JH, Chu Y, Hauser RA, Freeman TB, Olanow CW (2008). Lewy body-like pathology in long-term embryonic nigral transplants in Parkinson's disease. Nat Med. 14(5): 504-506.

[142] Kordower JH, Chu Y, Hauser RA, Olanow CW, Freeman TB (2008). Transplanted dopaminergic neurons develop PD pathologic changes: a second case report. Mov Disord. 23(16): 2303-2306.

[143] Li JY, Englund E, Holton JL, Soulet D, Hagell P, Lees AJ, Lashley T, Quinn NP, Rehncrona S, Björklund A, Widner H, Revesz T, Lindvall O, Brundin P (2008). Lewy bodies in grafted neurons in subjects with Parkinson's disease suggest host-to-graft disease propagation. Nat Med. 14(5): 501-503.

[144] Makin S (2016). Pathology: the prion principle. Nature 538(7626): S13-S16.

[145] Recasens A, Dehay B (2014). Alpha-synuclein spreading in Parkinson's disease. Front Neuroanat. 8: 159.

[146] Alvarez-Erviti L, Seow Y, Schapira AH, Gardiner C, Sargent IL, Wood MJ, Cooper JM (2011). Lysosomal dysfunction increases exosome-mediated alpha-synuclein release and transmission. Neurobiol Dis. 42(3): 360-367.

[147] Sung JY, Kim J, Paik SR, Park JH, Ahn YS, Chung KC (2001). Induction of neuronal cell death by Rab5A-dependent endocytosis of alpha-synuclein. J Biol Chem 276(29): 27441-27448.

[148] Gousset K, Schiff E, Langevin C, Marijanovic Z, Caputo A, Browman DT, Chenouard N, de Chaumont F, Martino A, Enninga J, Olivo-Marin JC, Männel D, Zurzolo C (2009). Prions hijack tunnelling nanotubes for intercellular spread. Nat Cell Biol. 11(3): 328-336.

[149] Ahn KJ, Paik SR, Chung KC, Kim J (2006). Amino acid sequence motifs and mechanistic features of the membrane translocation of alpha-synuclein. J Neurochem 97(1): 265-279.

[150] Freundt EC, Maynard N, Clancy EK, Roy S, Bousset L, Sourigues Y, Covert M, Melki R, Kirkegaard K, Brahic M (2012). Neuron-to-neuron transmission of α-synuclein fibrils through axonal transport. Ann Neurol. 72(4): 517-524.

[151] Rey NL, Steiner JA, Maroof N, Luk KC, Madaj Z, Trojanowski JQ, Lee VM, Brundin P (2016). Widespread transneuronal propagation of α-synucleinopathy triggered in olfactory bulb mimics prodromal Parkinson's disease. J Exp Med. 213(9): 1759-1778.

[152] Ulusoy A, Rusconi R, Pérez-Revuelta BI, Musgrove RE, Helwig M, Winzen-Reichert B, Di Monte DA (2013). Caudo-rostral brain spreading of α-synuclein through vagal connections. EMBO Mol Med. 5(7): 1119-1127.

[153] Peelaerts W, Baekelandt V (2016). α-Synuclein strains and the variable pathologies of synucleinopathies. J Neurochem. 139 Suppl. 1: 256-274.

[154] Xu L, Bhattacharya S, Thompson D (2018). The fold preference and thermodynamic stability of α-synuclein fibrils is encoded in the non-amyloid-β component region. Phys Chem Chem Phys. 20(6): 4502-4512.

[155] Roostaee A, Beaudoin S, Staskevicius A, Roucou X (2013). Aggregation and neurotoxicity of recombinant α-synuclein aggregates initiated by dimerization. Mol Neurodegener. 8: 5.

[156] Bengoa-Vergniory N, Roberts RF, Wade-Martins R, Alegre-Abarrategui J (2017). Alpha-synuclein oligomers: a new hope. Acta Neuropathol. 134(6): 819-838.

[157] Serio TR, Cashikar AG, Kowal AS, Sawicki GJ, Moslehi JJ, Serpell L, Arnsdorf MF, Lindquist SL (2000). Nucleated conformational conversion and the replication of conformational information by a prion determinant. Science 289(5483): 317-1321.

[158] Bousset L, Pieri L, Ruiz-Arlandis G, Gath J, Jensen PH, Habenstein B, Madiona K, Olieric V, Böckmann A, Meier BH, Melki R (2013). Structural and functional characterization of two alpha-synuclein strains. Nat Commun. 4: 2575.

[159] Peelaerts W, Bousset L, Van der Perren A, Moskalyuk A, Pulizzi R, Giugliano M, Van den Haute C, Melki R, Baekelandt V (2015). α-Synuclein strains cause distinct synucleinopathies after local and systemic administration. Nature 552(7556): 430-344.

[160] Guo JL, Covell DJ, Daniels JP, Iba M, Stieber A, Zhang B, Riddle DM, Kwong LK, Xu Y, Trojanowski JQ, Lee VM (2013). Distinct α-synuclein strains differentially promote tau inclusions in neurons. Cell 154(1): 103-117.

[161] Kim C, Lv G, Lee JS, Jung BC, Masuda-Suzukake M, Hong CS, Valera E, Lee HJ, Paik SR, Hasegawa M, Masliah E, Eliezer D, Lee SJ (2016). Exposure to bacterial enDotoxin generates a distinct strain of α-synuclein fibril. Sci Rep. 6: 30891.

[162] Watts JC, Giles K, Oehler A, Middleton L, Dexter DT, Gentleman SM, DeArmond SJ, Prusiner SB (2013). Transmission of multiple system atrophy prions to transgenic mice. Proc Natl Acad Sci U.S.A. 110(46): 19555-19560.

[163] Giasson BI, Duda JE, Quinn SM, Zhang B, Trojanowski JQ, Lee VM (2002). Neuronal alpha-synucleinopathy with severe movement disorder in mice expressing A53T human alpha-synuclein. Neuron 34(4): 521-533.

[164] Prusiner SB, Woerman AL, Mordes DA, Watts JC, Rampersaud R, Berry DB, Patel S, Oehler A, Lowe JK, Kravitz SN, Geschwind DH, Glidden DV, Halliday GM, Middleton LT, Gentleman SM, Grinberg LT, Giles K (2015). Evidence for α-synuclein prions causing multiple system atrophy in humans with parkinsonism. Proc Natl Acad Sci U.S.A. 112(38): E5308-5317.

[165] Peng C, Gathagan RJ, Covell DJ, Medellin C, Stieber A, Robinson JL, Zhang B, Pitkin RM, Olufemi MF, Luk KC, Trojanowski JQ, Lee VM (2018). Cellular milieu imparts distinct pathological α-synuclein strains in α-synucleinopathies. Nature 557(7706): 558-563.

[166] Biancalana M, Koide S (2010). Molecular mechanism of Thioflavin-T binding to amyloid fibrils. Biochem Biophy Acta 1804(7): 1405-1412.

[167] Vassar PS, Culling CF (1959). Fluorescent stains, with special reference to amyloid and connective tissues. Arch Pathol. 68: 487-498.

[168] Naiki H, Higuchi K, Hosokawa M, Takeda T (1989). Fluorometric determination of amyloid fibrils in vitro using the fluorescent dye, thioflavin T1. Anal Biochem. 177(2): 244-249.

[169] Naiki H, Higuchi K, Matsushima K, Shimada A, Chen WH, Hosokawa M, Takeda T (1990). Fluorometric examination of tissue amyloid fibrils in murine senile amyloidosis: use of the fluorescent indicator, thioflavine T. Lab Invest. 62(6): 768-773.

[170] Maskevich AA, Kurhuzenkau SA, Lavysh AV, Kivach LN, Maskevich SA (2015). Surface-Enhanced Raman Scattering Spectra of Thioflavin T: Manifestation of the Electromagnetic and Molecular Enhancement Mechanisms. J Appl Spectrosc 82:532.

[171] Sabaté R, Lascu I, Saupe SJ (2008). On the binding of Thioflavin-T to HET-s amyloid fibrils assembled at pH 2. J Struct Biol. 162(3): 387-396.

[172] De Ferrari GV, Mallender WD, Inestrosa NC, Rosenberry TL (2001). Thioflavin T is a fluorescent probe of the acetylcholinesterase peripheral site that reveals conformational interactions between the peripheral and acylation sites. J Biol Chem 276(26): 23284-23287.

[173] Sen P, Fatima S, Ahmad B, Khan RH (2009). Interactions of thioflavin T with serum albumins: spectroscopic analyses. Spectrochim Acta A Mol Biomol Spectrosc. 74(1): 94-99.

[174] Villar-Piqué A, Schmitz M, Candelise N, Ventura S, Llorens F, Zerr I (2018). Molecular and Clinical Aspects of Protein Aggregation Assays in Neurodegenerative Diseases. Mol Neurobiol. 55(9): 7588-7605.

[175] Lindgren M, Sörgjerd K, Hammarström P (2005). Detection and characterization of aggregates, prefibrillar amyloidogenic oligomers, and protofibrils using fluorescence spectroscopy. Biophys J. 88(6): 4200-4212.

[176] Pinotsi D, Buell AK, Galvagnion C, Dobson CM, Kaminski Schierle GS, Kaminski CF (2013). Direct observation of heterogeneous amyloid fibril growth kinetics via two-color super-resolution microscopy. Nano Lett. 14(1): 339-345.

[177] Perczel A, Park K, Fasman GD (1992). Deconvolution of the circular dichroism spectra of proteins: the circular dichroism spectra of the antiparallel beta-sheet in proteins. Proteins 13(1): 57-69.

[178] Miller LM, Bourassa MW, Smith RJ (2013). FTIR spectroscopic imaging of protein aggregation in living cells. Biochim Biophys Acta 1828(10): 2339-2346.

[179] Guerrini L, Arenal R, Mannini B, Chiti F, Pini R, Matteini P, Alvarez-Puebla RA (2015). SERS Detection of Amyloid Oligomers on Metallorganic-Decorated Plasmonic Beads. ACS Appl Mater Interfaces 7(18): 9420-9428.

[180] D'Andrea C, Foti A, Cottat M, Banchelli M, Capitini C, Barreca F, Canale C, de Angelis M, Relini A, Maragò OM, Pini R, Chiti F, Gucciardi PG, Matteini P (2018). Small 14(36): e1800890.

[181] Chiti F, Dobson CM (2017). Protein Misfolding, Amyloid Formation, and Human Disease: A Summary of Progress Over the Last Decade. Annu Rev Biochem. 86: 27-68.

[182] Pleshakova TO, Bukharina NS, Archakov AI, Ivanov YD (2018). Atomic Force Microscopy for Protein Detection and Their Physicochemical Characterization. Int J Mol Sci 19(4): pii: E1142.

[183] Come JH, Fraser PE, Lansbury PT Jr (1993). A kinetic model for amyloid formation in the prion diseases: importance of seeding.Proc Natl acad Sci U.S.A. 90(13): 5959-5963.

[184] Saborio GP, Permanne B, Soto C (2001). Sensitive detection of pathological prion protein by cyclic amplification of protein misfolding. Nature 411(6839): 810-813.

[185] Castilla J, Saá P, Hetz C, Soto C (2005). In vitro generation of infectious scrapie prions. Cell 12(2): 195-206.

[186] Saá P, Castilla J, Soto C (2006). Ultra-efficient replication of infectious prions by automated protein misfolding cyclic amplification. J Biol Chem. 281(46): 35245-35252.

[187] Morales R, Duran-Aniotz C, Diaz-Espinoza R, Camacho MV, Soto C (2012). Protein misfolding cyclic amplification of infectious prions. Nat. Protoc. 7(7): 1397-1409.

[188] Castilla J, Saá P, Soto C (2005). Detection of prions in blood. Nat Med. 11(9): 982-985.

[189] Murayama Y, Yoshioka M, Okada H, Takata M, Yokoyama T, Mohri S (2007). Urinary excretion and blood level of prions in scrapie-infected hamsters. J Gen Virol. 88(pt. 10): 2890-2898.

[190] Shahnawaz M, Tokuda T, Waragai M, Mendez N, Ishii R, Trenkwalder C, Mollenhauer B, Soto C (2017). Development of a Biochemical Diagnosis of Parkinson Disease by Detection of α-Synuclein Misfolded Aggregates in Cerebrospinal Fluid. JAMA Neurol. 74(2): 163-172.

[191] Salvadores N, Shahnawaz M, Scarpini E, Tagliavini F, Soto C (2014). Detection of misfolded Aβ oligomers for sensitive biochemical diagnosis of Alzheimer's disease. Cell Rep. 7(1): 261-268.

[192] Colby DW, Zhang Q, Wang S, Groth D, Legname G, Riesner D, Prusiner SB (2007). Prion detection by an amyloid seeding assay. Proc Natl Acad Sci U.S.A. 104(52): 20914-20919.

[193] Atarashi R, Wilham JM, Christensen L, Hughson AG, Moore RA, Johnson LM, Onwubiko HA, Priola SA, Caughey B (2008). Simplified ultrasensitive prion detection by recombinant PrP conversion with shaking. Nat Methods 5(3): 211-212.

[194] Orrú CD, Wilham JM, Hughson AG, Raymond LD, McNally KL, Bossers A, Ligios C, Caughey B (2009). Human variant Creutzfeldt-Jakob disease and sheep scrapie PrP(res) detection using seeded conversion of recombinant prion protein. Protein Eng Des Sel. 22(8): 515-521.

[195] Collins SR, Douglass A, Vale RD, Weissman JS (2004). Mechanism of prion propagation: amyloid growth occurs by monomer addition. PLoS Biol. 2(10): e321.

[196] Atarashi R, Satoh K, Sano K, Fuse T, Yamaguchi N, Ishibashi D, Matsubara T, Nakagaki T, Yamanaka H, Shirabe S, Yamada M, Mizusawa H, Kitamoto T, Klug G, McGlade A, Collins SJ, Nishida N (2011). Ultrasensitive human prion detection in cerebrospinal fluid by real-time quaking-induced conversion. Nat Med. 17(2): 175-178.

[197] Schmitz M, Cramm M, Llorens F, Müller-Cramm D, Collins S, Atarashi R, Satoh K, Orrú CD, Groveman BR, Zafar S, Schulz-Schaeffer WJ, Caughey B, Zerr I (2016). The real-time quaking-induced conversion assay for detection of human prion disease and study of other protein misfolding diseases. Nat Protoc. 11(11): 2233-2242.

[198] Cheng K, Sloan A, Avery KM, Coulthart M, Carpenter M, Knox JD (2014). Exploring physical and chemical factors influencing the properties of recombinant prion protein and the real-time quaking-induced conversion (RT-QuIC) assay. PLoS One. 9(1): e84812.

[199] Schmitz M, Candelise N, Llorens F, Zerr I (2018). Amplification and Detection of Minuscule Amounts of Misfolded Prion Protein by Using the Real-Time Quaking-Induced Conversion. Methods Mol Biol. 1779: 257-263.

[200] Cramm M, Schmitz M, Karch A, Mitrova E, Kuhn F, Schroeder B, Raeber A, Varges D, Kim YS, Satoh K, Collins S, Zerr I (2015). Stability and Reproducibility Underscore Utility of RT-QuIC for Diagnosis of Creutzfeldt-Jakob Disease.Mol Neurobiol. 53(3): 1896-1904.

[201] Candelise N, Schmitz M, Da Silva Correia SM, Arora AS, Villar-Piqué A, Zafar S, Llorens F, Cramm M, Zerr I (2017). Applications of the real-time quaking-induced conversion assay in diagnosis, prion strain-typing, drug pre-screening and other amyloidopathies. Expeet Rev Mol Diagn. 17(10): 897-904.

[202] Orrú CD, Wilham JM, Raymond LD, Kuhn F, Schroeder B, Raeber AJ, Caughey B (2011). Prion disease blood test using immunoprecipitation and improved quaking-induced conversion. MBio 2(3): e00078-11.

[203] Moda F, Gambetti P, Notari S, Concha-Marambio L, Catania M, Park KW, Maderna E, Suardi S, Haïk S, Brandel JP, Ironside J, Knight R, Tagliavini F, Soto C (2014). Prions in the urine of patients with variant Creutzfeldt-Jakob disease. N Eng J Med. 371(6): 530-539.

[204] Orrú CD, Yuan J, Appleby BS, Li B, Li Y, Winner D, Wang Z, Zhan YA, Rodgers M, Rarick J, Wyza RE, Joshi T, Wang GX, Cohen ML, Zhang S, Groveman BR, Petersen RB, Ironside JW, Quiñones-Mateu ME, Safar JG, Kong Q, Caughey B, Zou WQ (2017). Prion seeding activity and infectivity in skin samples from patients with sporadic Creutzfeldt-Jakob disease. Sci Transl Med. 9(417).

[205] Orrú CD, Groveman BR, Hughson AG, Zanusso G, Coulthart MB, Caughey B (2015). Rapid and sensitive RT-QuIC detection of human Creutzfeldt-Jakob disease using cerebrospinal fluid. MBio 6(1).

[206] Schmitz M, Cramm M, Llorens F, Candelise N, Müller-Cramm D, Varges D, Schulz-Schaeffer WJ, Zafar S, Zerr I (2016). Application of an in vitro-amplification assay as a novel pre-screening test for compounds inhibiting the aggregation of prion protein scrapie. Sci Rep. 6: 28711.

[207] Hyeon JW, Kim SY, Lee SM, Lee J, An SS, Lee MK, Lee YS (2017). Anti-Prion Screening for Acridine, Dextran, and Tannic Acid using Real Time-Quaking Induced Conversion: A Comparison with PrPSc-Infected Cell Screening. PLoS One. 12(1): e017026.

[208] Saijo E, Ghetti B, Zanusso G, Oblak A, Furman JL, Diamond MI, Kraus A, Caughey B (2017). Ultrasensitive and selective detection of 3-repeat tau seeding activity in Pick disease brain and cerebrospinal fluid. Acta Neuropathol. 133(5): 751-765.

[209] Fairfoul G, McGuire LI, Pal S, Ironside JW, Neumann J, Christie S, Joachim C, Esiri M, Evetts SG, Rolinski M, Baig F, Ruffmann C, Wade-Martins R, Hu MT, Parkkinen L, Green AJ (2016). Alpha-synuclein RT-QuIC in the CSF of patients with alpha-synucleinopathies. Ann Clin Transl Neurol. 3(10): 812-818.

[210] Sano K, Atarashi R, Satoh K, Ishibashi D, Nakagaki T, Iwasaki Y, Yoshida M, Murayama S, Mishima K, Nishida N (2018). Prion-Like Seeding of Misfolded α-Synuclein in the Brains of Dementia with Lewy Body Patients in RT-QUIC. Mol Neurobiol. 55(5): 3916-3930.

[211] Groveman BR, Orrù CD, Hughson AG, Raymond LD, Zanusso G, Ghetti B, Campbell KJ, Safar J, Galasko D, Caughey B (2018). Rapid and ultra-sensitive quantitation of disease-associated α-synuclein seeds in brain and cerebrospinal fluid by αSyn RT-QuIC. Acta Neuropathol Commun. 6(1): 7.

[212] Zea-Sevilla MA, Fernández-Blázquez MA, Calero M, Bermejo-Velasco P, Rábano A (2015). Combined Alzheimer's disease and cerebrovascular staging explains advanced dementia cognition. Alzheimers Dement. 11(11): 1358-1366.

[213] Martinez-Martin P (2010). Composite rating scales. J Neurol Sci 289(1-2): 7-11.

[214] Llorens F, Kruse N, Schmitz M, Shafiq M, da Cunha JE, Gotzman N, Zafar S, Thune K, de Oliveira JR, Mollenhauer B, Zerr I (2015). Quantification of CSF biomarkers using an electrochemiluminescence-based detection system in the differential diagnosis of AD and sCJD. J Neurol. 262(10): 2305-2311.

[215] Capitini C, Patel JR, Natalello A, D'Andrea C, Relini A, Jarvis JA, Birolo L, Peduzzo A, Vendruscolo M, Matteini P, Dobson CM, De Simone A, Chiti F (2018). Structural differences between toxic and nontoxic HypF-N oligomers. Chem commun (Camb). 54(62): 8637-8670.

[216] Dickson DW (2002). Misfolded, protease-resistant proteins in animal models and human neurodegenerative disease. J Clin Invest. 110(10): 1403-1405.

[217] Maiti NC, Apetri MM, Zagorski MG, Carey PR, Anderson VE (2004). Raman spectroscopic characterization of secondary structure in natively unfolded proteins: alpha-synuclein. J Am Chem Soc 126:2399-408.

[218] Zhu M, Li J, Fink AL (2003). The association of alpha-synuclein with membranes affects bilayer structure, stability, and fibril formation. J Biol Chem. 278(41): 40186-40197.

[219] Liu IH, Uversky VN, Munishkina LA, Fink AL, Halfter W, Cole GJ (2005). Agrin binds alpha-synuclein and modulates alpha-synuclein fibrillation. Glycobiology 15(12): 1320-1331.

[220] Heydorn WE, Joseph Creed G, Patel J, Jacobowitz DM (1986). Distribution of proteins in different subcellular fractions of rat brain studied by two-dimensional gel electrophoresis. Neurochem Int. 9(3): 357-370.

[221] Kramer ML, Behrens C, Schulz-Schaeffer WJ (2008). Selective detection, quantification, and subcellular location of alpha-synuclein aggregates with a protein aggregate filtration assay. Biotechniques. 44(3): 403-411.

[222] Luna E, Decker SC, Riddle DM, Caputo A, Zhang B, Cole T, Caswell C, Xie SX, Lee VMY, Luk KC (2018). Differential α-synuclein expression contributes to selective vulnerability of hippocampal neuron subpopulations to fibril-induced toxicity. Acta Neuropathol. 135(6): 855-875.